Title
VSP Site Characterization at NTS: OSSY '91 - Summary Report

Authors
Leonard, M.A.
Daley, T.M.
Johnson, L.R.

Publication Date
1992-04-01

LBL-32521
UC-000

Lawrence Berkeley Laboratory
UNIVERSITY OF CALIFORNIA

EARTH SCIENCES DIVISION

VSP Site Characterization at NTS: OSSY '91—Summary Report

M.A. Leonard, T.M. Daley, and L.R. Johnson

April 1992

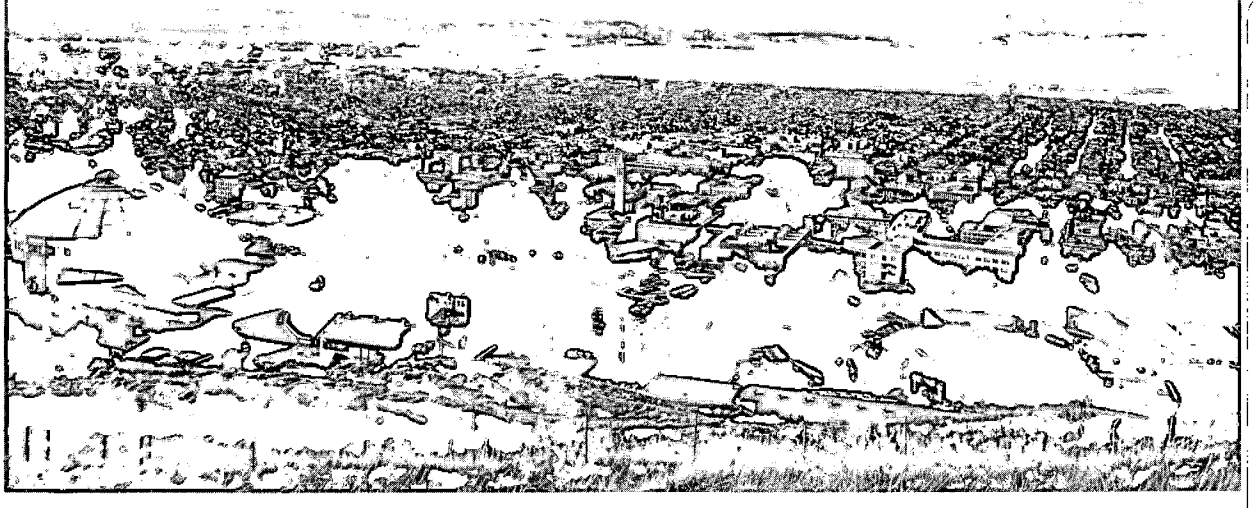

Prepared for the U.S. Department of Energy under Contract Number DE-AC03-76SF00098

This report has been reproduced directly from the
best available copy.

DISCLAIMER

LBL-32521

VSP Site Characterization at NTS: OSSY '91—Summary Report

M. A. Leonard, T. M. Daley, and L. R. Johnson

Center for Computational Seismology
Earth Sciences Division
Lawrence Berkeley Laboratory
University of California
Berkeley, California 94720

April 1992

This work was supported by Lawrence Livermore National Laboratory, under U.S. Department of Energy Contract No. W-7405-ENG-48, through U.S. Department of Energy Contract No. DE-AC03-76SF00098.

INTRODUCTION

In June of 1991 a Vertical Seismic Profiling (VSP) survey was conducted as part of the 1991 On Site Seismic Yield (OSSY) experiment in the Yucca Valley area of the Nevada Test Site. The OSSY '91 experiment has been a cooperative effort between Lawrence Livermore National Laboratory, the Lawrence Berkeley Laboratory, and Southern Methodist University. The principal goal of the project is to develop seismic methods to determine accurately the yield of underground nuclear explosions in a manner which is relatively inexpensive, non-invasive, and at least as reliable as existing methods. The ability to estimate nuclear yield accurately is fundamental in the verification of nuclear test ban treaties. The steps involved in this inverse problem for explosive yield can be described as follows:

1. Determine the physical properties controlling seismic wave propagation in the vicinity of the explosion,
2. Calibrate the yield-inversion method with small chemical explosions of known yield detonated at the working point of the subsequent nuclear explosion, and
3. Apply the method to the nuclear explosion

The critical first step of determining the seismic wave propagation properties was accomplished by the VSP survey in which P, SV, and SH surface vibrator sources generated wavefields which were recorded by 3-component seismometers at several depths in well UE4av in Yucca Valley. This data set was used to construct 3-dimensional P and S velocity models of the area, and to assess shear-wave anisotropy. Following the VSP survey, the source-receiver geometry was reversed, with 3-component seismometers occupying the surface VSP sites and 100 pound chemical calibration explosions detonated downhole. Later, a nuclear explosion was detonated in an adjacent well. The use of the same sites by VSP sources and explosion receivers ensured that the seismic properties described by the VSP analysis were appropriate for the paths traveled by the explosion-generated wavefields. The acquisition and processing of this data set follows closely that from the VSP site characterization study that was part of the 1989 OSSY experiment, described in Daley, *et al.* (1990).

DATA ACQUISITION AND PROCESSING

The VSP source locations fell along four azimuths about the receiver well, with two to four sites along each azimuth, totaling ten sites in all (Figure 1a). Source offsets from the well ranged between 46 and 1600 meters. At each source location we obtained three vibrator data sets, using P, SV, and SH sources, with an 8-80 Hz sweep and 3 seconds of correlated data. The downhole 3-component receiver was placed at spacings of 22.9 m (75 ft) from 41 to 439 m and 7.6 m (25 ft) beyond to the maximum receiver depth of to 523 m. (Figure 1b). The data

sampling interval was 2 msec. Initial data processing, including demultiplexing, correlation and sorting into depth-ordered common source point data sets, was performed by the contractor, Seismograph Service Corporation. The remaining processing took place at the Center for Computational Seismology (CCS) at Lawrence Berkeley Laboratory. This processing has consisted of the editing of bad traces, sorting by source type at each source location, stacking of individual sweeps, converting horizontal components to a consistent coordinate system, and travel time analysis for velocity structure. The number of data traces following stacking totaled about 2100.

The need for a consistent horizontal coordinate system arises because the downhole seismometer is locked into place with an unknown horizontal orientation. To estimate the orientation of the receiver, a P-wave polarization analysis of the P-source data is performed for each source location. The results from all source locations are averaged to obtain a mean horizontal orientation of the receiver at each depth. Once the coordinate system is defined in this way, the waveform data from each VSP site can be rotated into vertical, horizontal-radial, and horizontal-transverse components of motion. Following the rotations, P, SV, and SH travel times were picked off the appropriate component to serve as input for the velocity inversion discussed below. Three of the ten resulting 9-component data sets, from VSP sites 1, 8, and 14, are shown in Figures 2, 3, and 4. Were the earth laterally homogeneous and isotropic, the coordinate rotations done without error, and the source generation pure, we would see only P and P-to-SV motion on the vertical and radial components from the P source, SV and SV-to-P motion on the vertical and radial components from the SV source, and SH motion only on the transverse component from the SH source. However, as is typical at all sites, the transverse energy from the P and SV sources and the vertical and radial energy from the SH source are significant.

This presence of this "out-of-plane" energy in the 9-component VSP is due to the combined factors of:

1) distortion of source polarization by near-surface material heterogeneities, though it is difficult to estimate the extent of this,

2) bending of the wavefield out of the source-receiver plane due to lateral heterogeneities along a particular azimuth and the resulting bias this will cause along other azimuths in the computation of the mean horizontal receiver orientation,

3) the difficulty in estimating receiver orientation from the polarization analysis due to poor data quality, i.e., low signal-to-noise ratios and waveform complexity.

With regard to 3) above, the orientation of rectilinear P-wave particle motion at a given receiver could, on the average, be confidently estimated from only 3 to 5 of the 10 VSP source locations, with the standard deviation of the resulting receiver orientations averaging about 20 degrees. This is in contrast to an average standard deviation of only 9.5 degrees with the OSSY '89 data set (Daley, *et al.* 1990), however in OSSY '89 all but one VSP site was within just 600 meters of the receiver well. In OSSY '91, VSP source offsets were taken out twice as far, suggesting that horizontal offset of the VSP source has a strong effect on the quality of data, as one might expect as wavefields increasingly distort as they travel a greater distance through a heterogeneous medium.

ANISOTROPY AND HETEROGENEITY

The multi-source three-dimensional design of the experiment clearly provides an excellent opportunity to assess shear-wave anisotropy and heterogeneity in the sub-surface structure. An illustrative example of both is given in Figure 5, which shows horizontal (radial and transverse) components of motion from all ten VSP source locations recorded at the deepest recorder depth of 523 meters. The source number is indicated to the left and the horizontal offset to the right of each waveform, which is normalized to unit amplitude. The transverse waveforms (solid lines) were constructed by summing the transverse component motion from all three source types (P, SV, and SH), and likewise the radial waveforms (dotted lines) by summing the radial components from all source types. Summing in this way was done in an attempt to enhance the SV and SH arrivals and give the best approximation of an explosive-generated waveform. Comparing the SV and SH traces, some anisotropy does appear to exist, though it is not great. For example, at site 12, which is 1143 meters away, there is an SH-SV time difference of only 10 msec in a travel time of over 1 sec, indicating less than 1% apparent anisotropy. Recordings from other VSP sites, e.g., site 9 in the figure, display no observable anisotropy.

The extent of heterogeneity is reflected in the differences between recordings having different source locations but identical horizontal offset. Here not only does waveform complexity vary, particularly among the 686 meter offset recordings, but there are also distinct differences in the S-wave arrival time, notably the relatively early arrival from VSP site 14 and the relatively late arrival from site 6 (see Figure 5). The velocity inversion procedure described below is an attempt to account for these differences in terms of laterally varying velocity structures.

VELOCITY INVERSION

The inversions of travel-time data produced three two-dimensional cross sections of P and S velocity along different source-receiver azimuths, i.e., to the southwest with VSP sites 1, 14, 15, 16, along the northwest-southeast with sites 6, 5, 1, 11, 12, and to the east with sites 1, 8, 9. VSP site 1 travel times, near zero offset, were used for all cross sections to give a consistent result at the borehole. The travel-time inversions performed were based on a method proposed by Thurber (1983) and modified by Michelini (1991). The method inverts for velocity values at discrete nodes in the model and interpolates between node points using a cubic B-spline parameterization of velocity. Along each of our cross sections the model was discretized with a horizontal node spacing of 300 meters and a vertical node spacing of 100 meters. The inversions for P and S velocity can be done separately or jointly with *a priori* constraints on Vp/Vs ratios. Here they were done separately. The inversions are non-linear and so require starting velocity models. These were obtained by first analyzing interval travel times from VSP site 1 and then using the resulting one-dimensional model as a starting model in inversions for one-dimensional, average models along each azimuth. An average of these one-dimensional models was then used as the starting model along each azimuth. Because of the scarcity of clear S-wave arrivals, there were in all cases fewer S-wave travel times available than for P, which adversely affected our ability to resolve lateral S-wave velocity structure.

One example of inversion results is shown in Figure 6 which displays ray paths and velocity contours from the P-wave velocity inversion along the southwest azimuth. The well is at zero offset and southwest is towards the right of the figure. The velocity values that are contoured were obtained from a cubic B-spline interpolation of the node values. The resolution of the inverted velocity values is primarily controlled by the characteristics of ray coverage within the model, which is quite variable. The velocities near the well in the figure are in fair agreement with the down-hole measurements. The increase in velocity near 300 meters depth correlates with the depth of the alluvium-tuff interface logged in the well. The depth to the Paleozoic basement is about 800 meters and so falls outside of the depth range of our models. The horizontal transition to greater velocity values beyond an offset of about 500 meters in the figure correlates with an upthrown block mapped in this southwest area. The lack of a sharper horizontal velocity contrast below 300 m may be due to insufficient ray coverage. Note that the ray paths from VSP site 14 sample the shallow high velocities, which would explain the relatively short travel times from this source location compared to the other VSP sites at the same offset but different azimuth (see Figure 5).

Among the three cross sections, the alluvial P velocity typically ranges between about 0.8 km/sec at the surface to about 2 km/sec at depth and the S velocity between about 0.5 km/sec at the surface to 1.1 km/sec at depth. Within the tuff at the depth of the well bottom, 523 meters, the P velocity increases to between about 2.8 and 3.2 km/sec, depending on the cross section, and S velocities to between 1.4 and 1.8 km/sec. See appendix 1 for further discussion of inversion results and color plots of P and S velocity and their associated resolution function along each azimuth.

The travel-time inversion analysis has also revealed a basic drawback in the design of the OSSY '91 VSP survey. As can be seen in Figure 6, with this source-receiver configuration, at the larger offsets most of the energy is concentrated in narrow bundles and hence samples the medium rather poorly. A much better experimental design would use fewer downhole receiver locations and a finer sampling of VSP source points at the surface. This would result in a more uniform sampling of the medium with many overlapping ray paths, and, assuming vibrator trucks can be moved and oriented faster than a downhole receiver can be raised and properly clamped, might reduce the time and cost of data acquisition.

SPECTRAL ANALYSIS

The vibroseis VSP data has been analyzed for spectral content. This analysis used the direct arrival from the site 1 P-wave and SH-wave sources at all receiver depths except the most shallow (23 m). The time window for analysis is small because we did not want scattered or reflected energy to bias the spectral estimate. Because of the short time series (about 36 samples at 2 ms sample rate), we did not use a standard fast fourier transform (FFT), instead a maximum entropy spectral analysis method was used. This is a data adaptive method used to obtain higher spectral resolution of a short time series. Figure 7 shows normalized spectra of the P-source P-wave arrival of the vertical component for all depths recorded. The spectral amplitude (complex absolute value of the transform) at each depth is plotted over the 8 to 80Hz range used for the source sweep. There is a broad peak of amplitude from about 20 to 50 Hz, a drop from 50 to 65 Hz, and a smaller peak near 70 Hz. The 70 Hz peak is at least partially due to resonance of the receiver. Figure 8 shows the normalized spectra for the SH-source S-wave arrival on the horizontal-transverse component. There is more noise and scatter in this shear-wave data, however the dominant trend is still apparent. The shear-wave has a spectral peak between 15 and 25 Hz, with a strong drop in amplitude with increasing frequency. The shear-wave amplitude at 70 Hz is nearly 2 orders of magnitude less than the peak.

CONCLUSIONS

The VSP method provides a flexible tool for evaluating the subsurface prior to acquisition of costly, non-repeatable explosive-source data. We are able to obtain velocity models and estimates of anisotropy and heterogeneities which can aid interpretation of explosive data. In this year's study (OSSY '91), we attempted to extend the VSP source sites to offsets of up to 1.5 km. While this was basically successful (waveforms were recorded and velocity models were derived), there was a definite degradation of data quality as compared to OSSY '89 (Daley, *et al.*, 1990). Since the subsurface material in the two studies was comparable, we feel that the reduced data quality was due to the larger offsets and the raypath bending associated with long offset VSP data. In many cases the deeper receiver depths had good quality arrivals, but the shallower depths were not usable for first arrival information. For receiver depths less than 500 m, source offsets of 1 km appear to be the limit of good quality VSP data in the alluvium and tuffs of NTS. Also, a design which uses fewer receiver points and more source points seems warranted for future experiments.

The velocity models derived from inversion of VSP travel time data have been used in yield estimations within the OSSY '91 experiment. These models are used to help interpret structural features such as the upthrown block indicated in the southwest cross section (Figure 6). The SV and SH data have been analyzed for shear-wave anisotropy with no significant (>1%) findings. This negative result with respect to anisotropy in the subsurface is in agreement with the results of OSSY '89, which found some shallow anisotropic material, but no anisotropy at depth. There is clear evidence of azimuthal and lateral heterogeneities within the subsurface from the VSP waveforms. Such heterogeneities will affect the explosive-generated wavefield as recorded at the surface. Unfortunately, we are currently limited in our ability to describe structure outside the source-receiver planes. However, we are exploring ways to utilize the information in the entire VSP waveforms, rather than just travel times, to improve our characterization of the seismic response to the heterogeneous medium for the purpose of yield estimation.

REFERENCES

Daley, T. M., T. V. McEvilly, and A. Michelini, 1990. VSP Site Characterization at NTS - Summary Report , Lawrence Berkeley Laboratory Report LBL-29778.

Michelini, A., 1991. Fault zone structure determined through the analysis of earthquake arrival times, Ph.D. Thesis, University of California at Berkeley.

Thurber, C. H., 1983. Earthquake locations and three-dimensional crustal structure in the Coyote Lake area, Central California. J. Geophys. Res., v. 88, p. 8226-8236

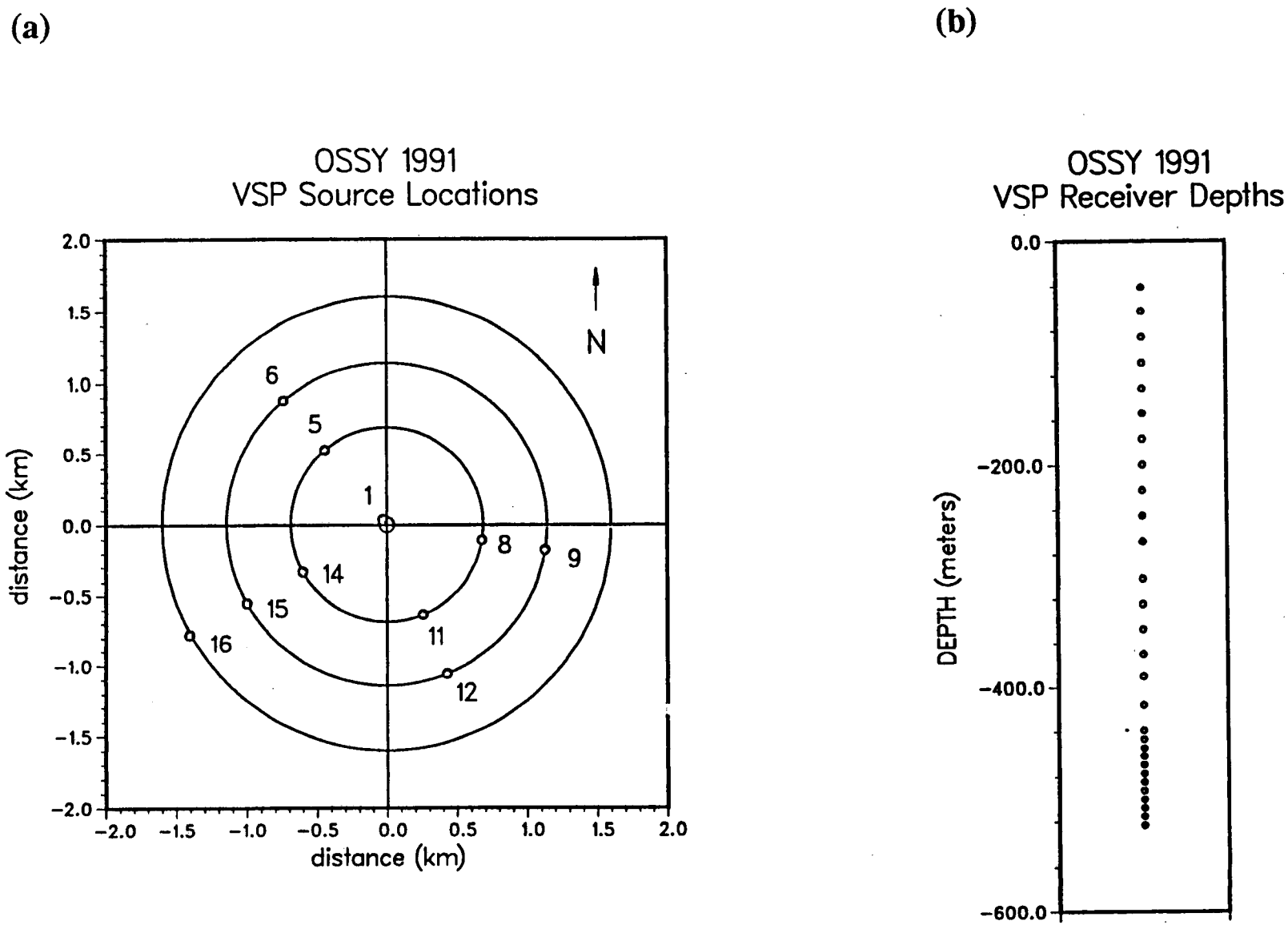

Figure 1 **(a)** VSP source locations with site numbers indicated. **(b)** VSP receiver depths. The six most shallow receivers recorded data from VSP sites 1 and 5 only.

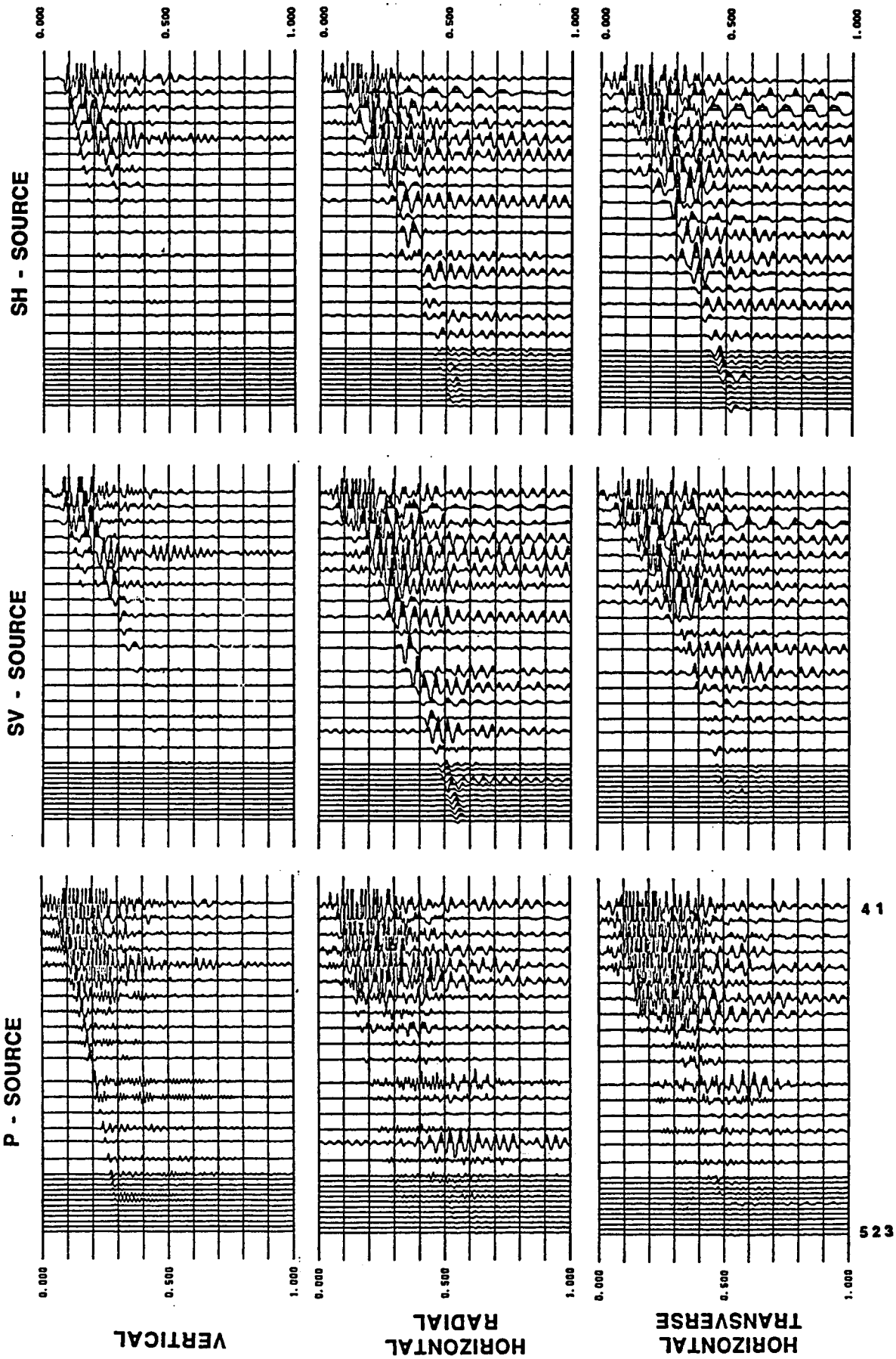

Figure 2 9-component VSP data set from site 1 (41 m offset). Data traces are normalized to a constant value, giving true relative amplitudes. The minimum and maximum depths of recording in meters are indicated in the lower left.

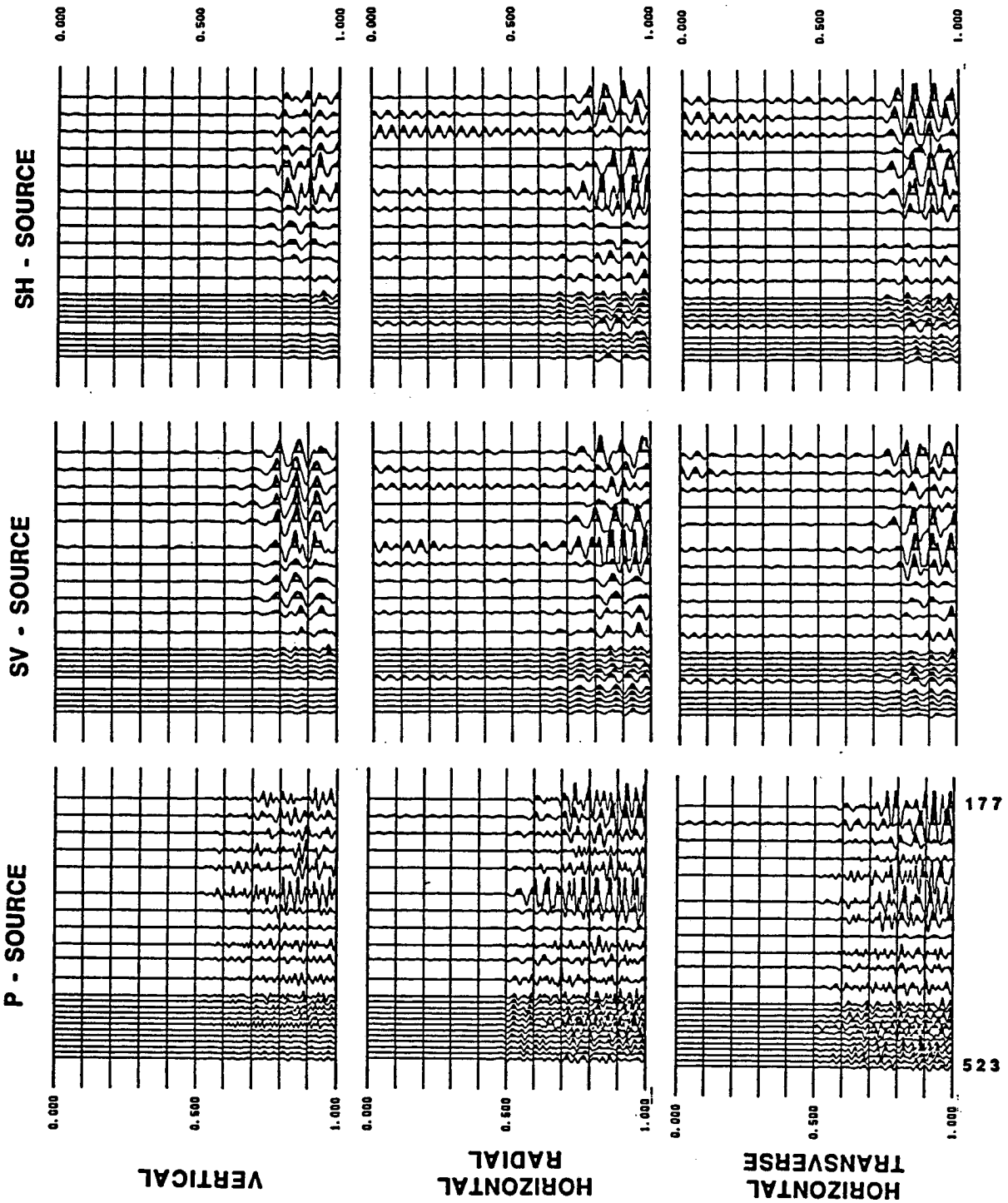

Figure 3 9-component VSP data set from site 8 (686 m offset). Data traces are normalized to a constant value, giving true relative amplitudes. The minimum and maximum depths of recording in meters are indicated in the lower left.

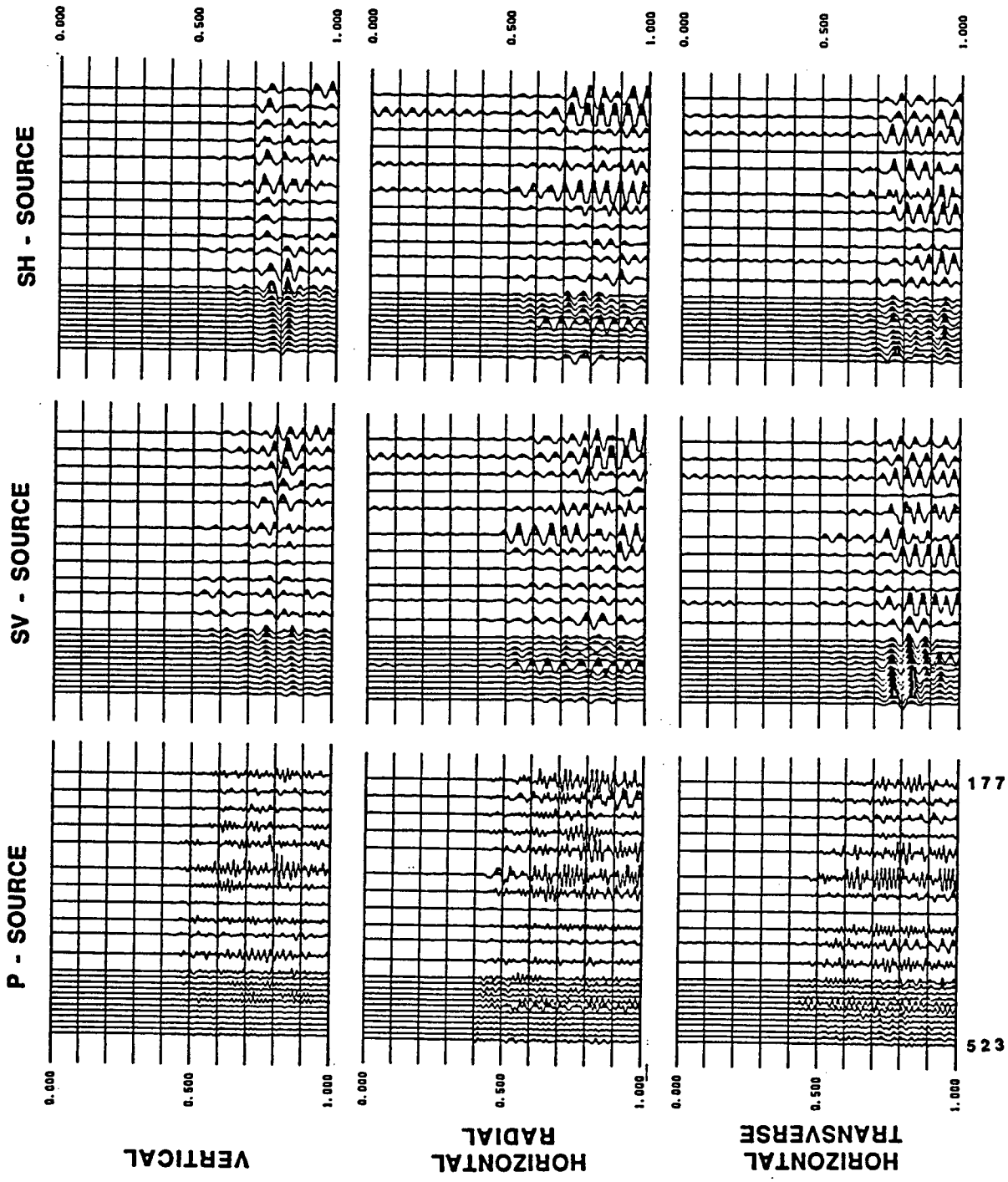

Figure 4 9-component VSP data set from site 14 (686 m offset). Data traces are normalized to a constant value, giving true relative amplitudes. The minimum and maximum depths of recording in meters are indicated in the lower left.

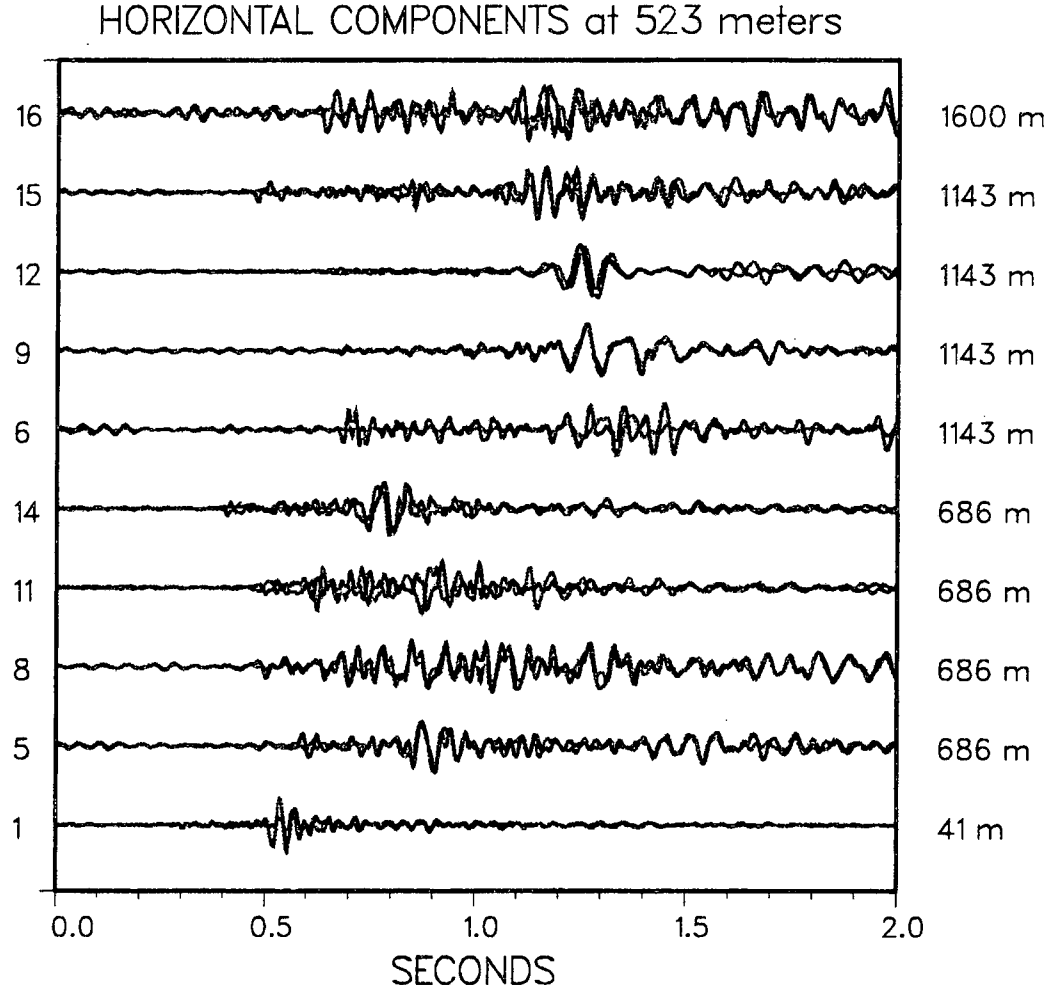

Figure 5 Horizontal component data traces for a receiver at 523 m depth and sources at each site. The VSP source location number is indicated on the left and the receiver offset to the right of the figure. The radial component is plotted in red and the transverse component is plotted in blue. The traces shown are a sum of data from all three sources (P, SV and SH). Note the large variation is frequency content and waveform character between sites.

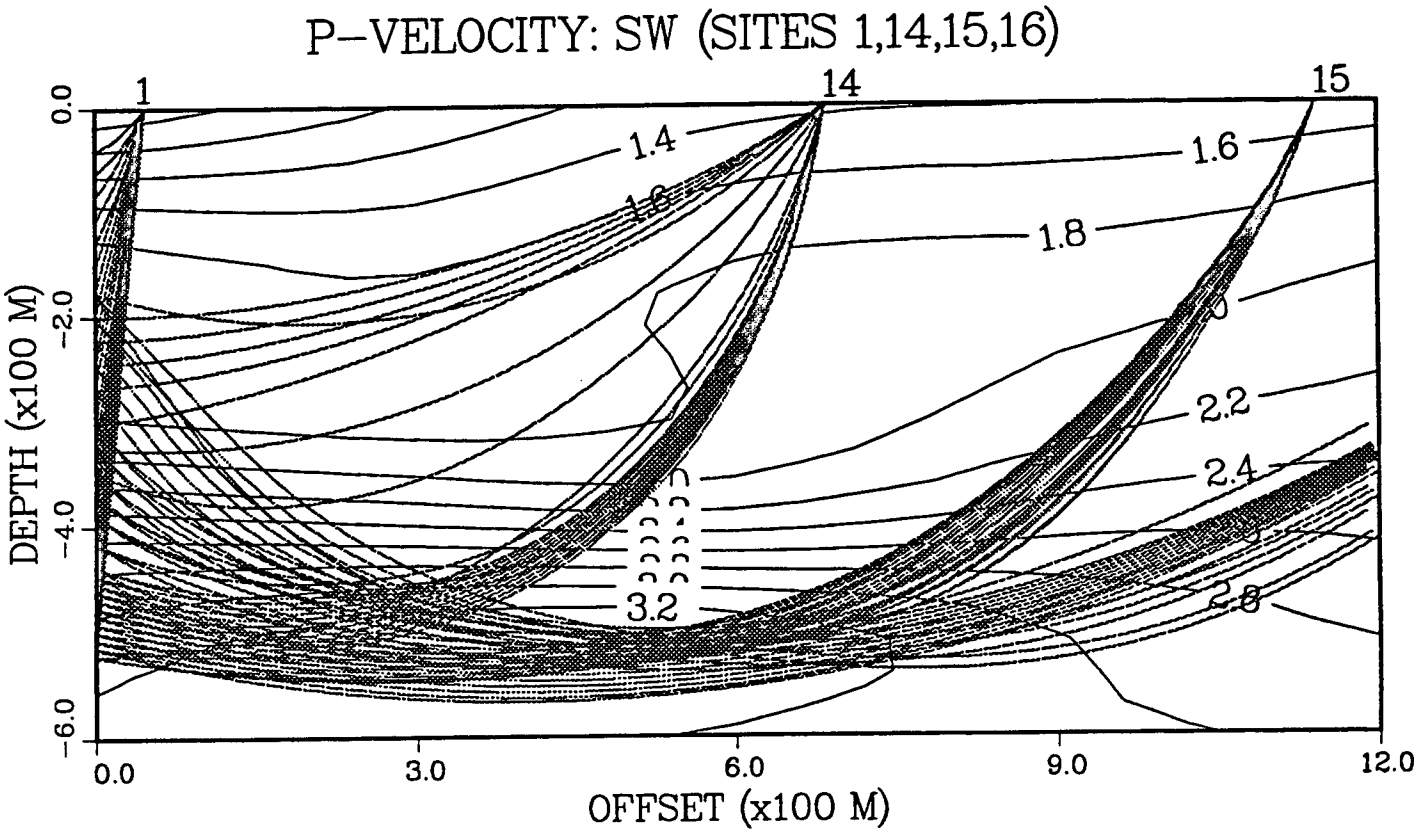

Figure 6 P-wave velocity inversion for the southwest cross-section with raypaths shown. The well is located at zero offset, and VSP site numbers are indicated at the top of the figure. Additional cross-sections are shown in appendix 1.

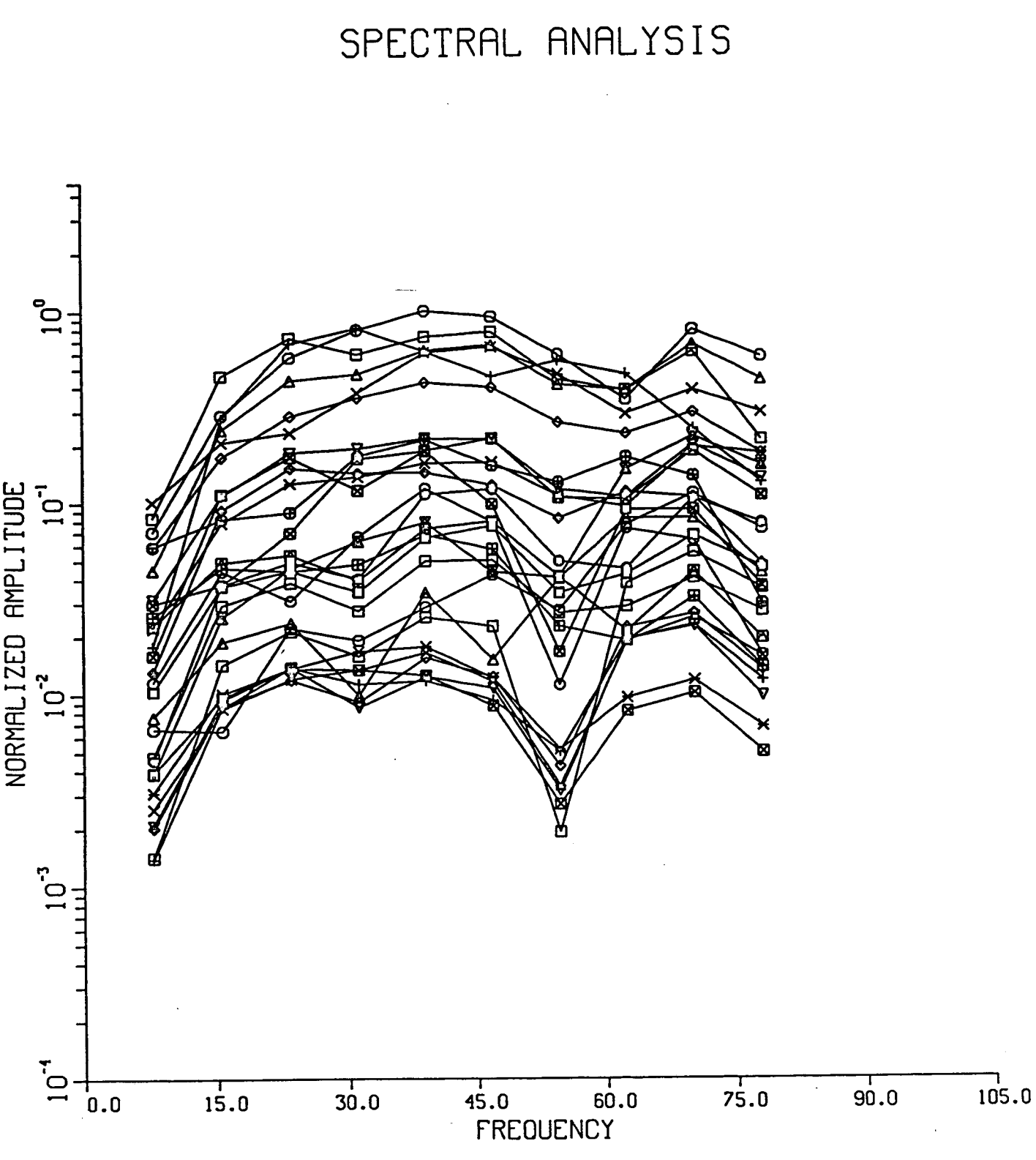

Figure 7 P-wave spectral amplitude. Each line is the spectrum for a different depth of the VSP receiver. The spectra were computed for a short time window (about 70 ms) around the first P-wave arrival on the vertical component for the P-wave source at site 1.

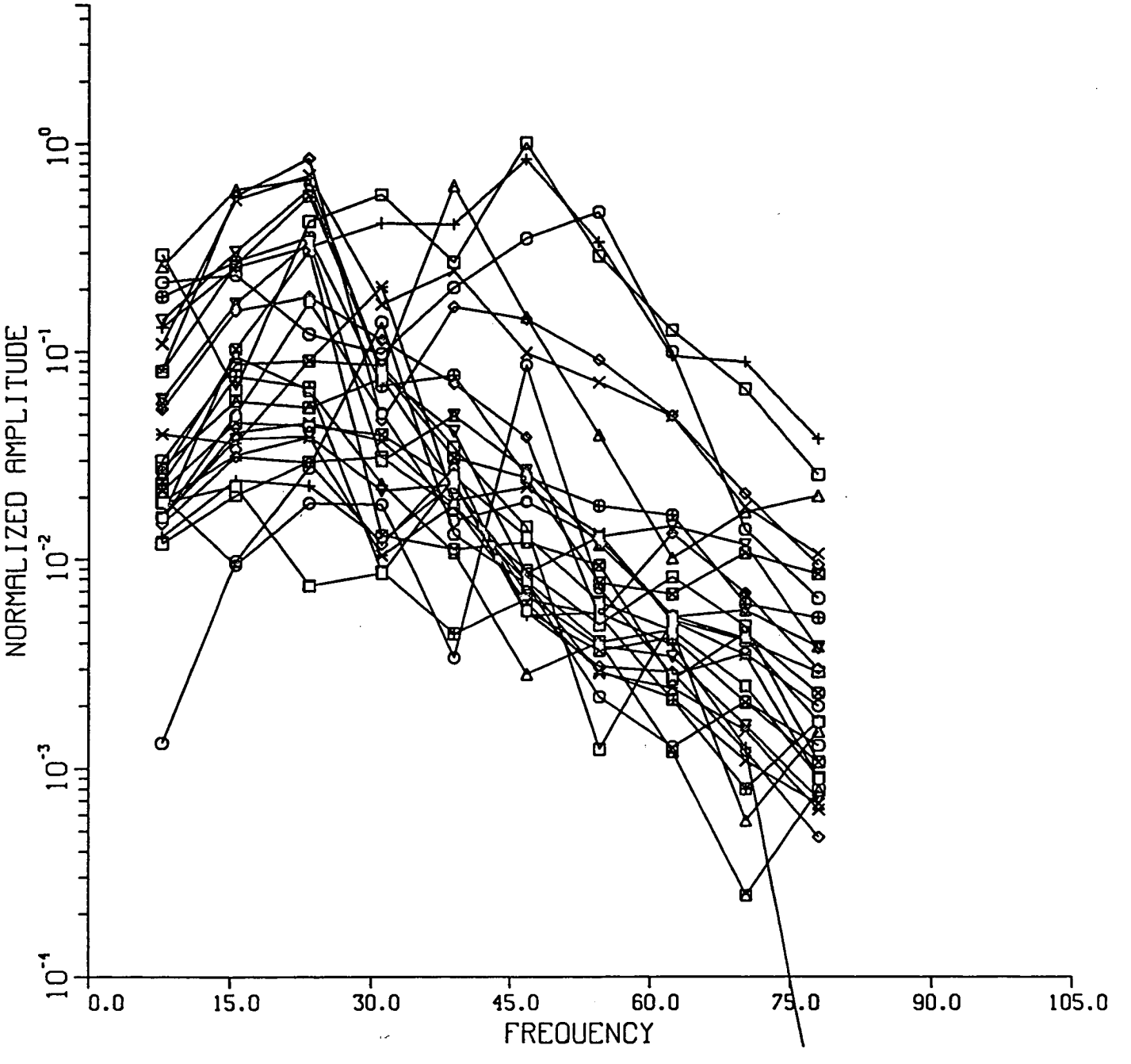

Figure 8 S-wave spectral amplitude. Each line is the spectrum for a different depth of the VSP receiver. The spectra were computed for a short time window (about 70 ms) around the first S-wave arrival on the horizontal-transverse component for the SH-source at site 1.

APPENDIX 1

OSSY '91 P & S Velocity Cross-sections

This appendix contains plots of P and S velocity inversion results along the northwest-southeast (NW-SE), southwest (SW), and east (E) source-receiver azimuths. The velocity values are color-coded and contoured. The degree to which the inverted velocities are resolved by the travel time inversion is reflected in the resolving width (RW), which is indicated by the intensity of the color, as shown on the plot legends. Fainter colors correspond to relatively poorer resolution. The resolution is essentially controlled by the characteristics of ray coverage within the model. Resolution is best when we have a large number of crisscrossing rays. Recall that the node spacing of the models is 100 meters in the vertical direction and 300 meters in the horizontal direction. In the plots that follow both the resolution and velocity values are plotted on a finer grid following a cubic B-spline interpolation of nearby values at the inversion nodes. Though plots differ in their range of horizontal offset, the horizontal scale is kept the same

It is important to keep ray coverage and resolution in mind when interpreting the models. For example, initial velocity values at nodes are more apt be adjusted if there are a lot of nearby rays, and conversely if there are few or no rays. Therefore, the juxtaposition of a well-sampled and poorly-sampled node can create the artifact of lateral heterogeneity. This appears to be the case in some of the following plots where the high density of rays from VSP site 1 cause the velocity contours to peak near zero offset. Another artifact from poor ray coverage is an oscillation in the inversion solution, i.e., nearby velocity values which differ significantly. The S-wave velocity model along the southwest azimuth is probably an example of this, with a shallow 1.7 km/sec velocity anomaly near 8 km offset, underlain by an 0.6 km/sec anomaly near 3 km offset.

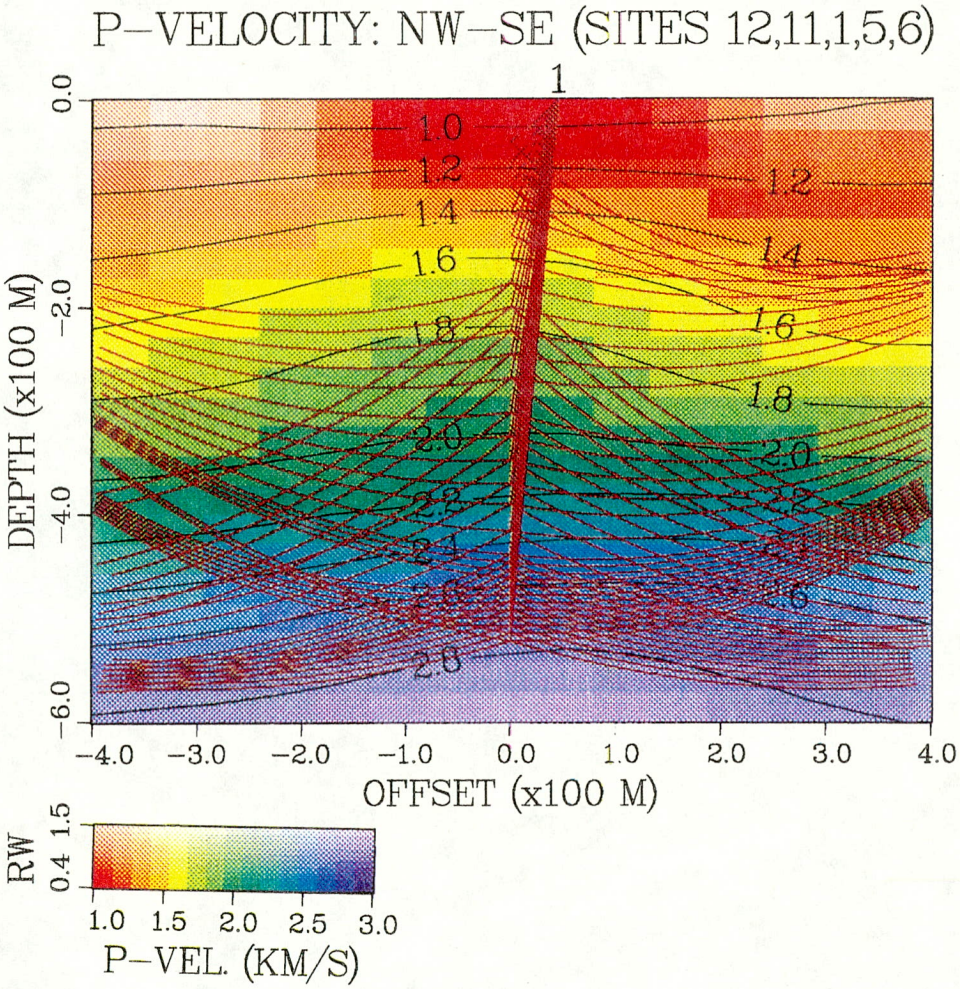
P–VELOCITY: NW–SE (SITES 12,11,1,5,6)
1
DEPTH (x100 M)
0.0
−2.0
−4.0
−6.0
1.0
1.2
1.4
1.6
1.8
2.0
2.2
2.4
2.6
2.8
−4.0 −3.0 −2.0 −1.0 0.0 1.0 2.0 3.0 4.0
OFFSET (x100 M)
RW
0.4 1.5
1.0 1.5 2.0 2.5 3.0
P–VEL. (KM/S)

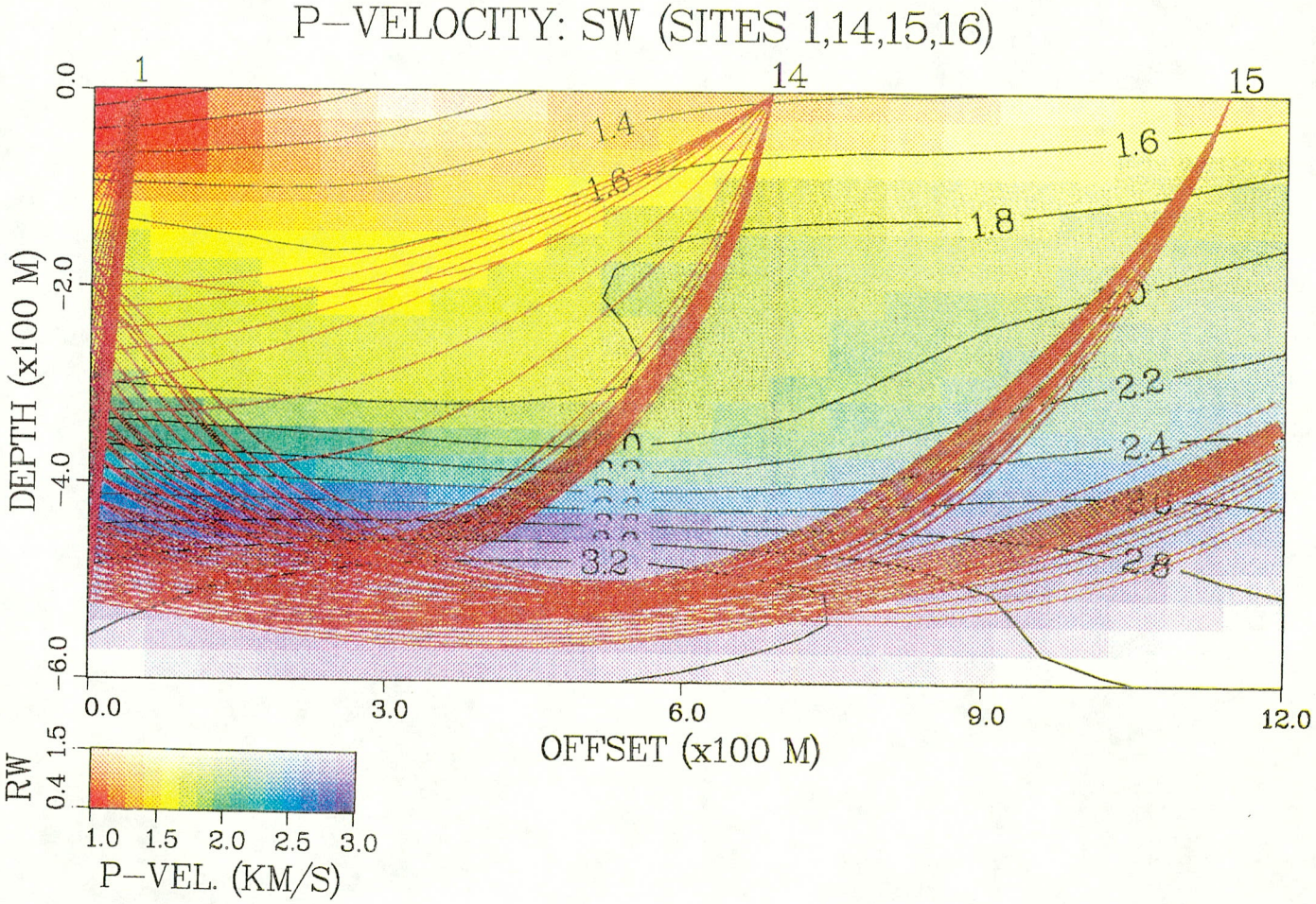
P–VELOCITY: SW (SITES 1,14,15,16)
1
14
15
0.0
-2.0
-4.0
-6.0
DEPTH (x100 M)
1.4
1.6
1.8
2.2
2.4
2.8
3.2
0.0
3.0
6.0
9.0
12.0
OFFSET (x100 M)
RW
0.4 1.5
1.0 1.5 2.0 2.5 3.0
P–VEL. (KM/S)

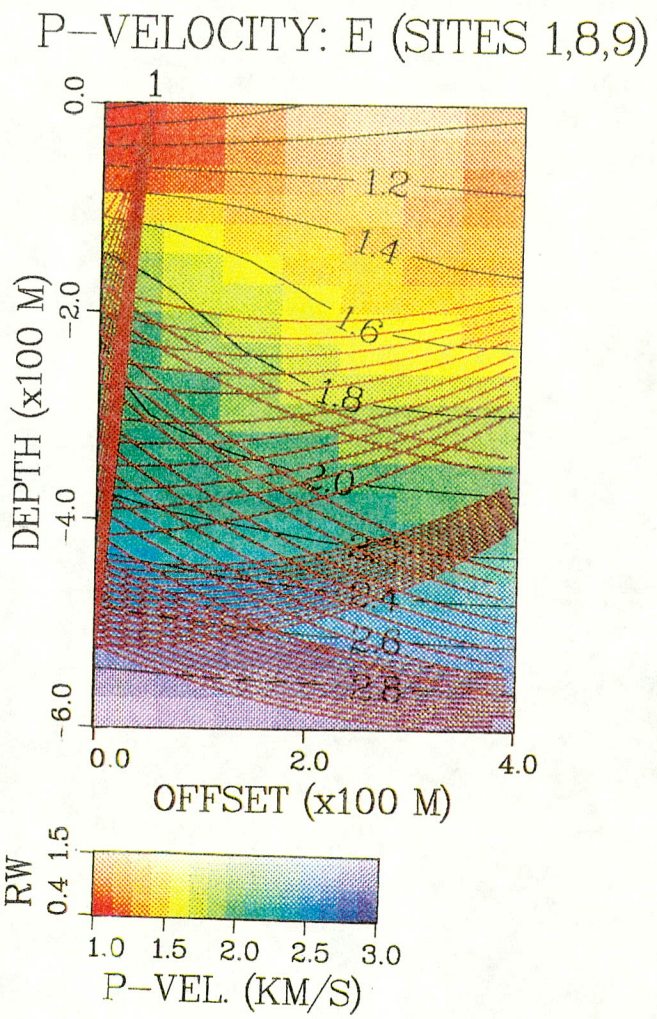
P–VELOCITY: E (SITES 1,8,9)
1
1.2
1.4
1.6
1.8
2.0
2.4
2.6
2.8
0.0
-2.0
-4.0
-6.0
DEPTH (x100 M)
0.0
2.0
4.0
OFFSET (x100 M)
RW
0.4 1.5
1.0 1.5 2.0 2.5 3.0
P–VEL. (KM/S)

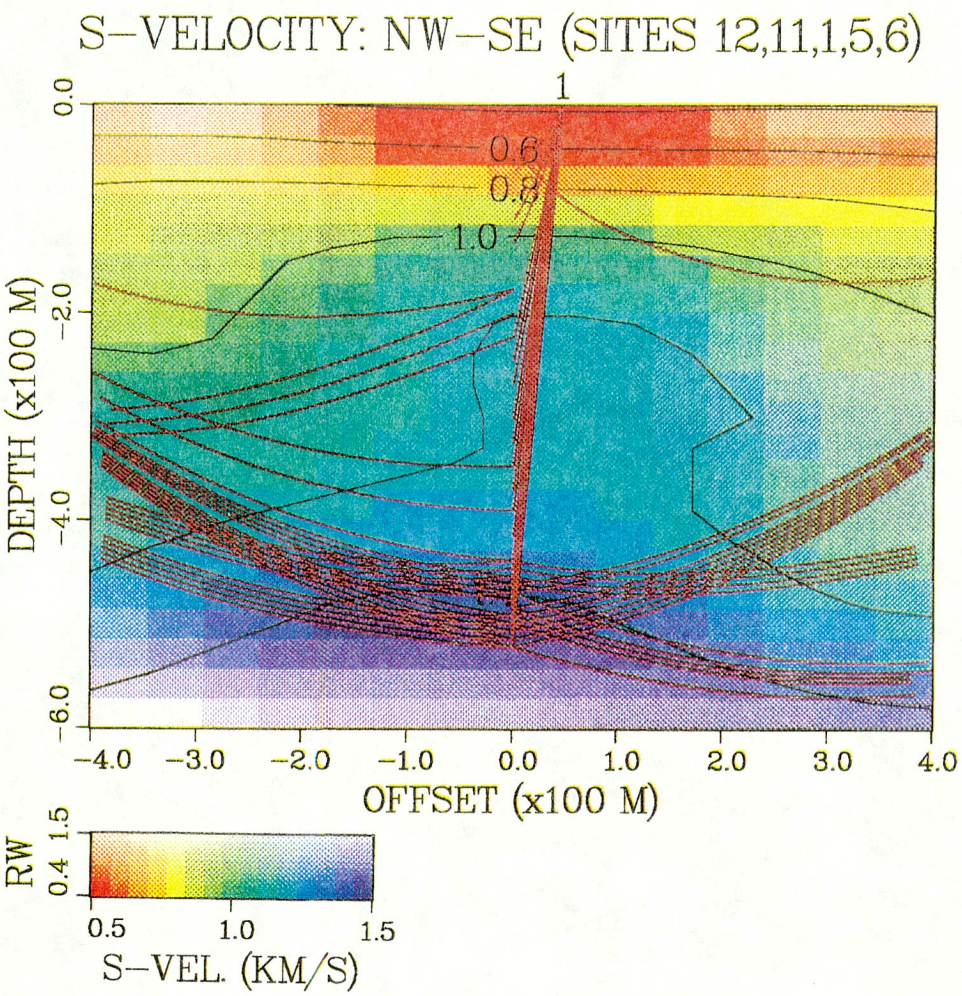
S–VELOCITY: NW–SE (SITES 12,11,1,5,6)
1
0.6
0.8
1.0
0.0
−2.0
−4.0
−6.0
DEPTH (x100 M)
−4.0
−3.0
−2.0
−1.0
0.0
1.0
2.0
3.0
4.0
OFFSET (x100 M)
RW
0.4
1.5
0.5
1.0
1.5
S–VEL. (KM/S)

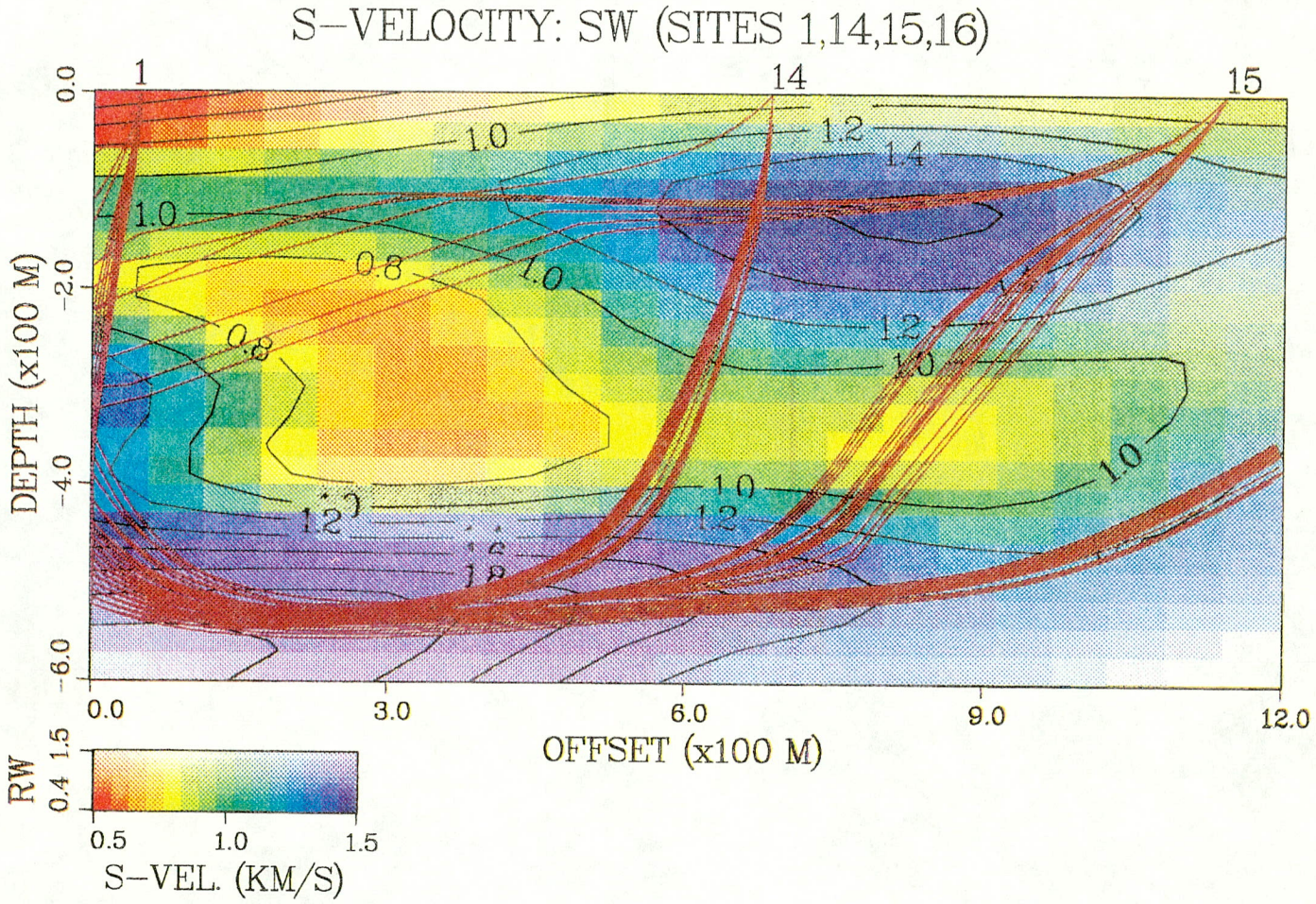
S–VELOCITY: SW (SITES 1,14,15,16)
1
14
15
0.0
-2.0
-4.0
-6.0
DEPTH (x100 M)
1.0
1.2
1.4
0.8
1.0
1.2
1.0
0.8
1.0
1.2
1.0
1.2
1.0
0.0
3.0
6.0
9.0
12.0
OFFSET (x100 M)
RW
0.4 1.5
0.5
1.0
1.5
S–VEL. (KM/S)

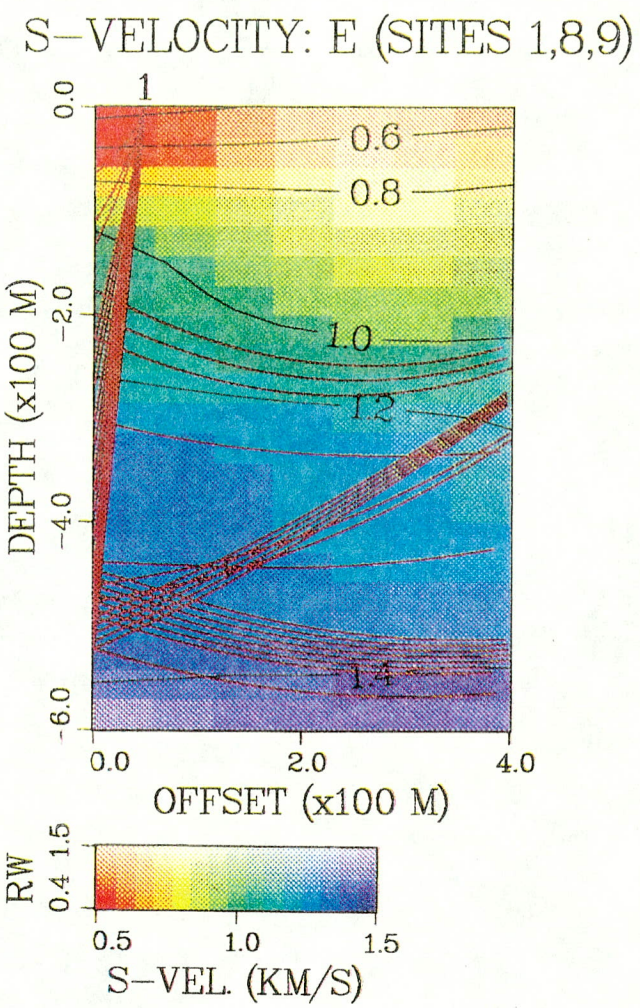
S–VELOCITY: E (SITES 1,8,9)
1
0.0
-2.0
-4.0
-6.0
DEPTH (x100 M)
0.6
0.8
1.0
1.2
1.4
0.0
2.0
4.0
OFFSET (x100 M)
RW
0.4 1.5
0.5
1.0
1.5
S–VEL. (KM/S)

APPENDIX 2

OSSY '91 Normalized 9-component VSP Recordings from all Source Locations

This appendix displays the OSSY '91 data set in its entirety. Three-component record sections from P-, SV-, and SH-vibrator sources are plotted for each source location. The data shown have been rotated into a horizontal-radial and horizontal-transverse receiver coordinate system, as described in the text. The plots are ordered by increasing VSP source location number. The receiver depth in feet is indicated next to each data trace. To compensate for the variable signal-to-noise ratio (which varies with depth and source offset) and to more clearly display coherent arrivals, all waveforms are normalized by their maximum amplitude.

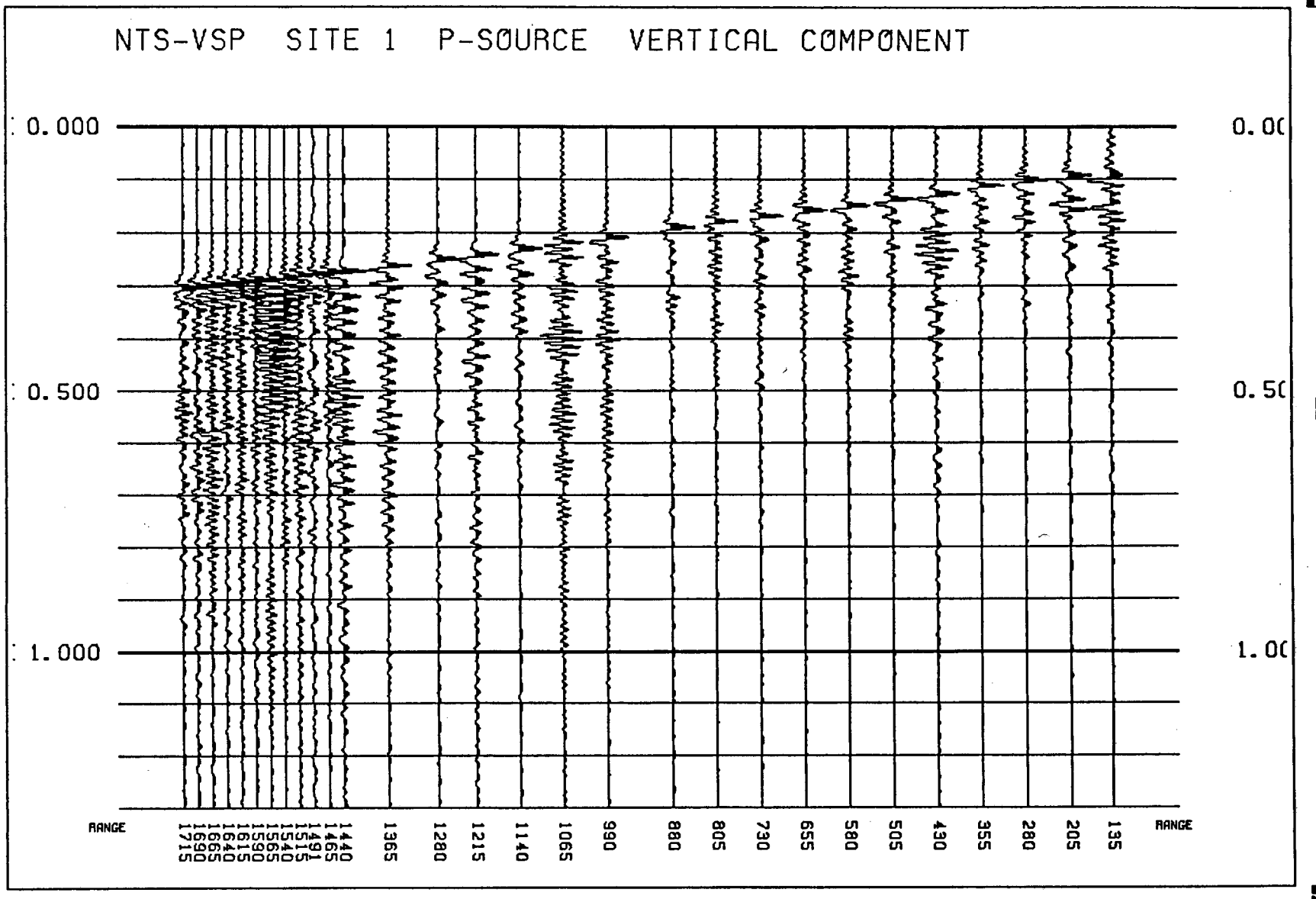

View File | Decimate
Stop | Redraw

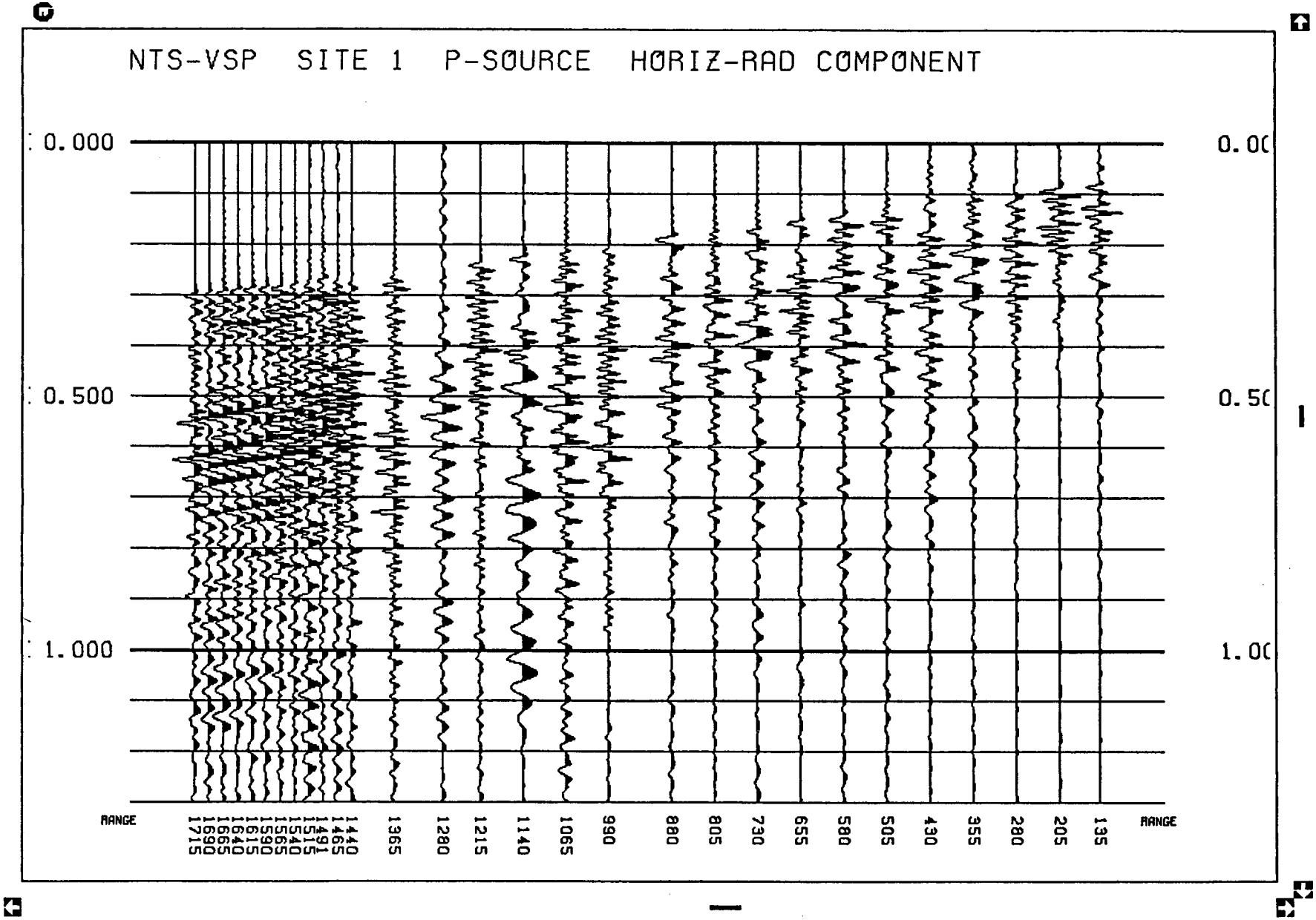

View File | Decimate

Stop | Redraw

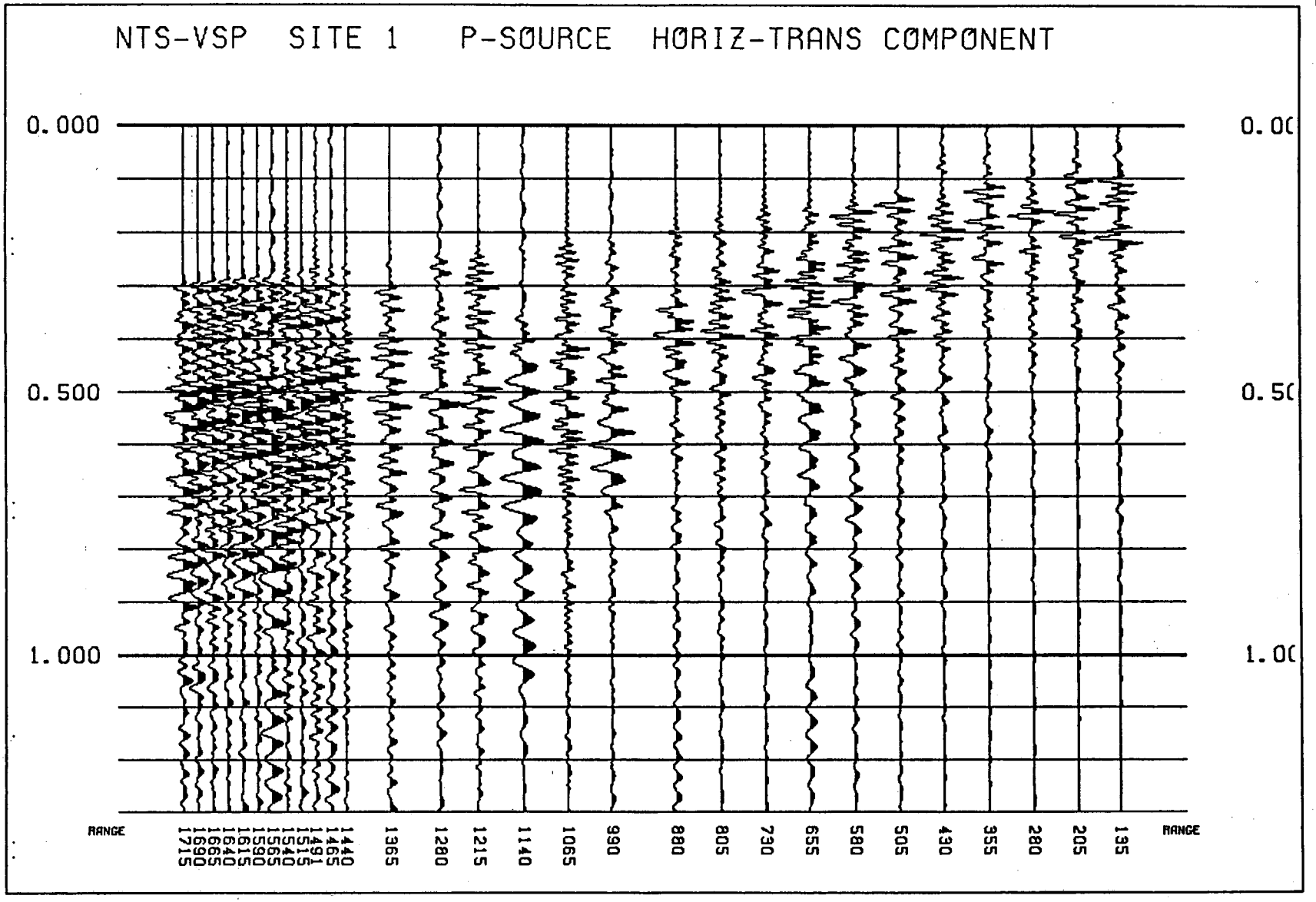

View File | Decimate

Stop | Redraw

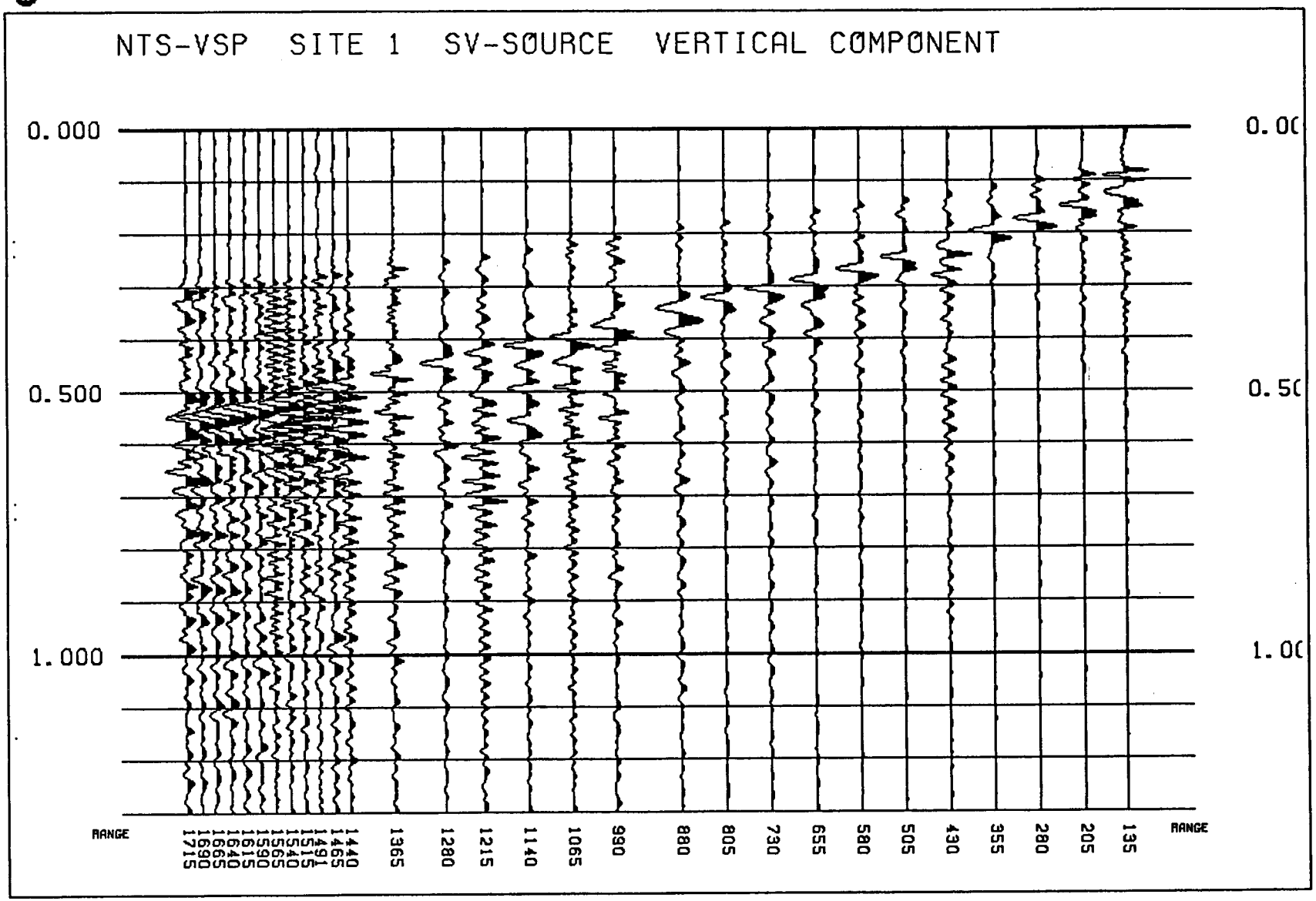

View File | Decimate

Stop | Redraw

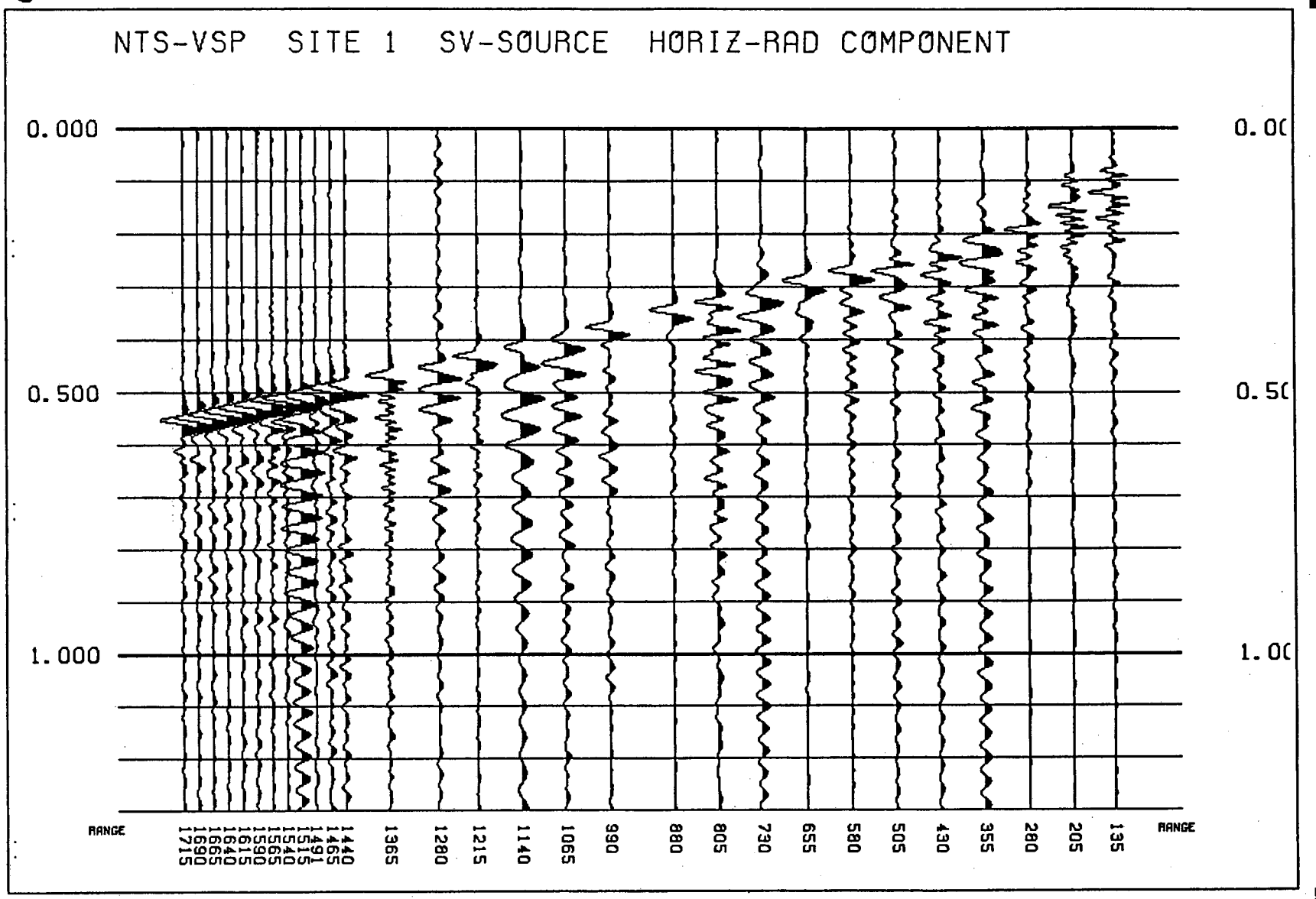

View File | Decimate

Stop | Redraw

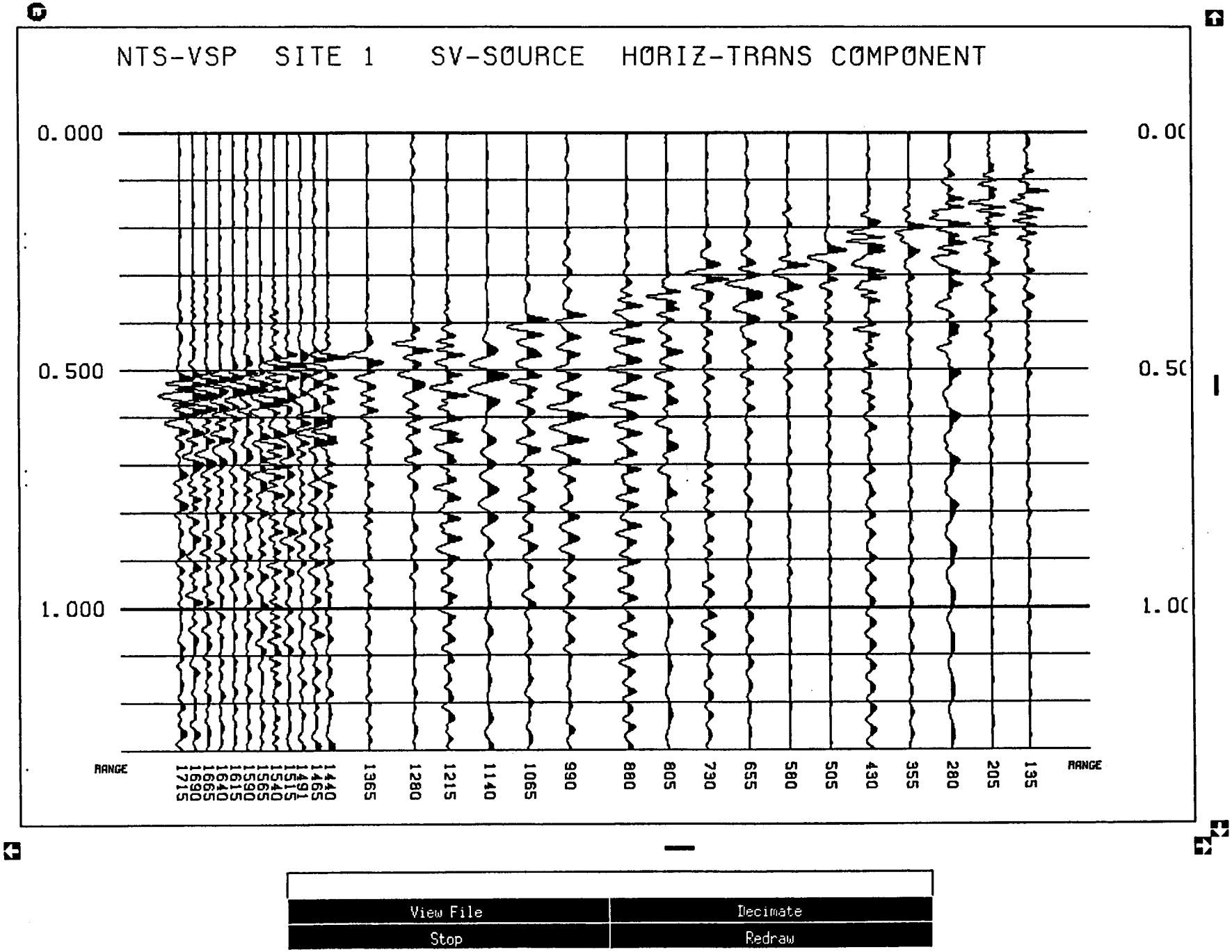

View File | Decimate

Stop | Redraw

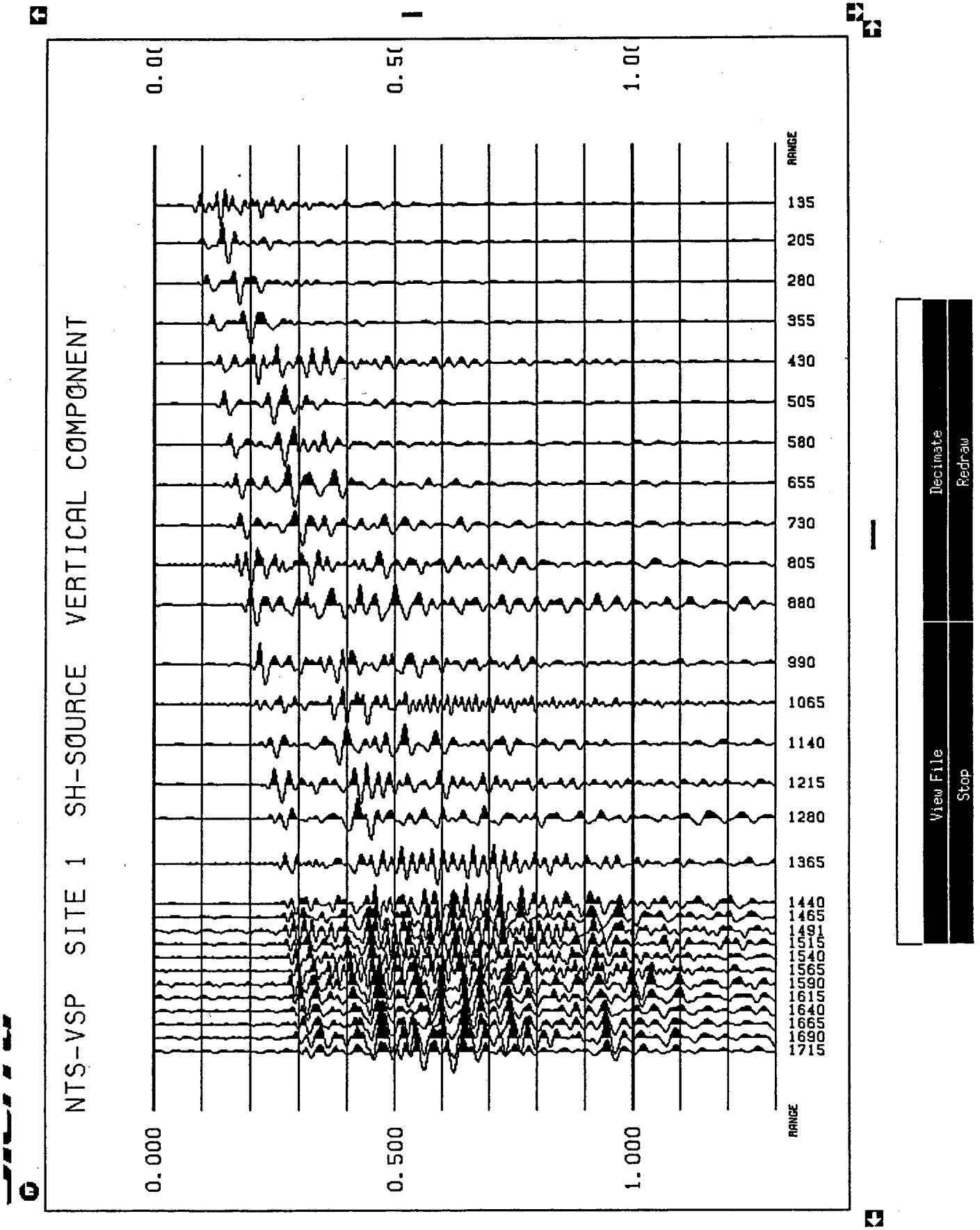
NTS-VSP SITE 1 SH-SOURCE VERTICAL COMPONENT
0.000
0.500
1.000
RANGE
135
205
280
355
430
505
580
655
730
805
880
990
1065
1140
1215
1280
1365
1440
1465
1491
1515
1540
1565
1590
1615
1640
1665
1690
1715
Decimate
Redraw
View File
Stop

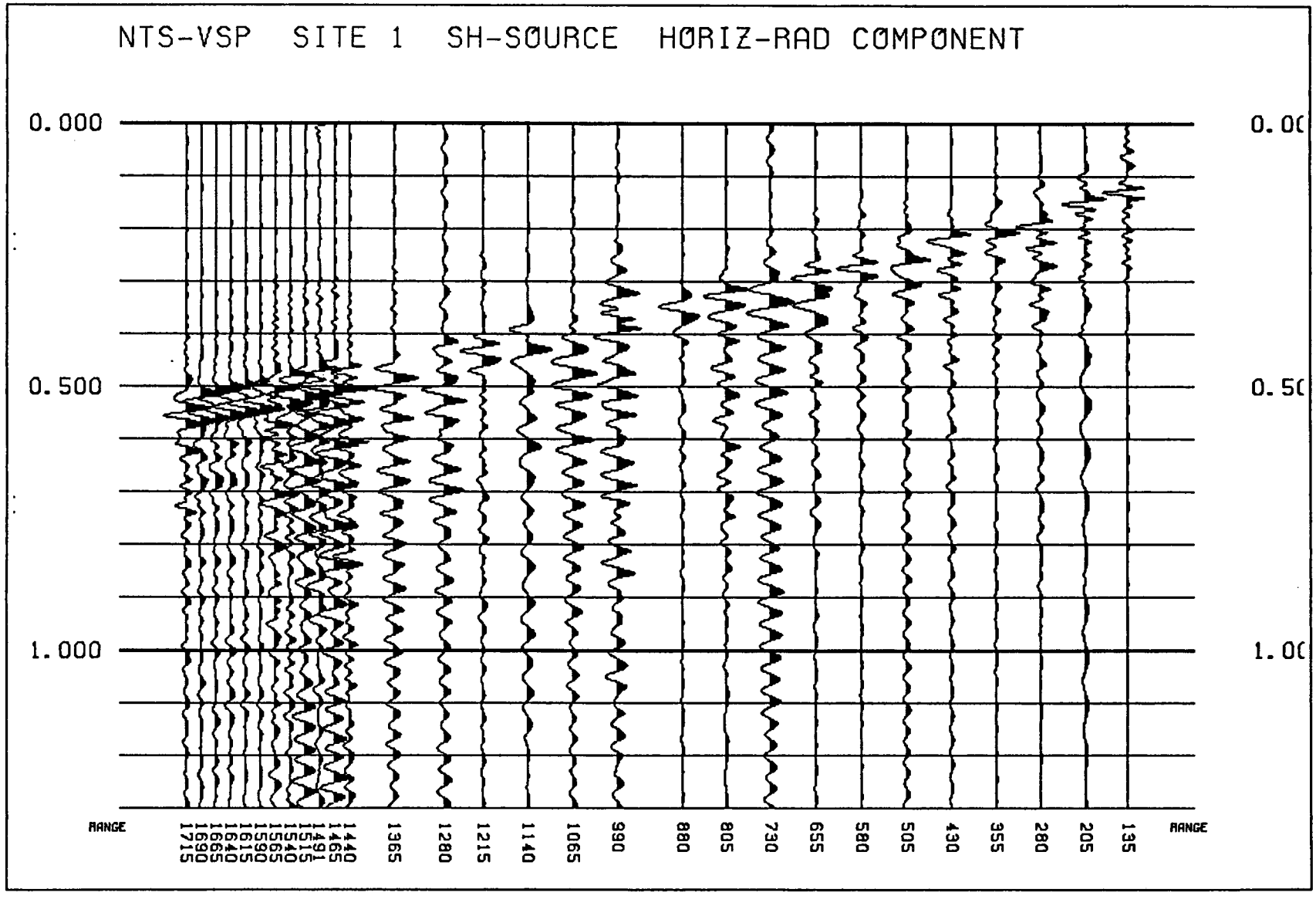

View File | Decimate

Stop | Redraw

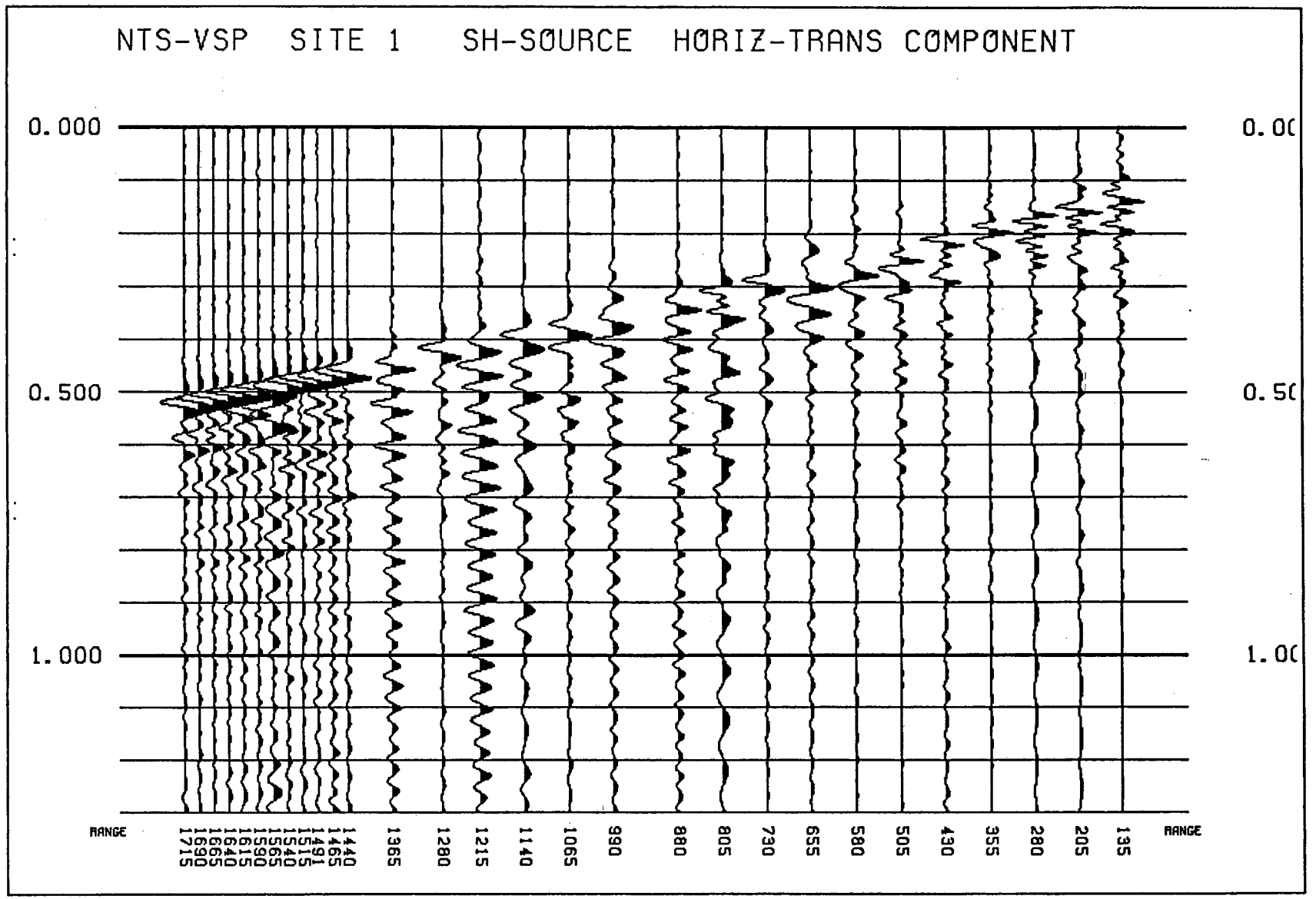

View File | Decimate

Stop | Redraw

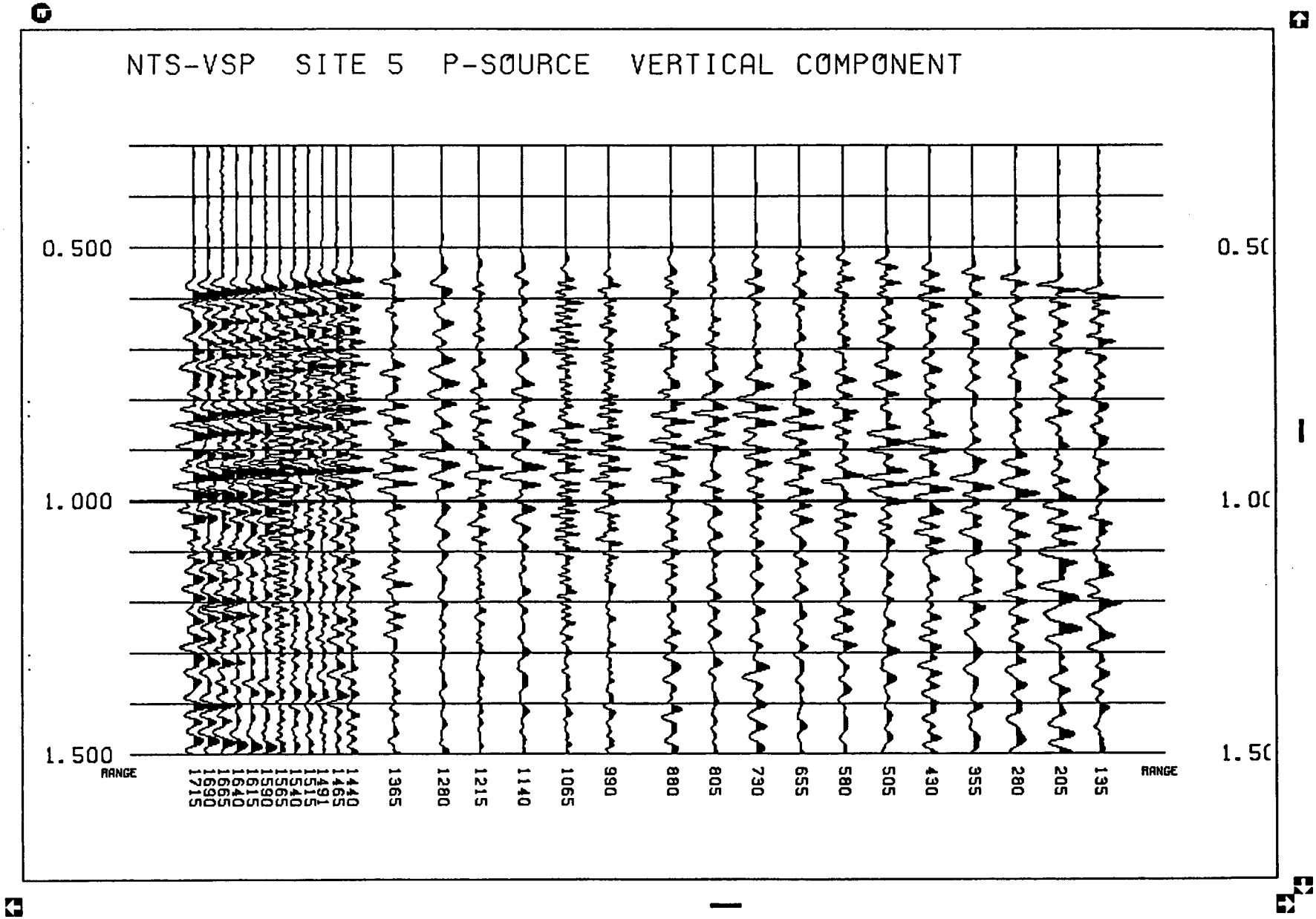
NTS-VSP SITE 5 P-SOURCE VERTICAL COMPONENT
0.500
1.000
1.500
0.5(
1.0(
1.5(
RANGE
1715
1690
1665
1640
1615
1590
1565
1540
1515
1491
1465
1440
1365
1280
1215
1140
1065
990
880
805
730
655
580
505
430
355
280
205
135
RANGE
View File
Decimate
Stop
Redraw

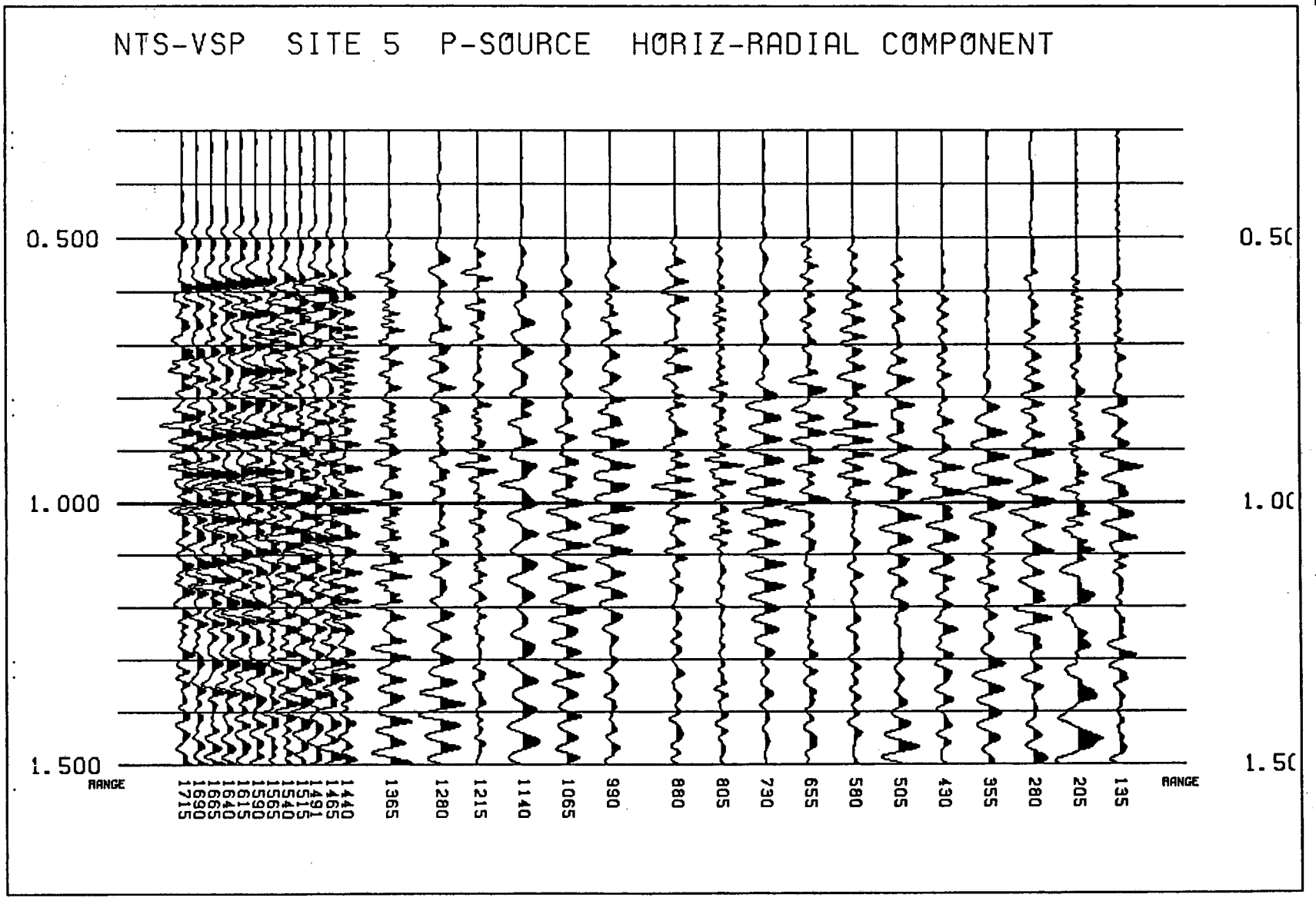

View File | Decimate

Stop | Redraw

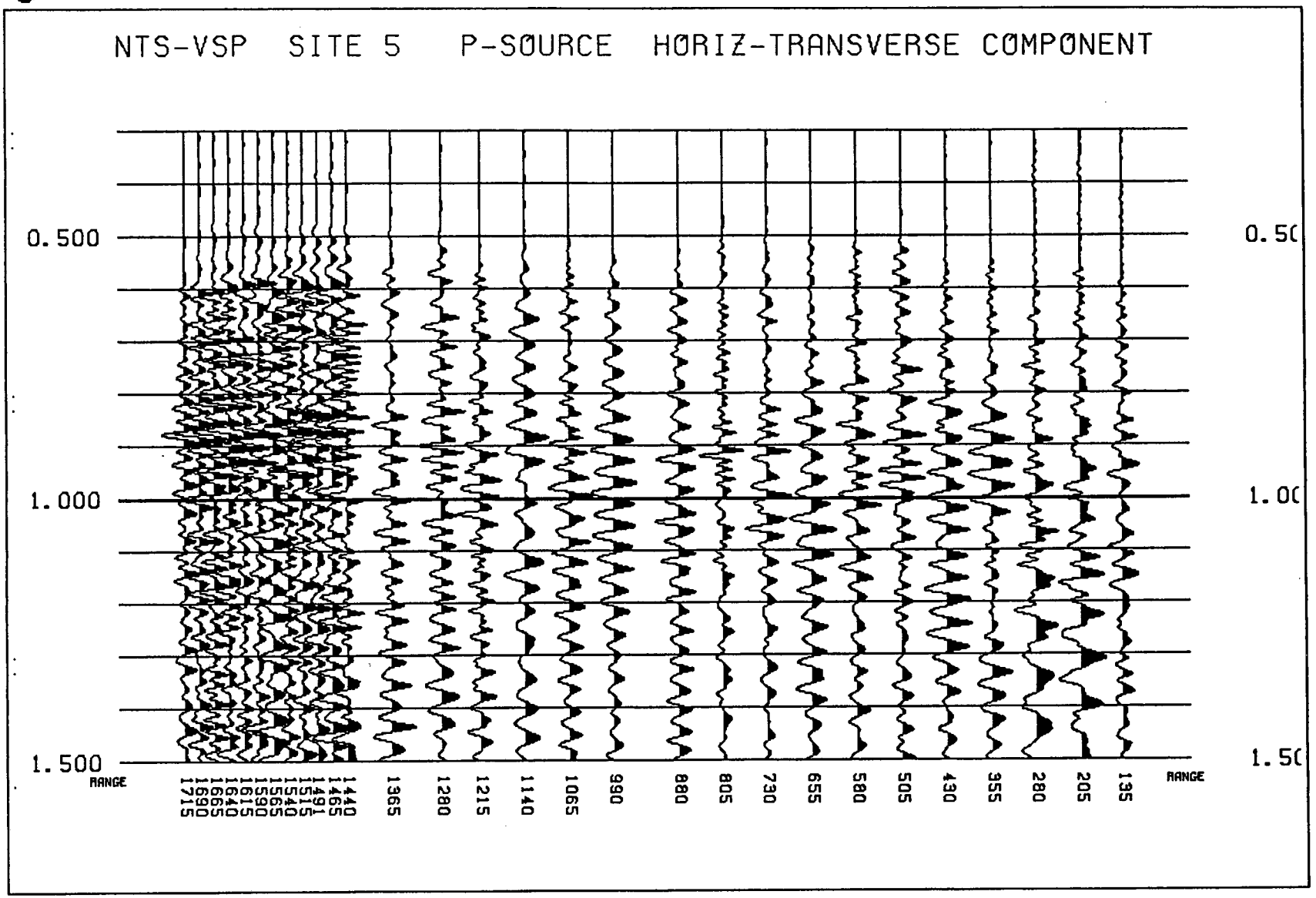
NTS-VSP SITE 5 P-SOURCE HORIZ-TRANSVERSE COMPONENT
0.500
1.000
1.500
RANGE
1715
1690
1665
1640
1615
1590
1565
1540
1515
1491
1465
1440
1365
1280
1215
1140
1065
990
880
805
730
655
580
505
430
355
280
205
135
RANGE
View File
Decimate
Stop
Redraw

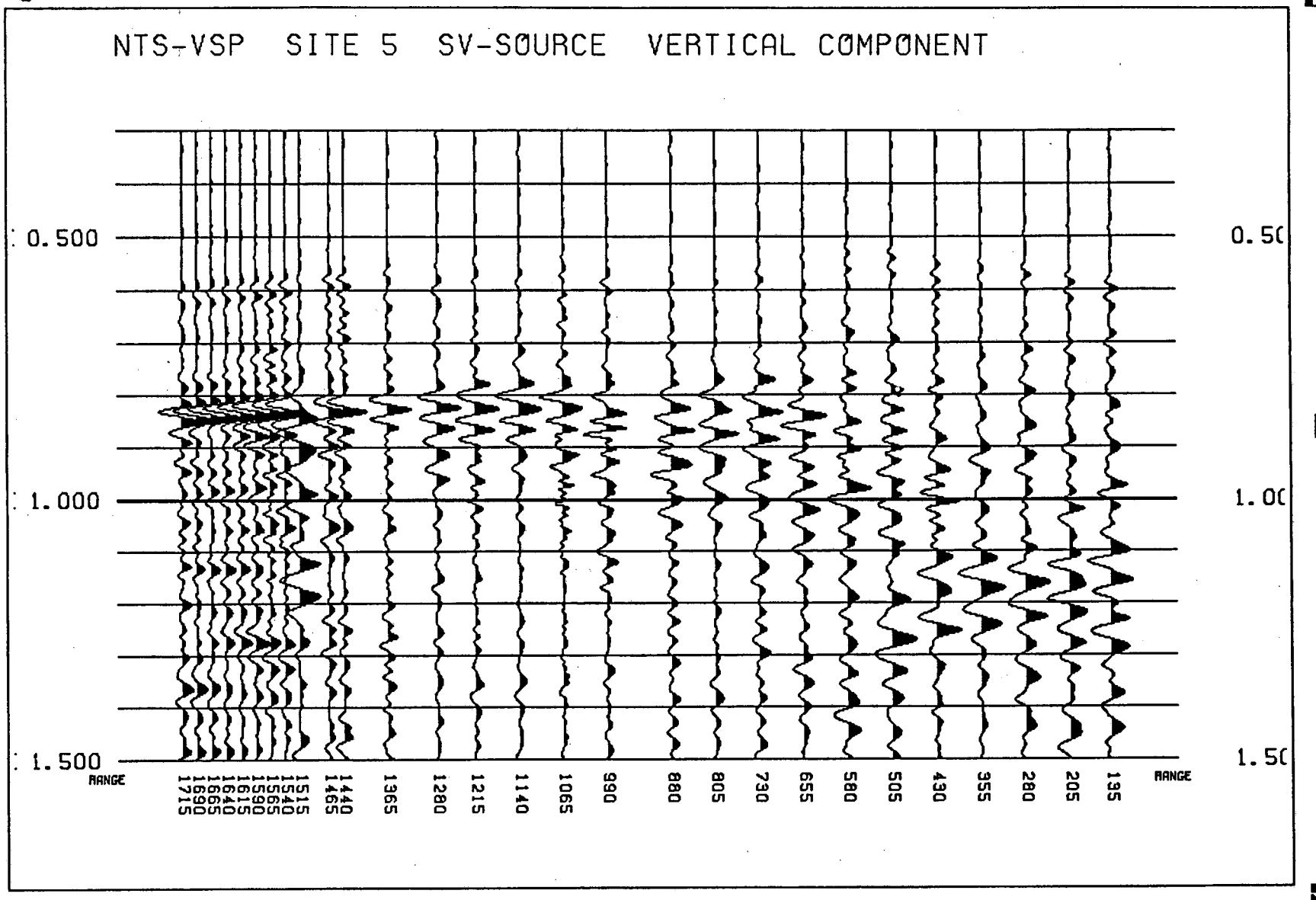

View File | Decimate

Stop | Redraw

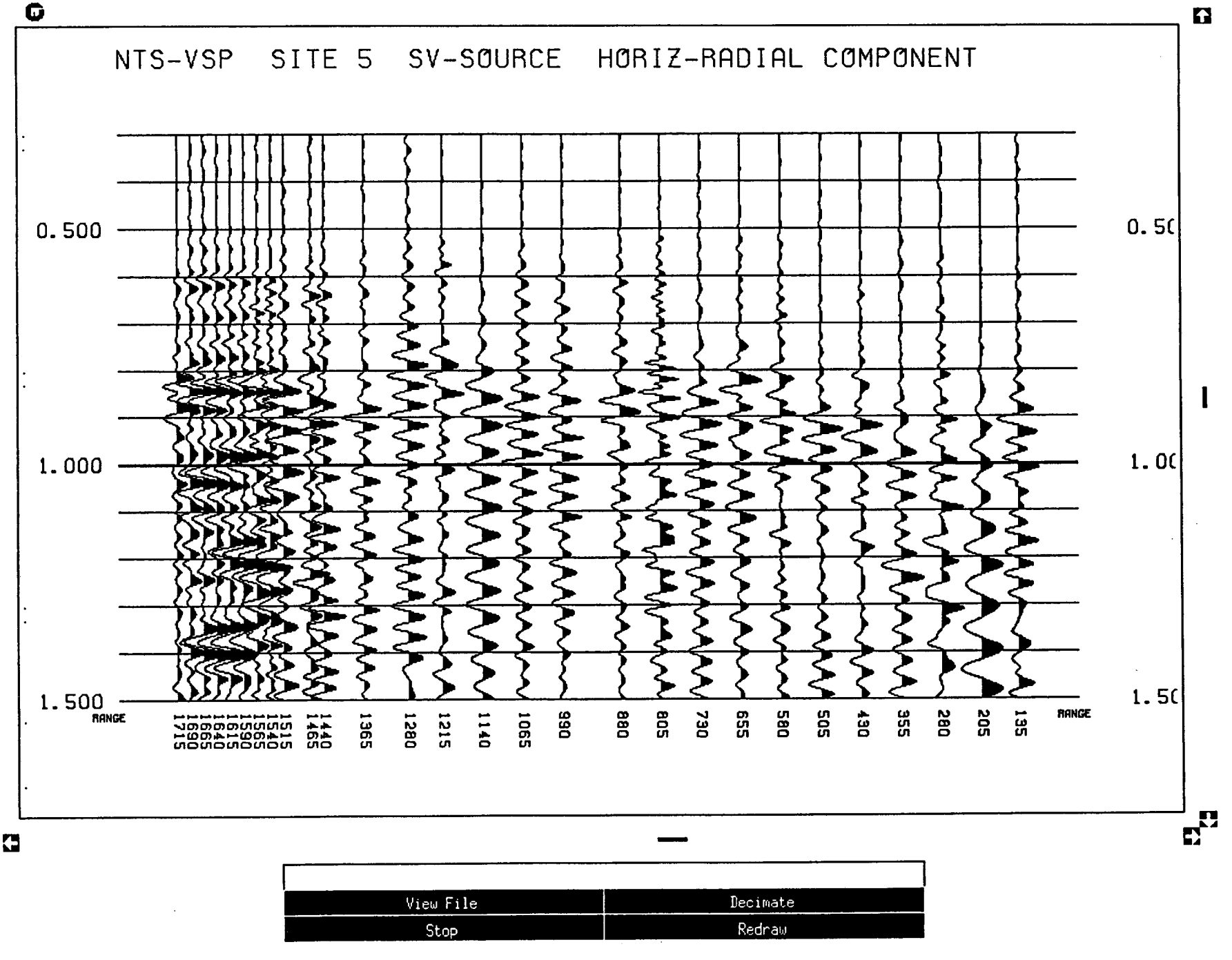
NTS-VSP SITE 5 SV-SOURCE HORIZ-RADIAL COMPONENT
0.500
1.000
1.500
RANGE
1715
1690
1665
1640
1615
1590
1565
1540
1515
1465
1440
1365
1280
1215
1140
1065
990
880
805
730
655
580
505
430
355
280
205
135
RANGE
View File
Decimate
Stop
Redraw

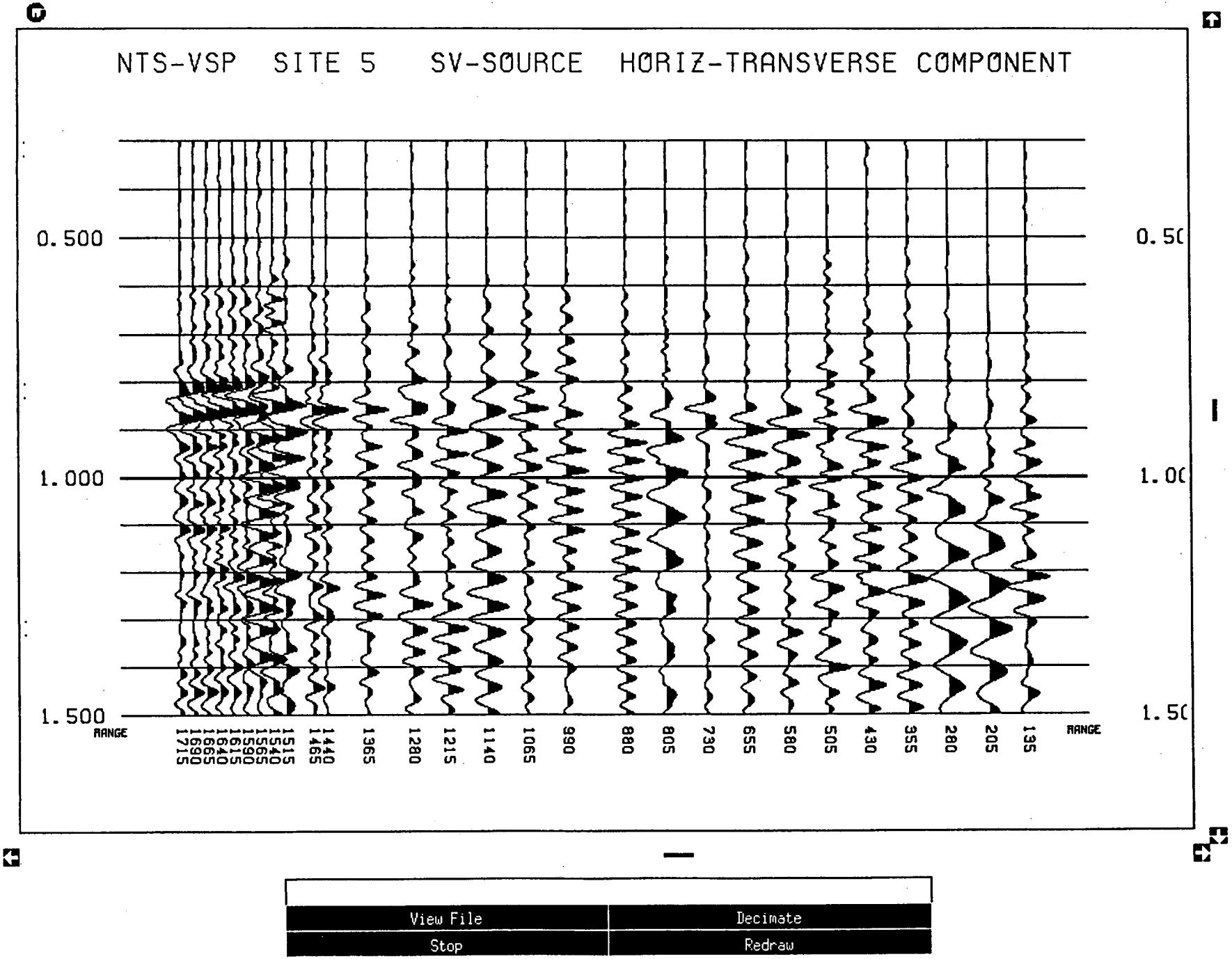
NTS-VSP SITE 5 SV-SOURCE HORIZ-TRANSVERSE COMPONENT
0.500
1.000
1.500
RANGE
1715
1690
1665
1640
1615
1590
1565
1540
1515
1465
1440
1365
1280
1215
1140
1065
990
880
805
730
655
580
505
430
355
280
205
135
RANGE
View File
Decimate
Stop
Redraw

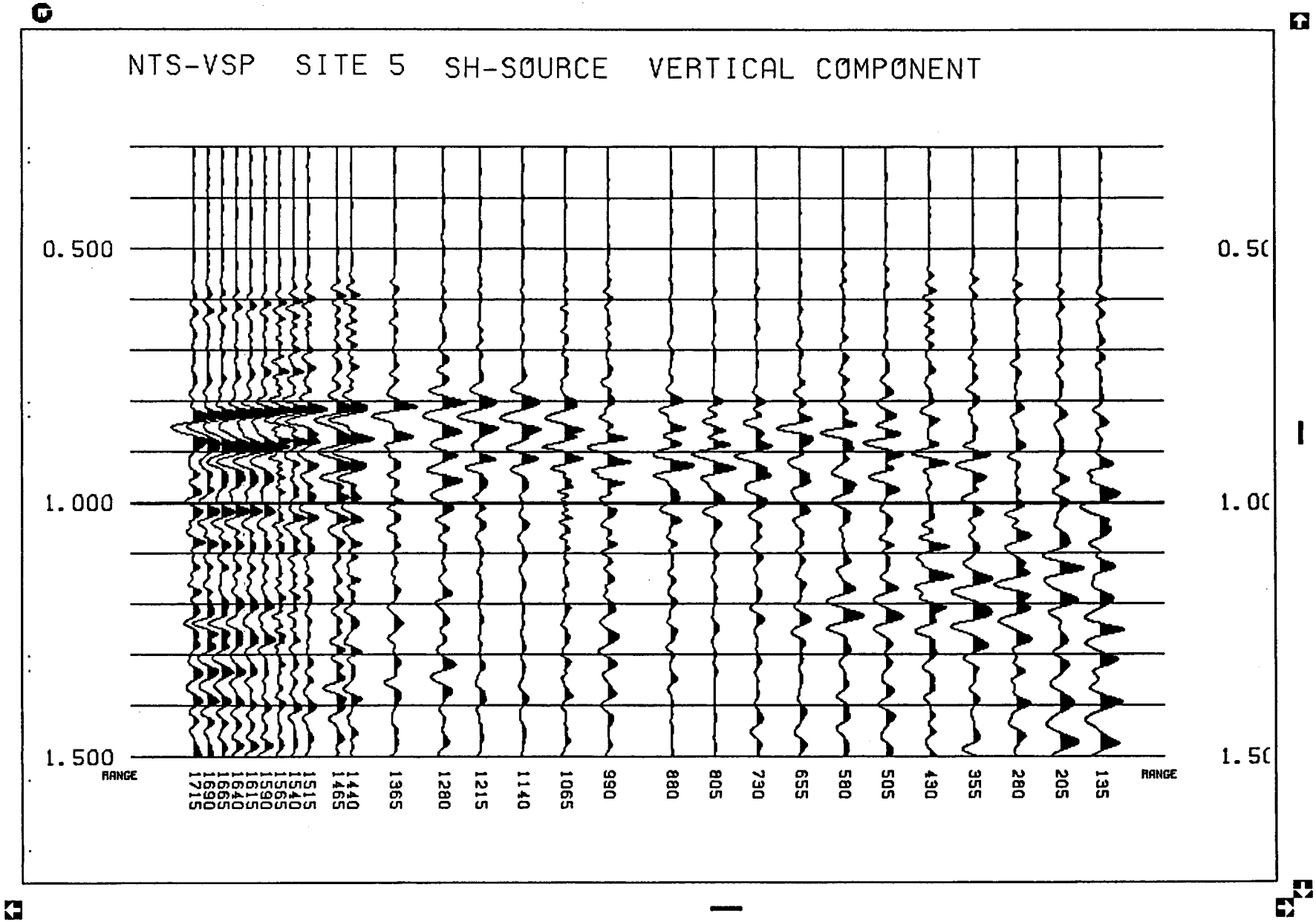
NTS-VSP SITE 5 SH-SOURCE VERTICAL COMPONENT
0.500
1.000
1.500
RANGE
1715
1690
1665
1640
1615
1590
1565
1540
1515
1465
1440
1365
1280
1215
1140
1065
990
880
805
730
655
580
505
430
355
280
205
135
RANGE
View File
Decimate
Stop
Redraw

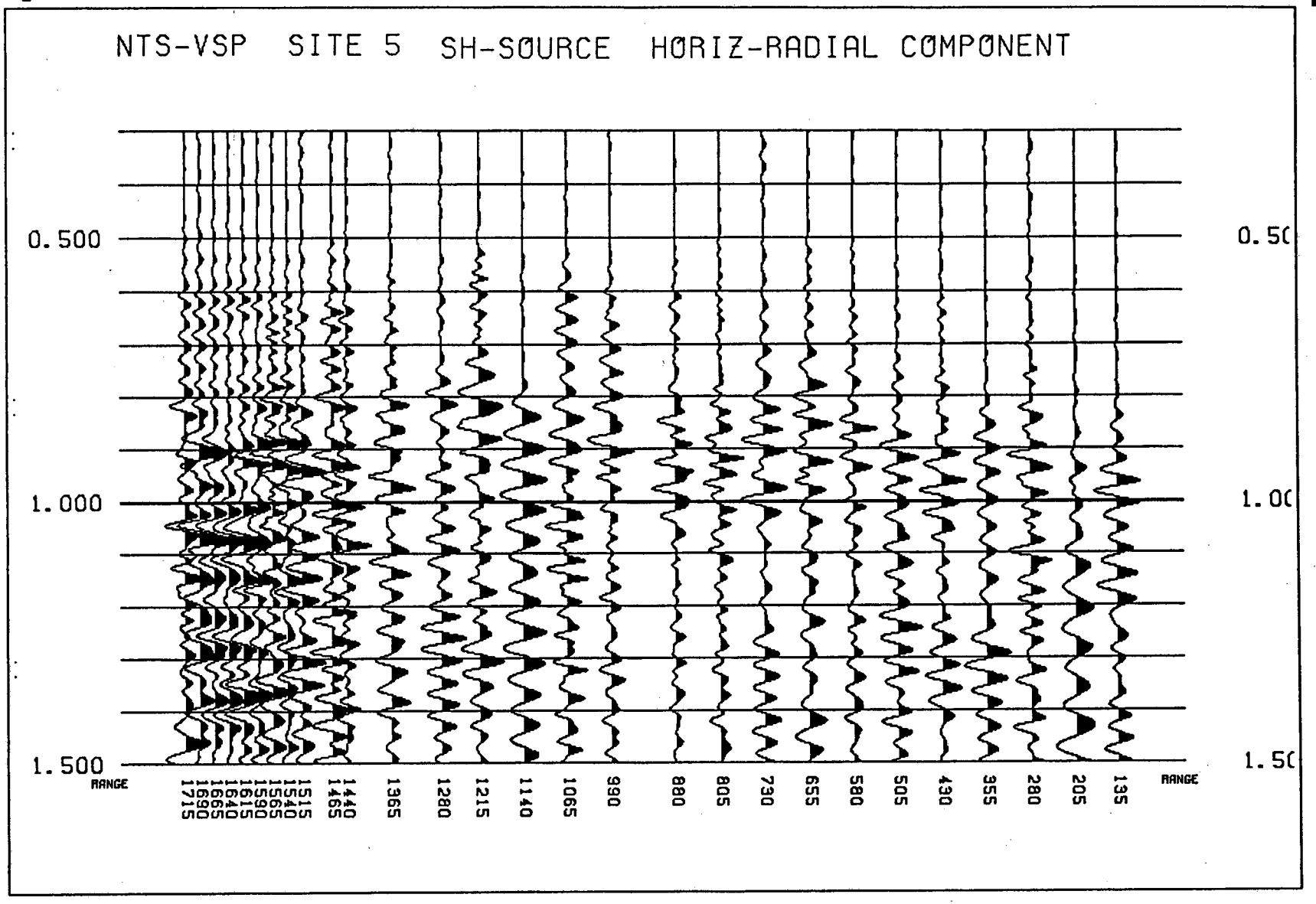

View File | Decimate

Stop | Redraw

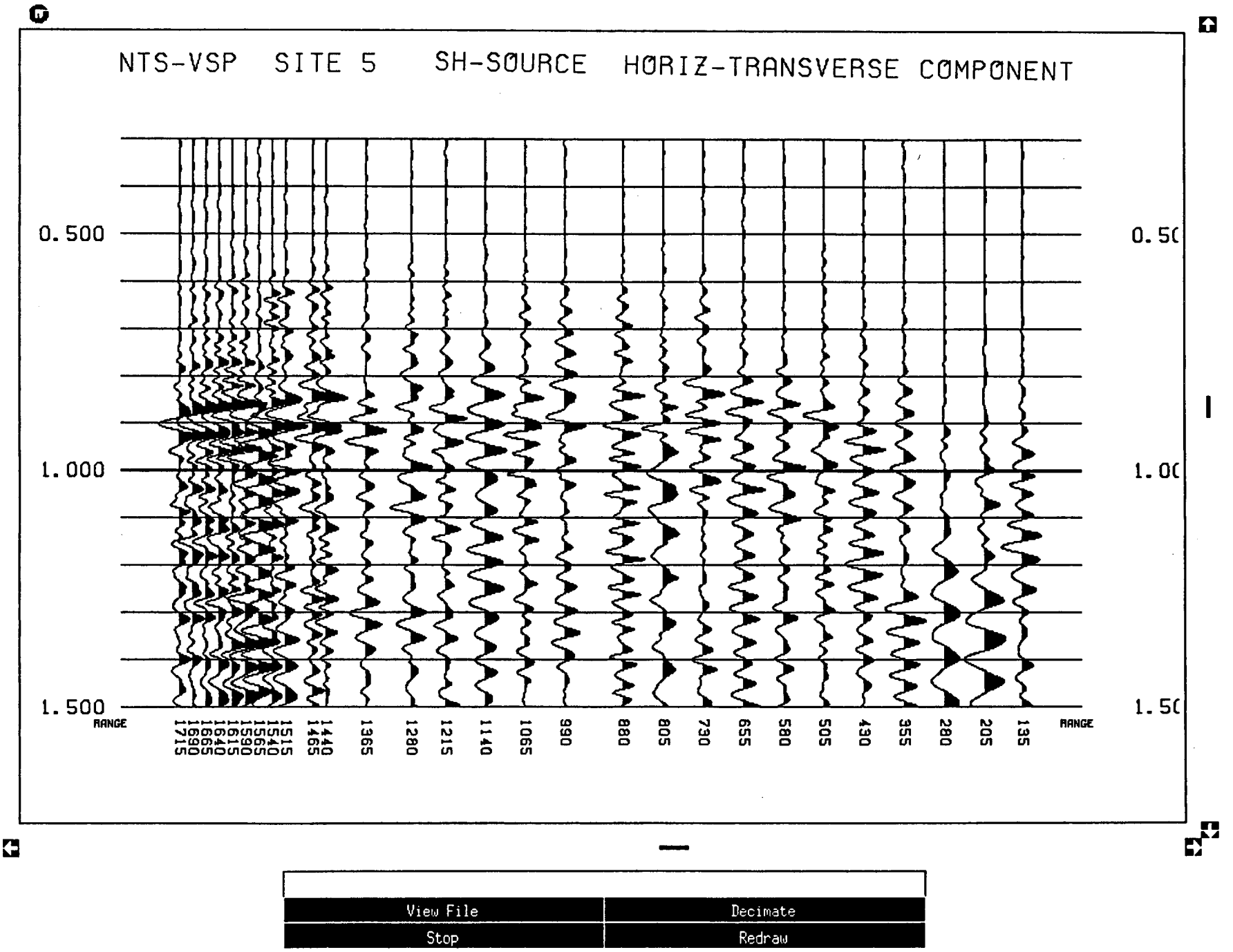
NTS-VSP SITE 5 SH-SOURCE HORIZ-TRANSVERSE COMPONENT
0.500
1.000
1.500
0.5(
1.0(
1.5(
RANGE
1715
1690
1665
1640
1615
1590
1565
1540
1515
1465
1440
1365
1280
1215
1140
1065
990
880
805
730
655
580
505
430
355
280
205
135
RANGE
View File
Decimate
Stop
Redraw

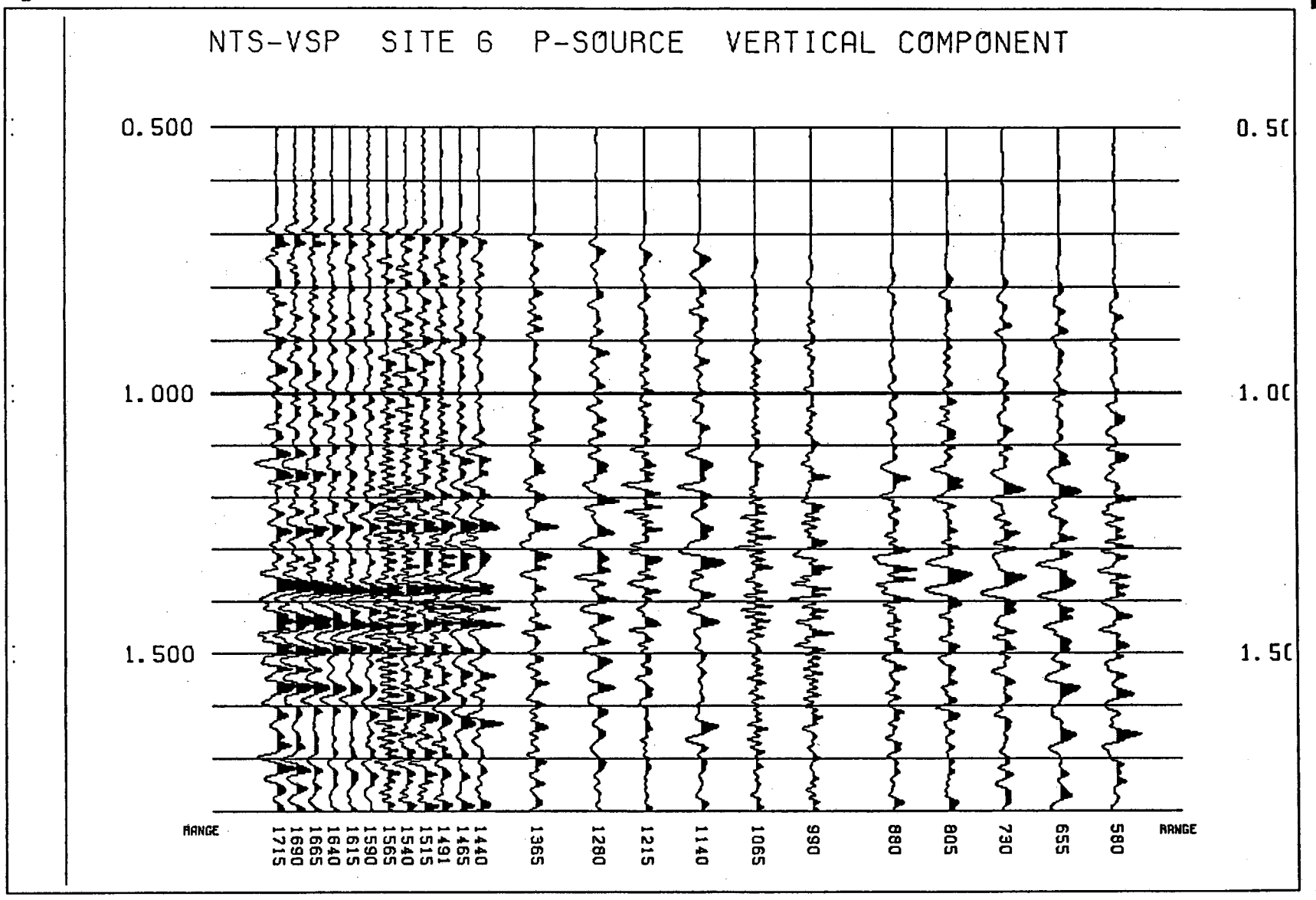
NTS-VSP SITE 6 P-SOURCE VERTICAL COMPONENT
0.500
1.000
1.500
0.5(
1.0(
1.5(
RANGE
1715
1690
1665
1640
1615
1590
1565
1540
1515
1491
1465
1440
1365
1280
1215
1140
1065
990
880
805
730
655
580
RANGE
View File
Decimate
Stop
Redraw

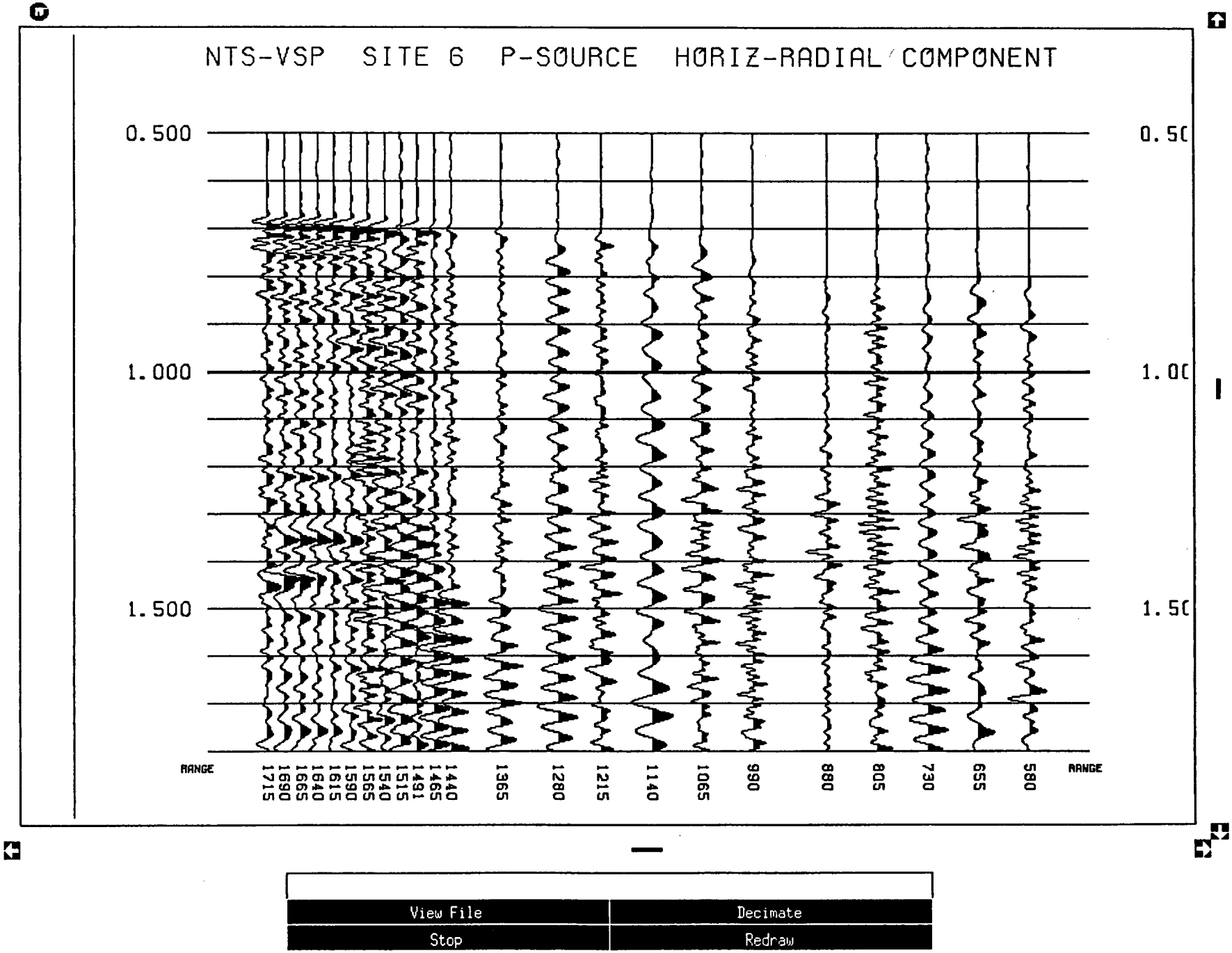
NTS-VSP SITE 6 P-SOURCE HORIZ-RADIAL COMPONENT
0.500
1.000
1.500
RANGE
1715
1690
1665
1640
1615
1590
1565
1540
1515
1491
1465
1440
1365
1280
1215
1140
1065
990
880
805
730
655
580
RANGE
View File
Decimate
Stop
Redraw

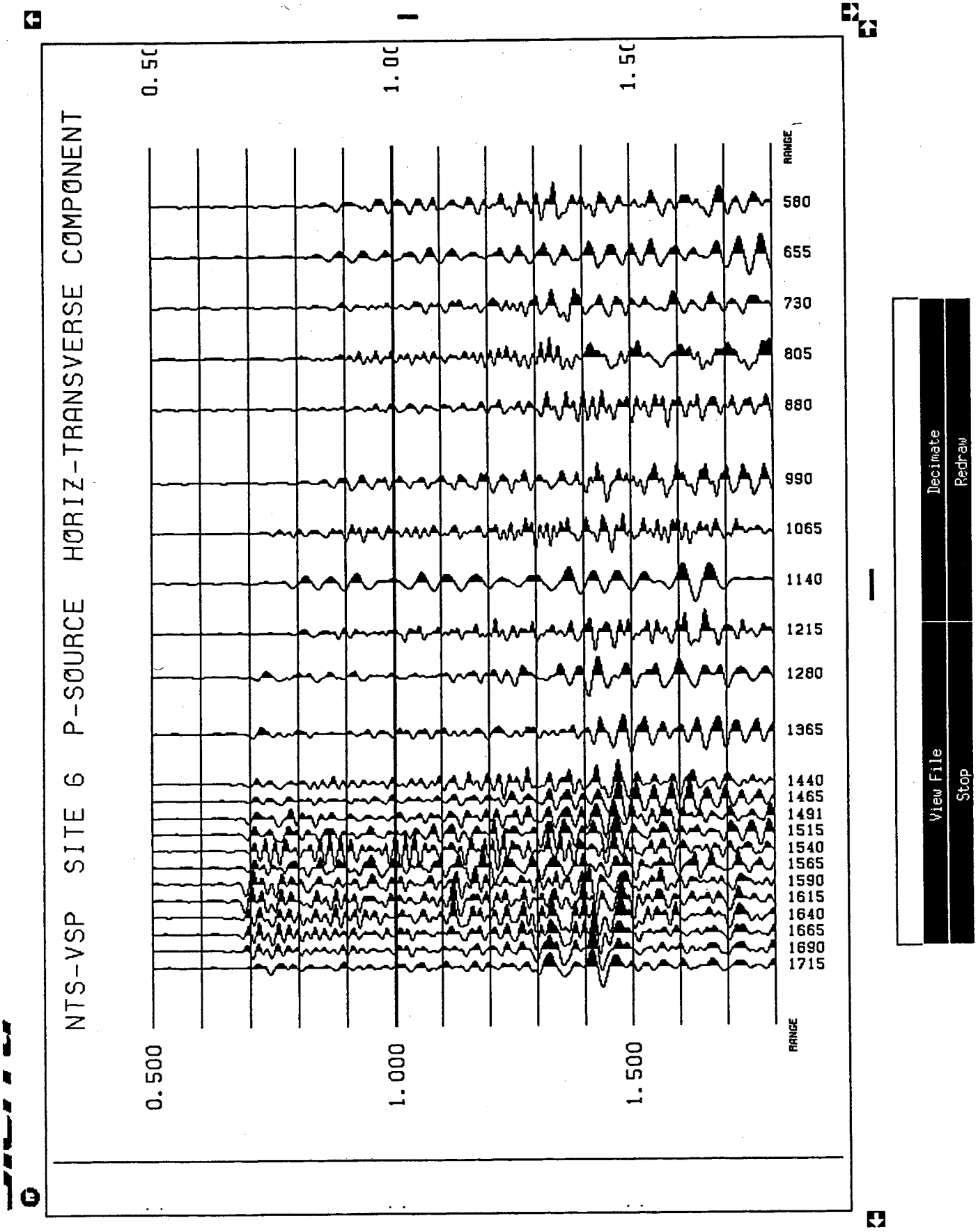
NTS-VSP SITE 6 P-SOURCE HORIZ-TRANSVERSE COMPONENT
0.500
1.000
1.500
RANGE
580
655
730
805
880
990
1065
1140
1215
1280
1365
1440
1465
1491
1515
1540
1565
1590
1615
1640
1665
1690
1715
Decimate
Redraw
View File
Stop

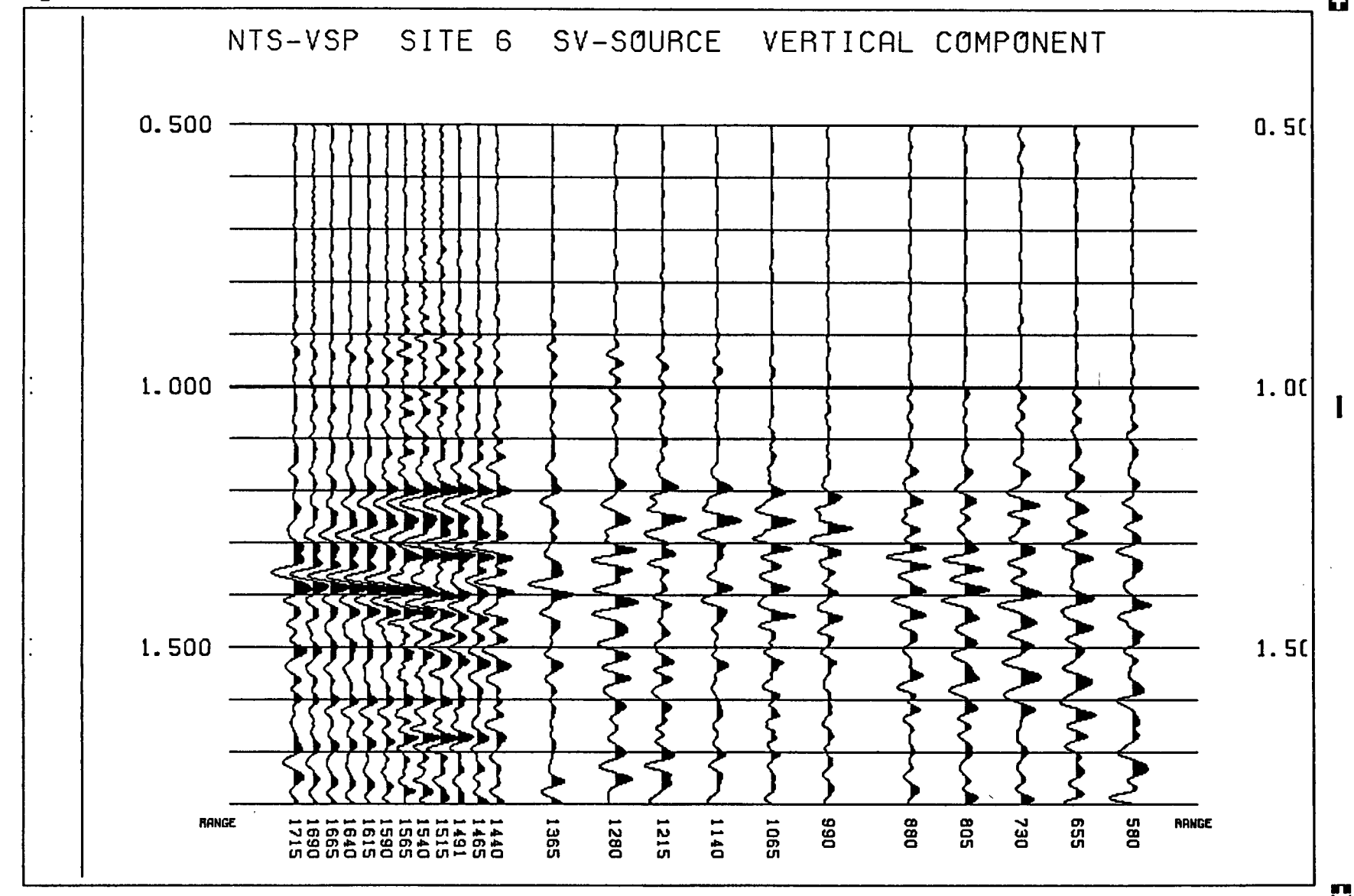
NTS-VSP SITE 6 SV-SOURCE VERTICAL COMPONENT
0.500
1.000
1.500
0.5(
1.0(
1.5(
RANGE
1715
1690
1665
1640
1615
1590
1565
1540
1515
1491
1465
1440
1365
1280
1215
1140
1065
990
880
805
730
655
580
RANGE
View File
Decimate
Stop
Redraw

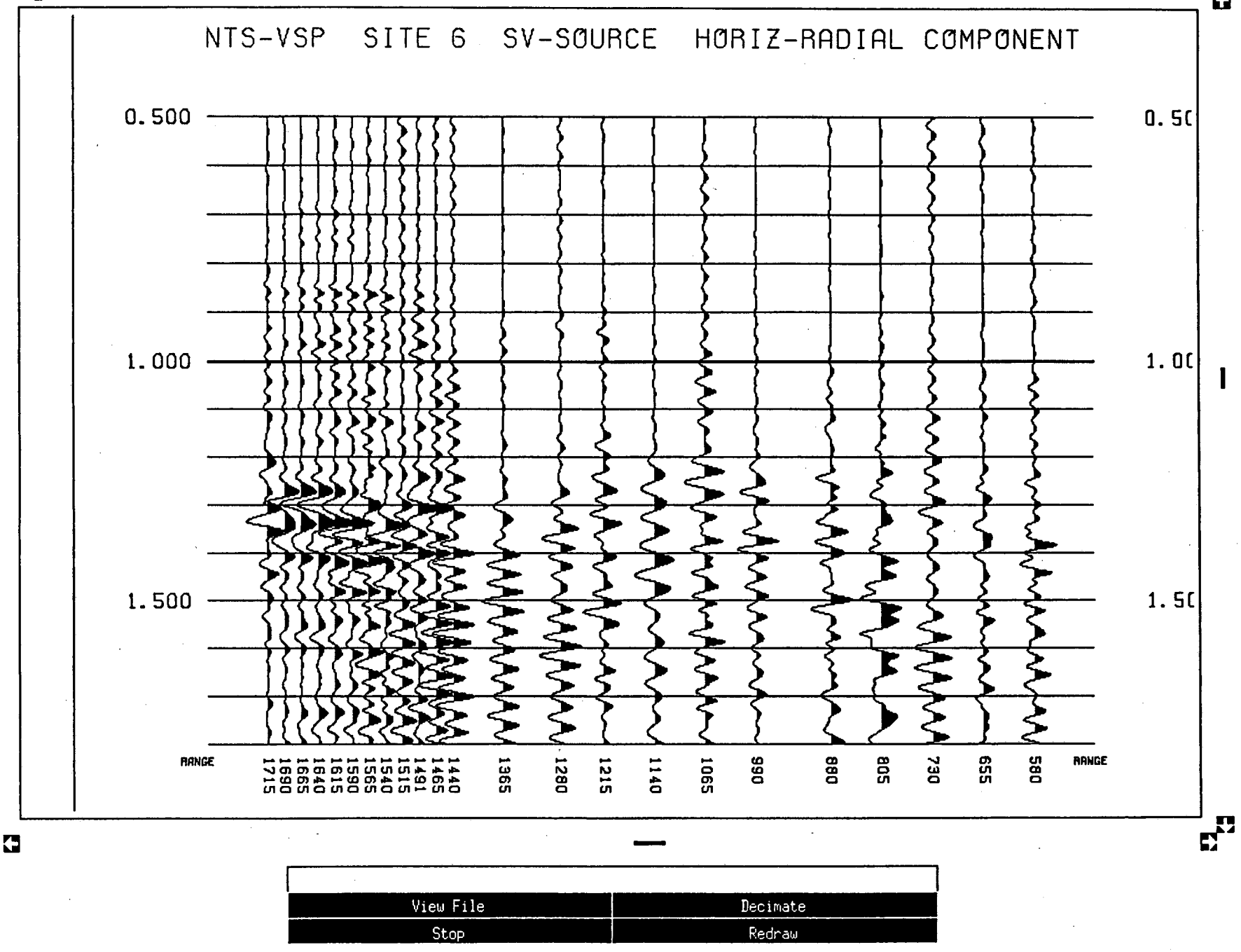
NTS-VSP SITE 6 SV-SOURCE HORIZ-RADIAL COMPONENT
0.500
1.000
1.500
RANGE
1715
1690
1665
1640
1615
1590
1565
1540
1515
1491
1465
1440
1365
1280
1215
1140
1065
990
880
805
730
655
580
RANGE
View File
Decimate
Stop
Redraw

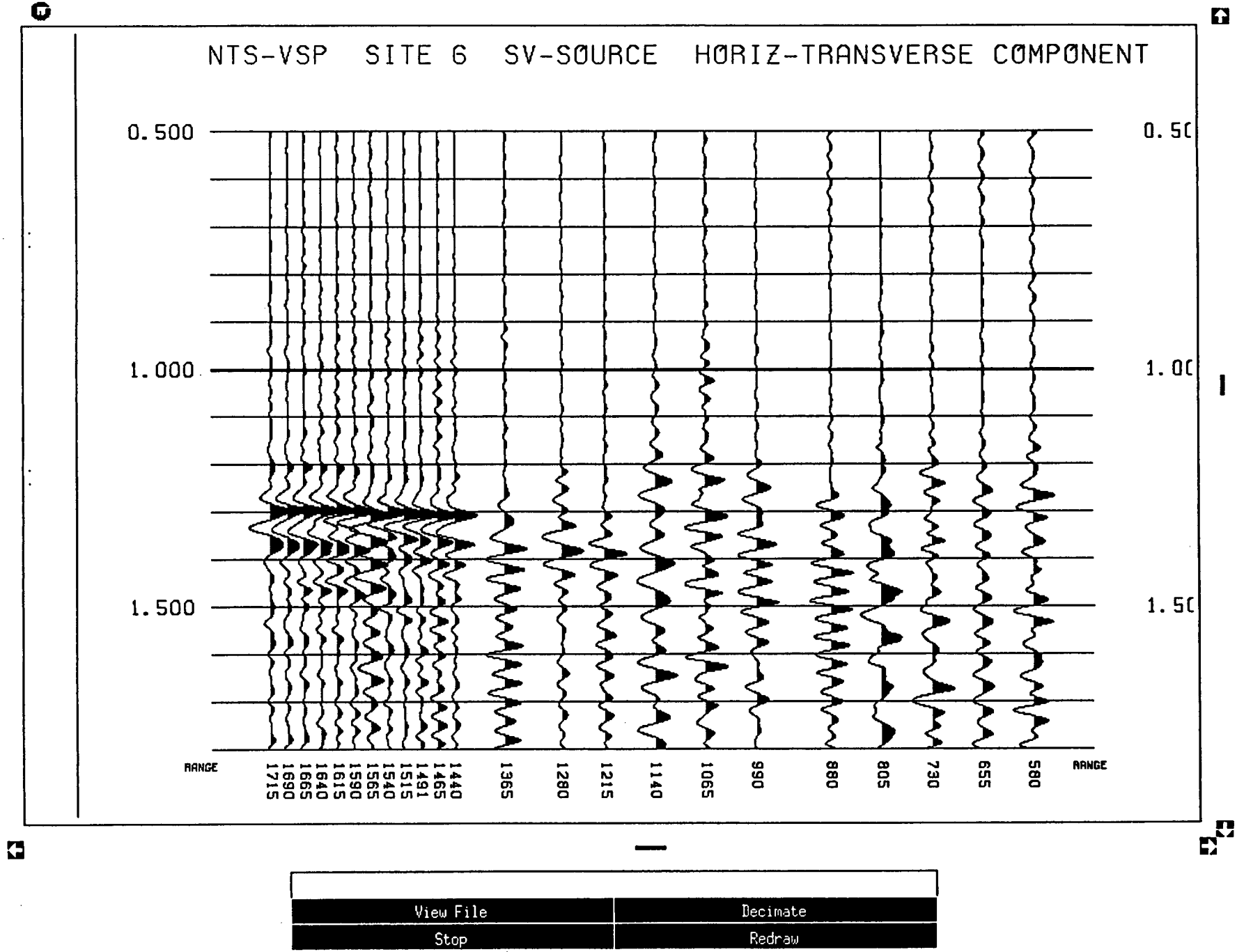
NTS-VSP SITE 6 SV-SOURCE HORIZ-TRANSVERSE COMPONENT
0.500
1.000
1.500
0.5C
1.0C
1.5C
RANGE
1715
1690
1665
1640
1615
1590
1565
1540
1515
1491
1465
1440
1365
1280
1215
1140
1065
990
880
805
730
655
580
RANGE
View File
Decimate
Stop
Redraw

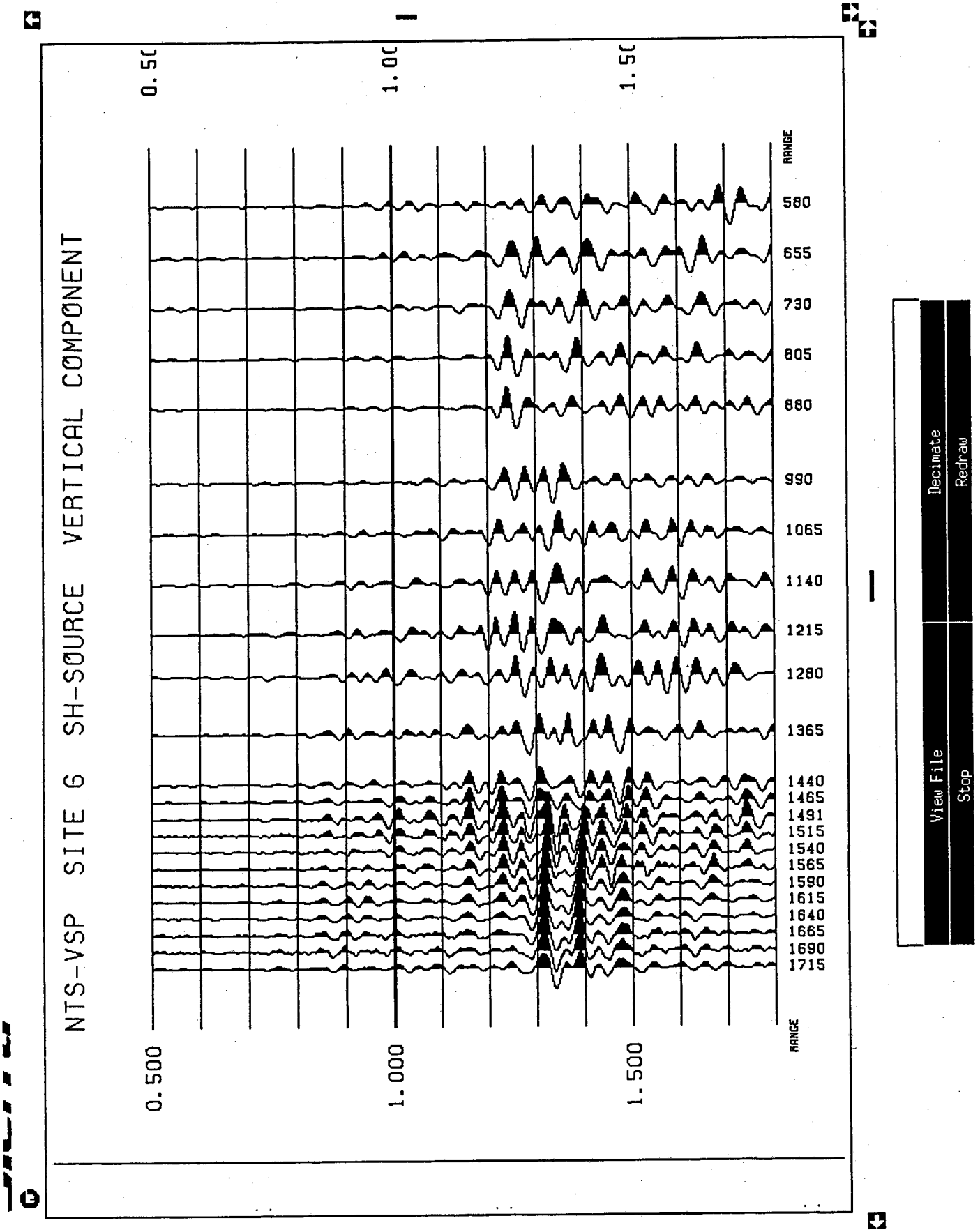
NTS-VSP SITE 6 SH-SOURCE VERTICAL COMPONENT
0.5
1.0
1.5
RANGE
580
655
730
805
880
990
1065
1140
1215
1280
1365
1440
1465
1491
1515
1540
1565
1590
1615
1640
1665
1690
1715
RANGE
0.500
1.000
1.500
Decimate
Redraw
View File
Stop

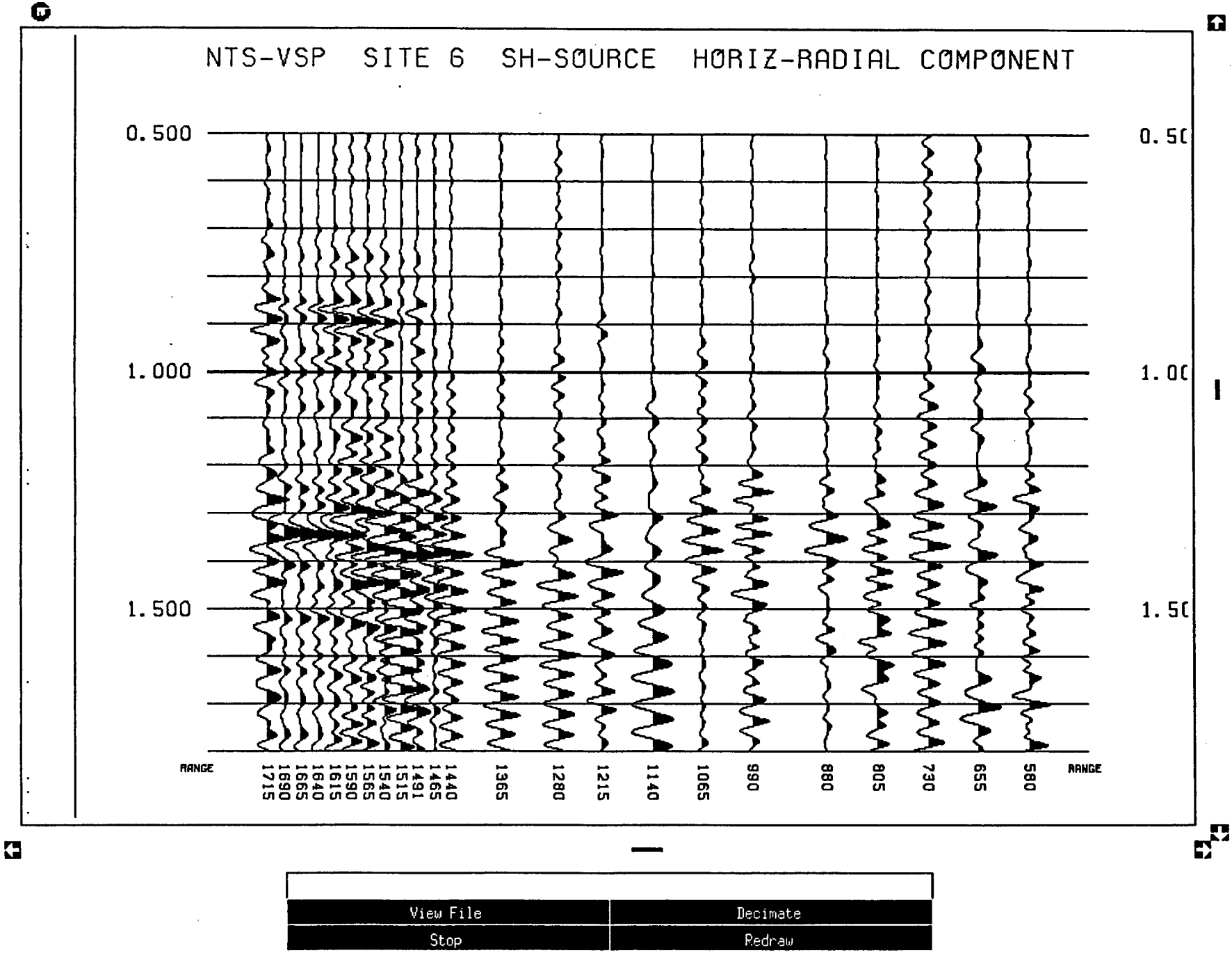
NTS-VSP SITE 6 SH-SOURCE HORIZ-RADIAL COMPONENT
0.500
1.000
1.500
0.50
1.00
1.50
RANGE
1715
1690
1665
1640
1615
1590
1565
1540
1515
1491
1465
1440
1365
1280
1215
1140
1065
990
880
805
730
655
580
RANGE
View File
Decimate
Stop
Redraw

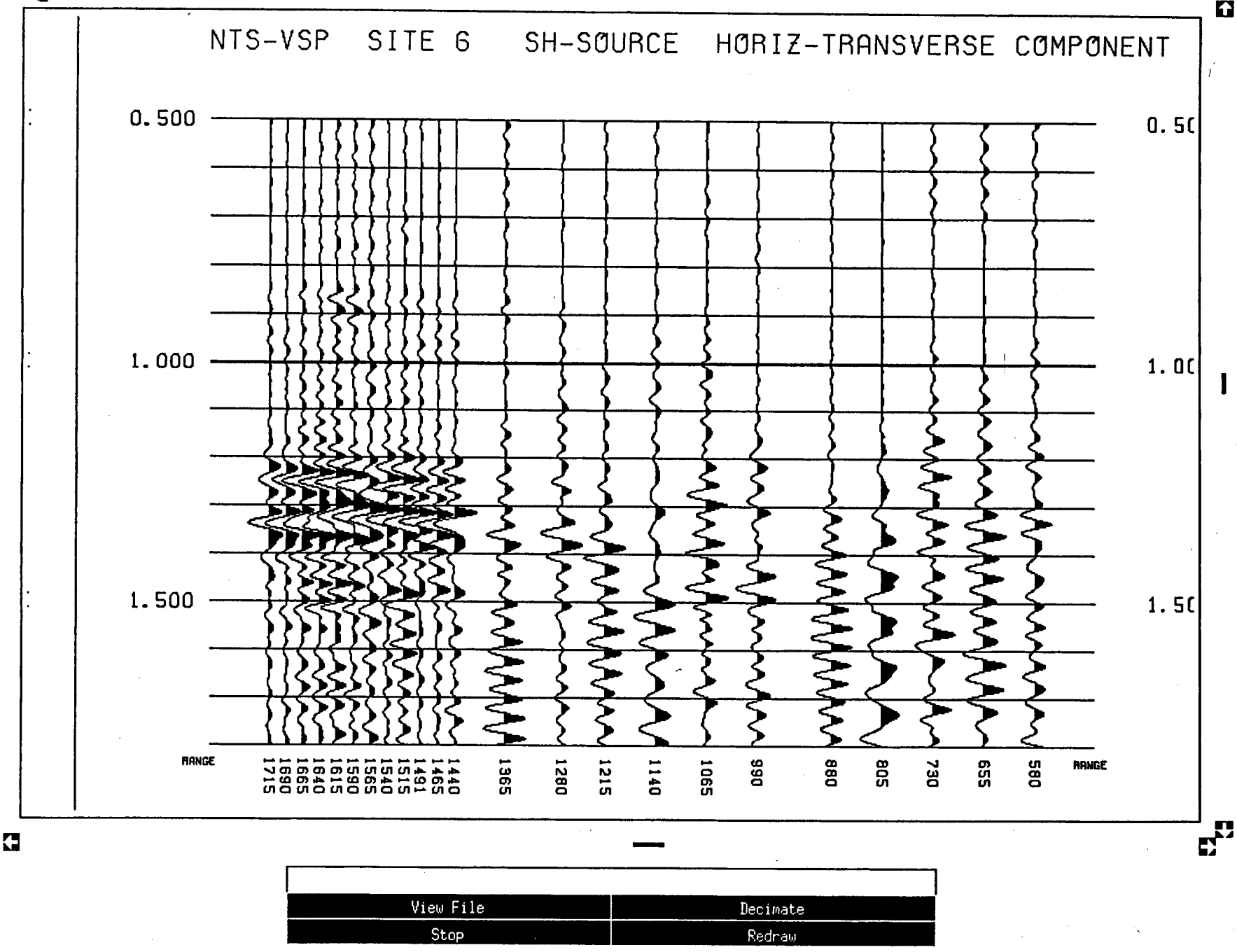
NTS-VSP SITE 6 SH-SOURCE HORIZ-TRANSVERSE COMPONENT
0.500
1.000
1.500
0.5C
1.0C
1.5C
RANGE
1715
1690
1665
1640
1615
1590
1565
1540
1515
1491
1465
1440
1365
1280
1215
1140
1065
990
880
805
730
655
580
RANGE
View File
Decimate
Stop
Redraw

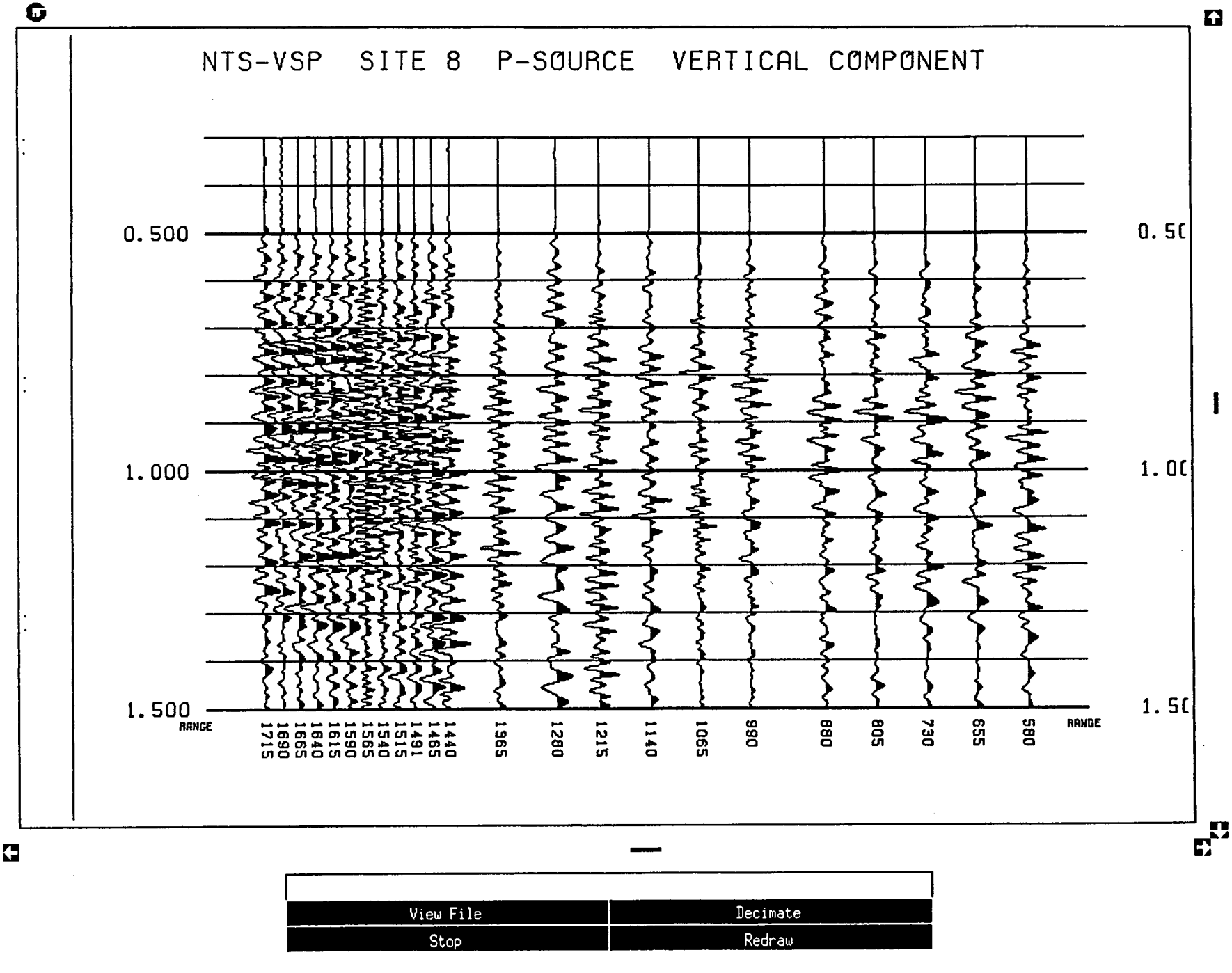
NTS-VSP SITE 8 P-SOURCE VERTICAL COMPONENT
0.500
1.000
1.500
RANGE
1715
1690
1665
1640
1615
1590
1565
1540
1515
1491
1465
1440
1365
1280
1215
1140
1065
990
880
805
730
655
580
RANGE
View File
Decimate
Stop
Redraw

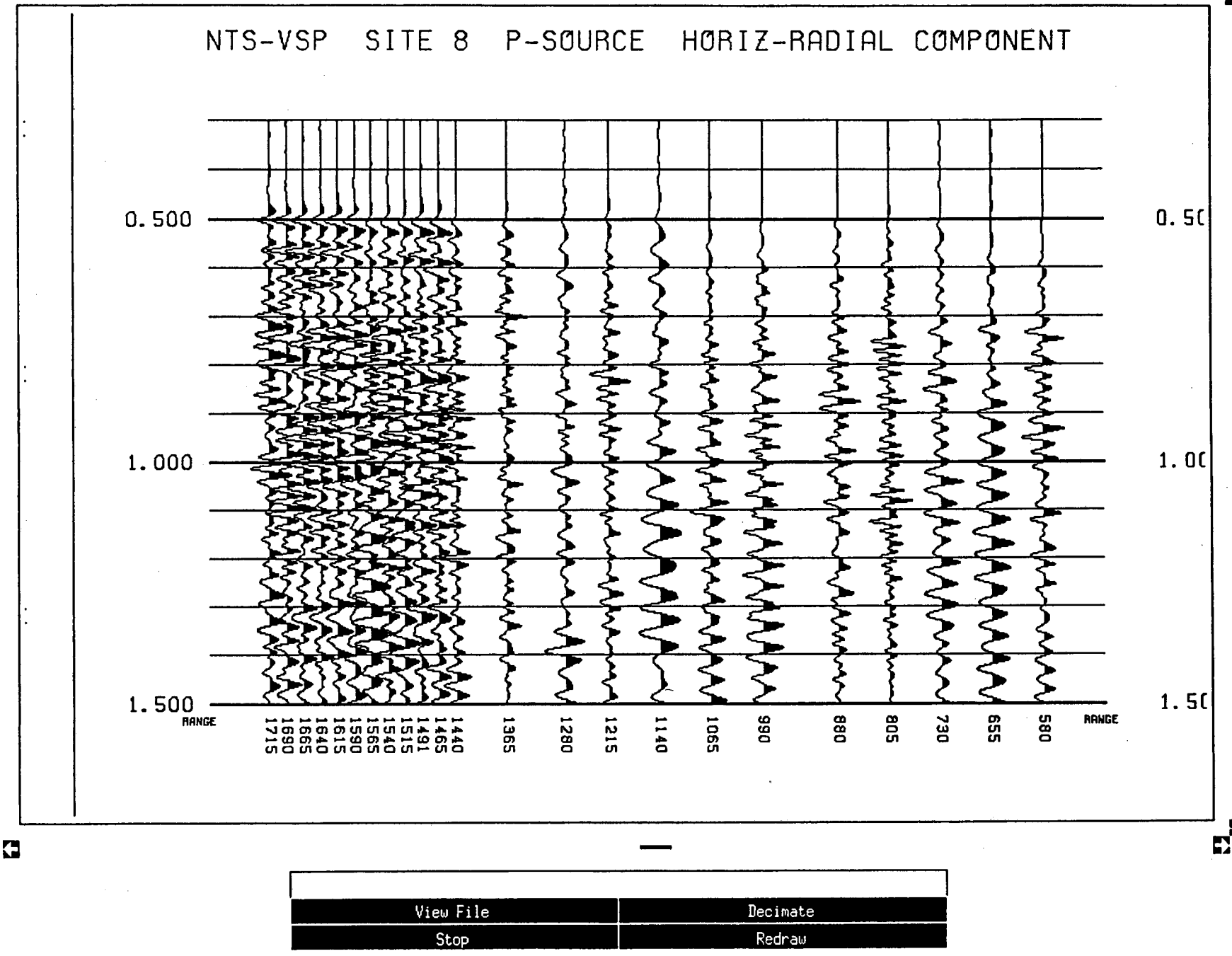
NTS-VSP SITE 8 P-SOURCE HORIZ-RADIAL COMPONENT
0.500
1.000
1.500
RANGE
1715
1690
1665
1640
1615
1590
1565
1540
1515
1491
1465
1440
1365
1280
1215
1140
1065
990
880
805
730
655
580
RANGE
View File
Decimate
Stop
Redraw

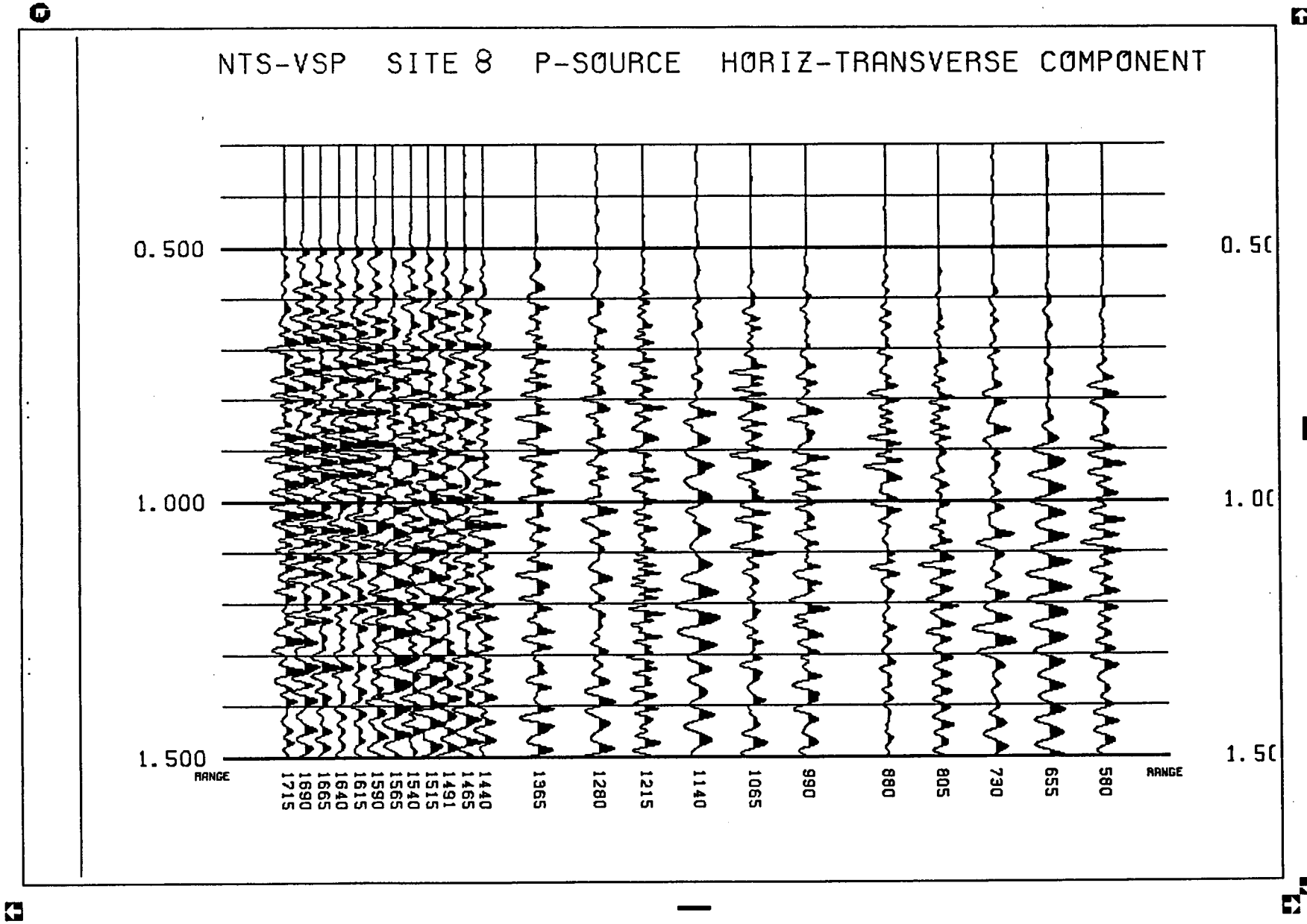
NTS-VSP SITE 8 P-SOURCE HORIZ-TRANSVERSE COMPONENT
0.500
1.000
1.500
RANGE
1715
1690
1665
1640
1615
1590
1565
1540
1515
1491
1465
1440
1365
1280
1215
1140
1065
980
880
805
730
655
580
RANGE
View File
Decimate
Stop
Redraw

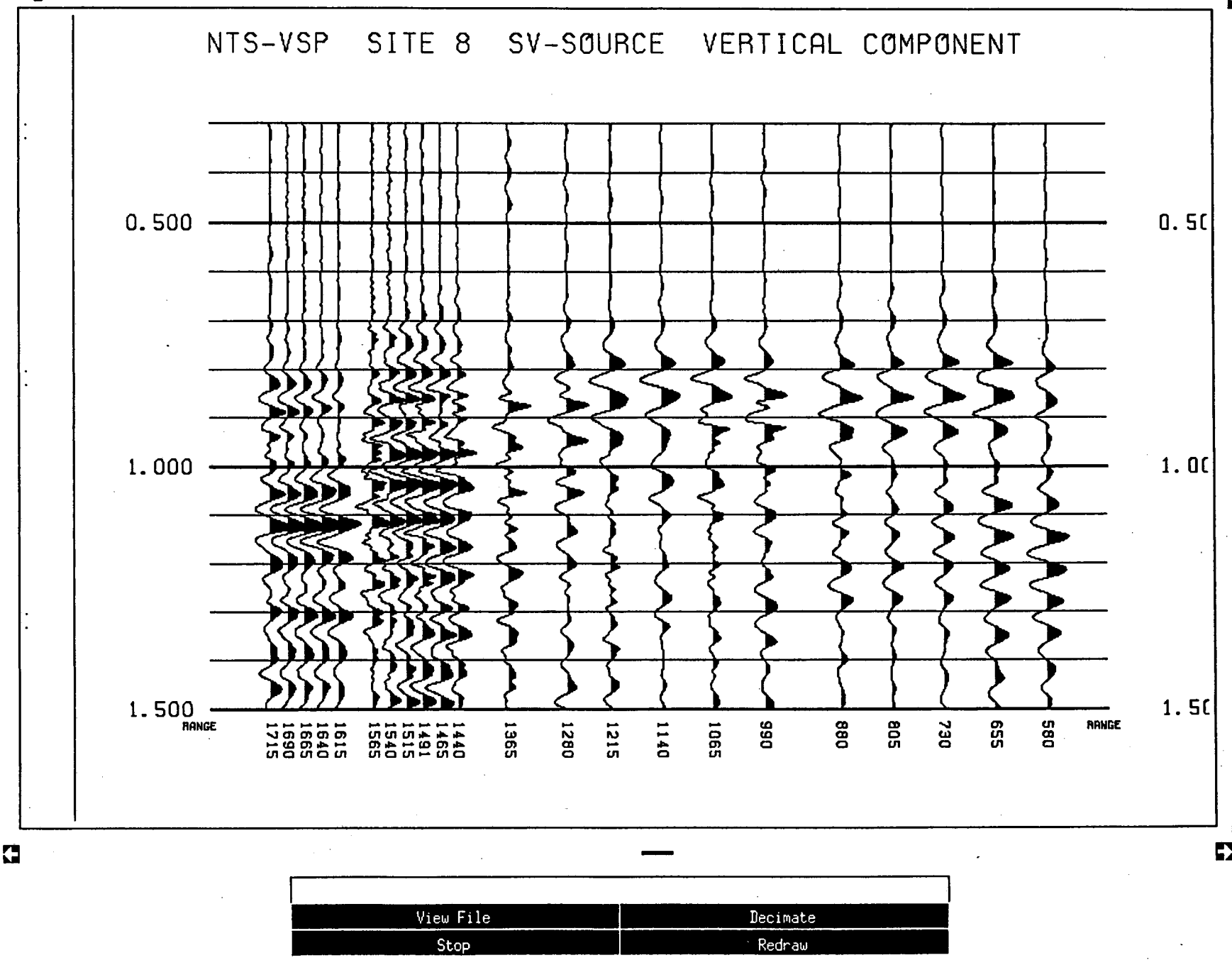
NTS-VSP SITE 8 SV-SOURCE VERTICAL COMPONENT
0.500
1.000
1.500
0.5C
1.0C
1.5C
RANGE
1715
1690
1665
1640
1615
1565
1540
1515
1491
1465
1440
1365
1280
1215
1140
1065
990
880
805
730
655
580
RANGE
View File
Decimate
Stop
Redraw

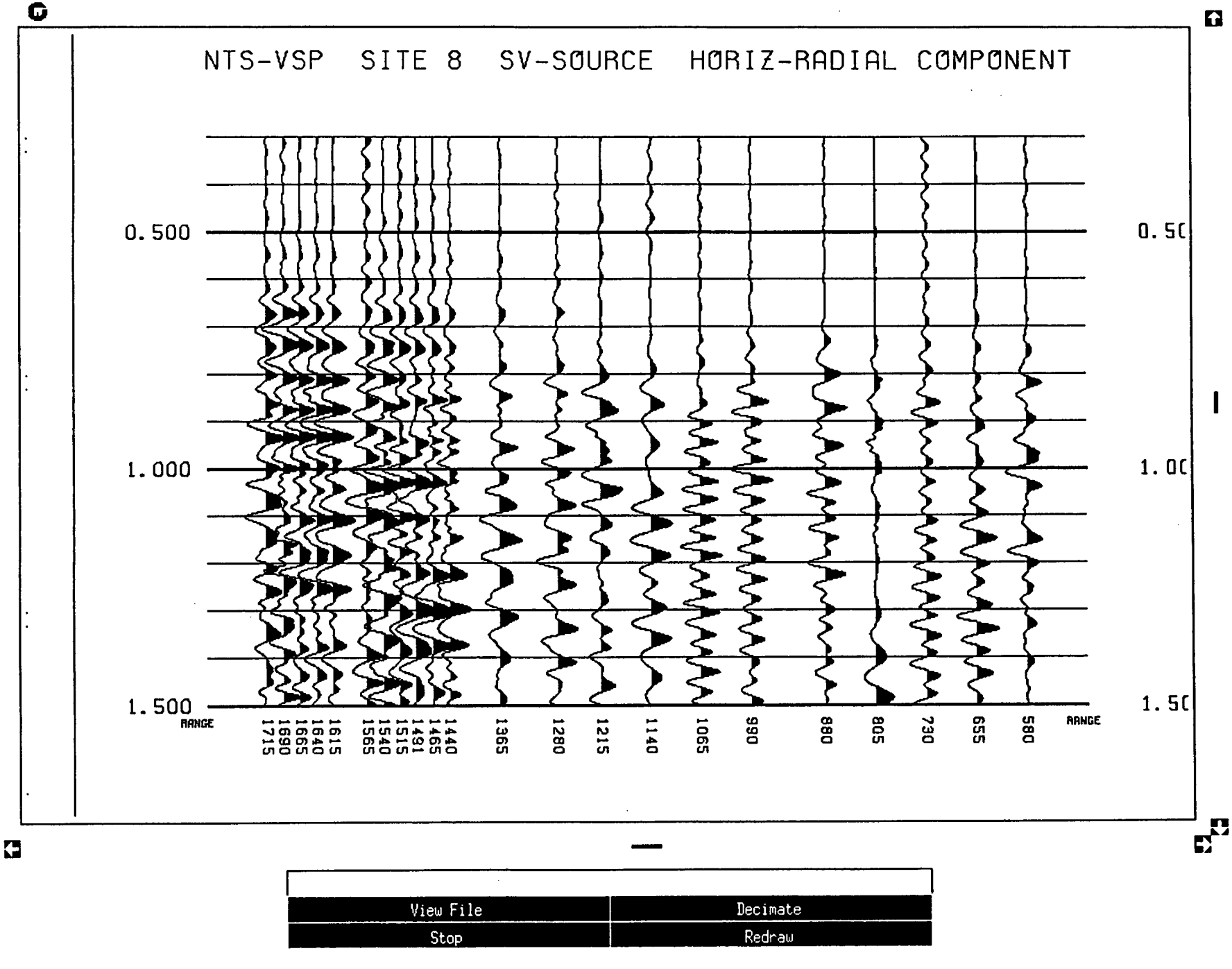
NTS-VSP SITE 8 SV-SOURCE HORIZ-RADIAL COMPONENT
0.500
1.000
1.500
RANGE
1715
1690
1665
1640
1615
1565
1540
1515
1491
1465
1440
1365
1280
1215
1140
1065
990
880
805
730
655
580
RANGE
View File
Decimate
Stop
Redraw

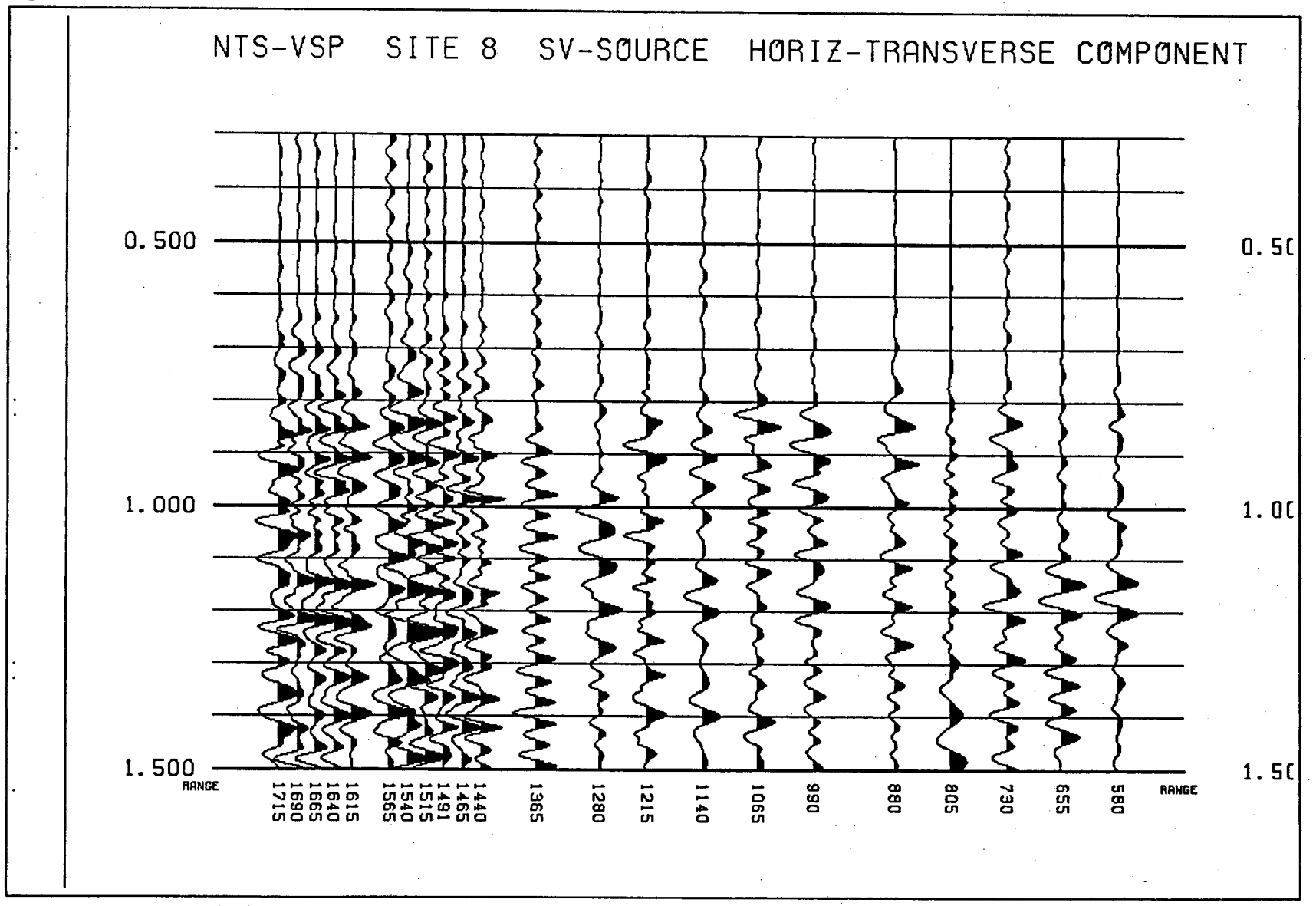

View File | Decimate

Stop | Redraw

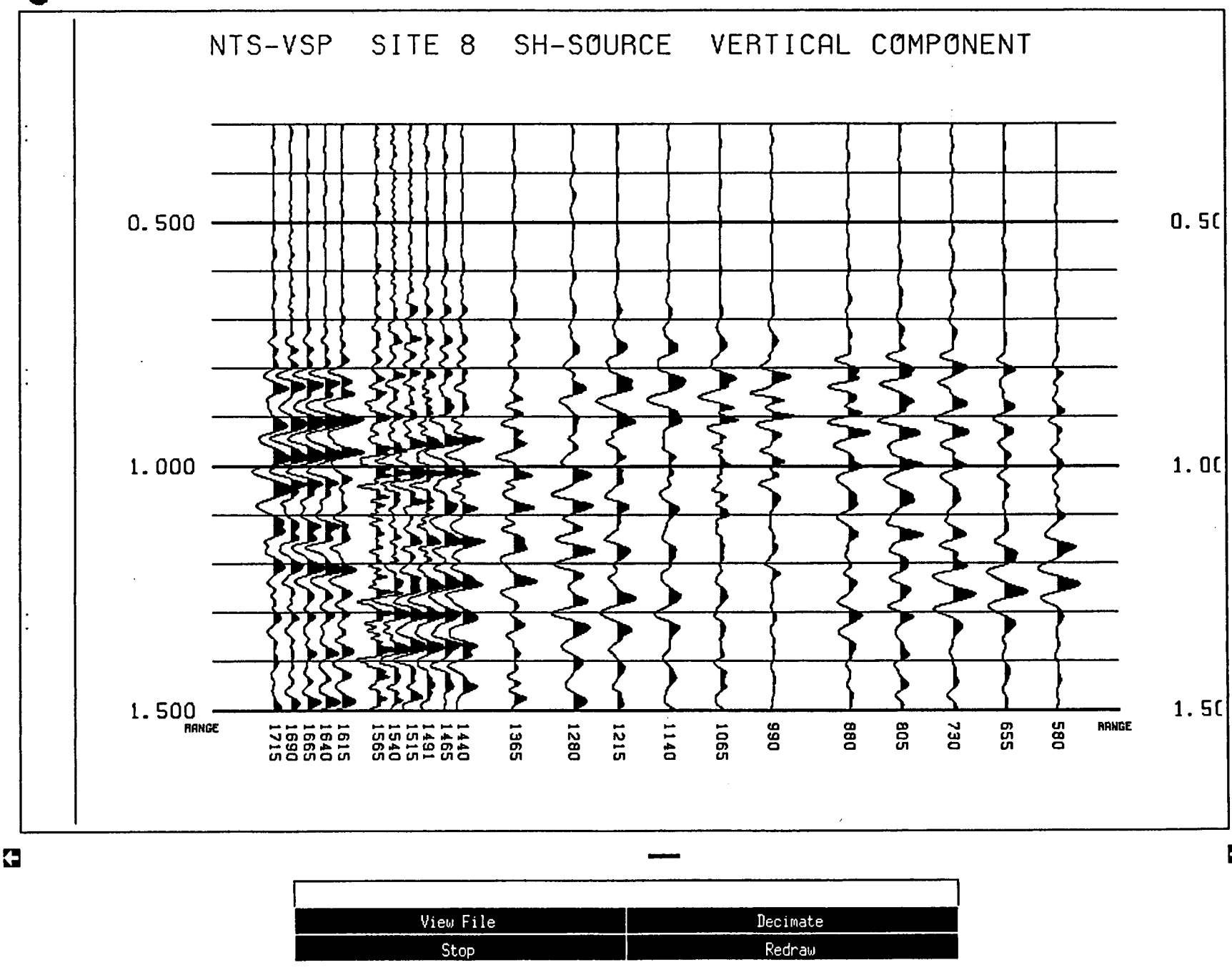
NTS-VSP SITE 8 SH-SOURCE VERTICAL COMPONENT
0.500
1.000
1.500
0.5C
1.0C
1.5C
RANGE
1715
1690
1665
1640
1615
1565
1540
1515
1491
1465
1440
1365
1280
1215
1140
1065
990
880
805
730
655
580
RANGE
View File
Decimate
Stop
Redraw

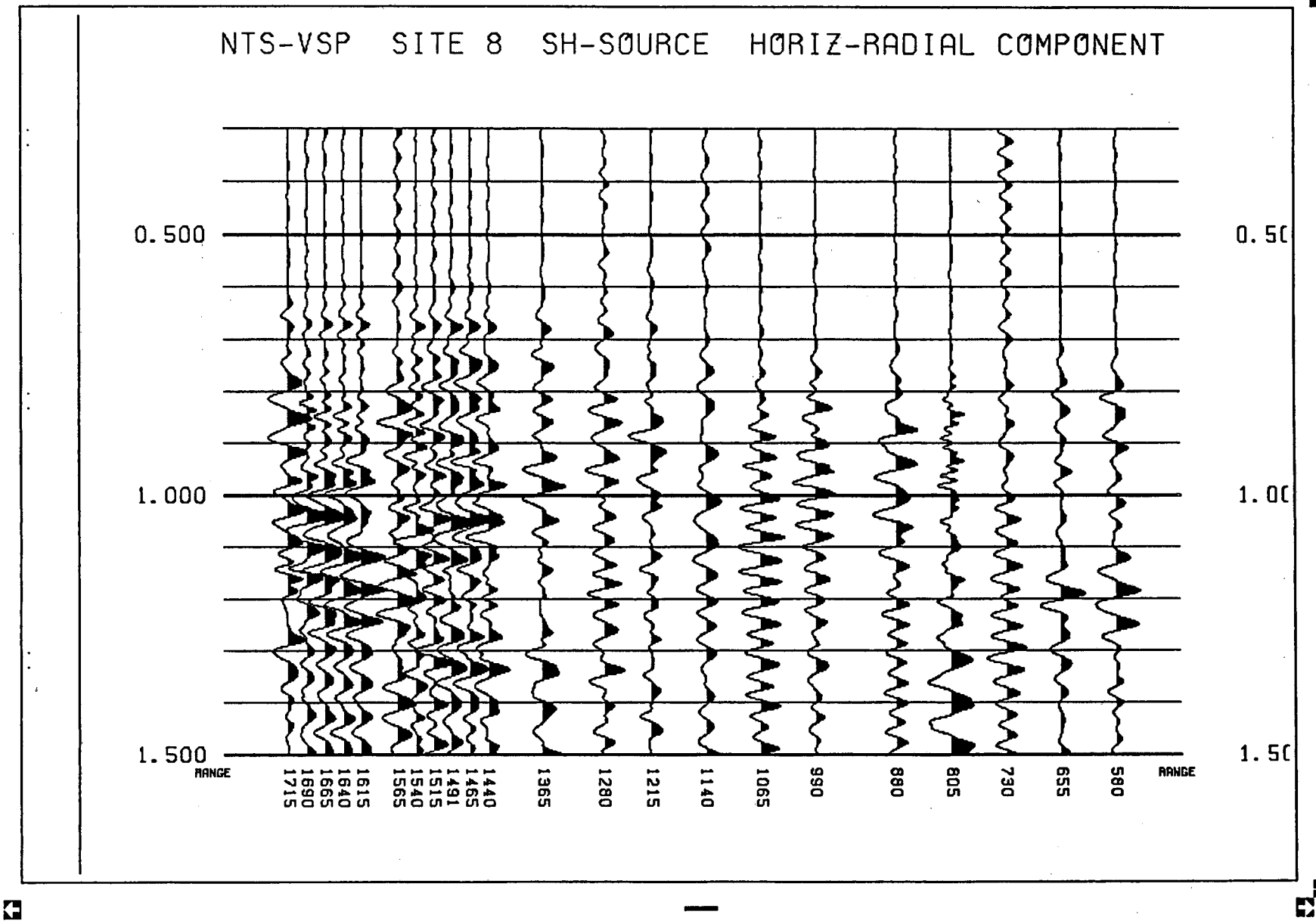
NTS-VSP SITE 8 SH-SOURCE HORIZ-RADIAL COMPONENT
0.500
1.000
1.500
RANGE
1715
1690
1665
1640
1615
1590
1565
1540
1515
1491
1465
1440
1365
1280
1215
1140
1065
980
880
805
730
655
580
RANGE

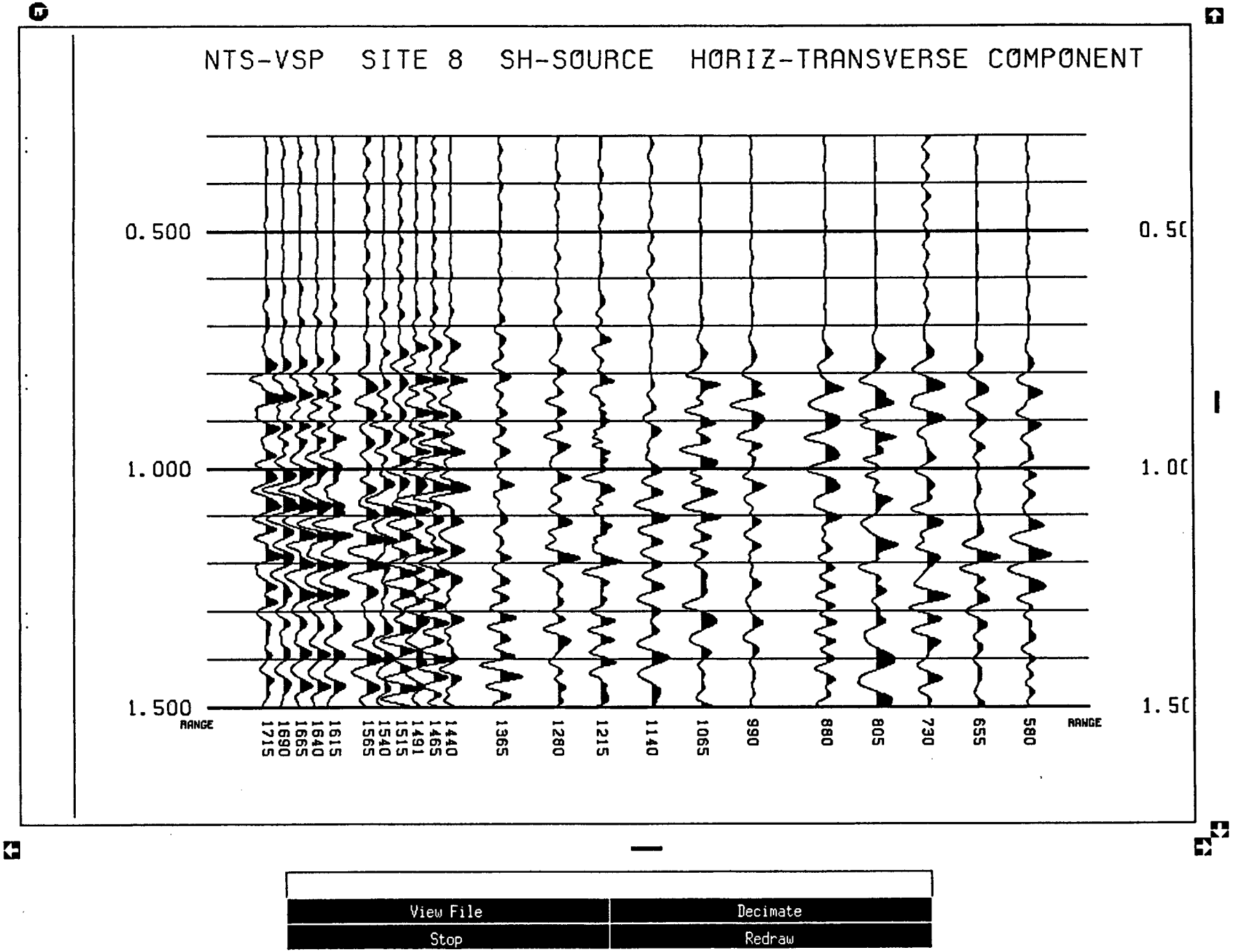
NTS-VSP SITE 8 SH-SOURCE HORIZ-TRANSVERSE COMPONENT
0.500
1.000
1.500
RANGE
1715
1690
1665
1640
1615
1565
1540
1515
1491
1465
1440
1365
1280
1215
1140
1065
990
880
805
730
655
580
RANGE
View File
Decimate
Stop
Redraw

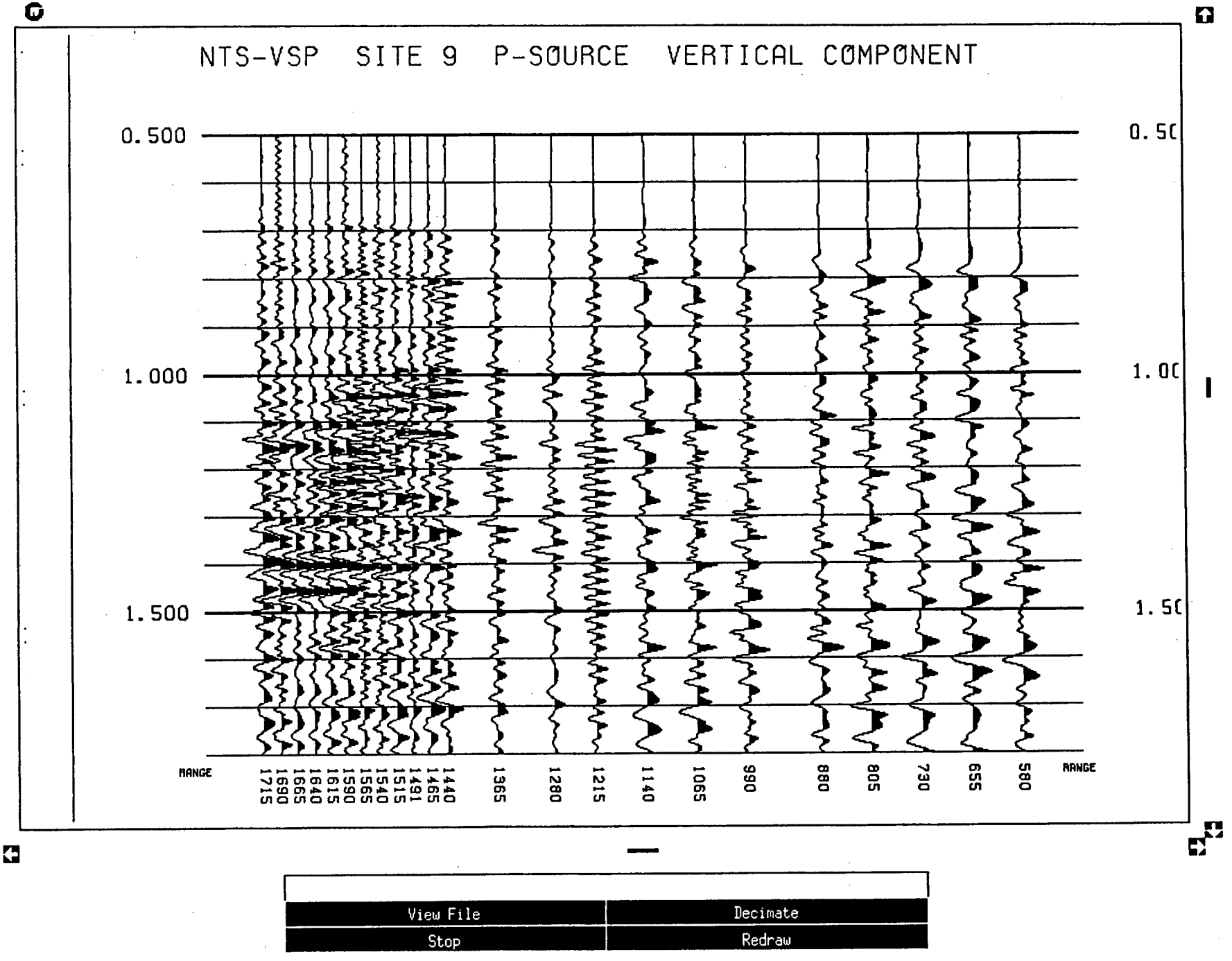
NTS-VSP SITE 9 P-SOURCE VERTICAL COMPONENT
0.500
1.000
1.500
0.5C
1.0C
1.5C
RANGE
1715
1690
1665
1640
1615
1590
1565
1540
1515
1491
1465
1440
1365
1280
1215
1140
1065
990
880
805
730
655
580
RANGE
View File
Decimate
Stop
Redraw

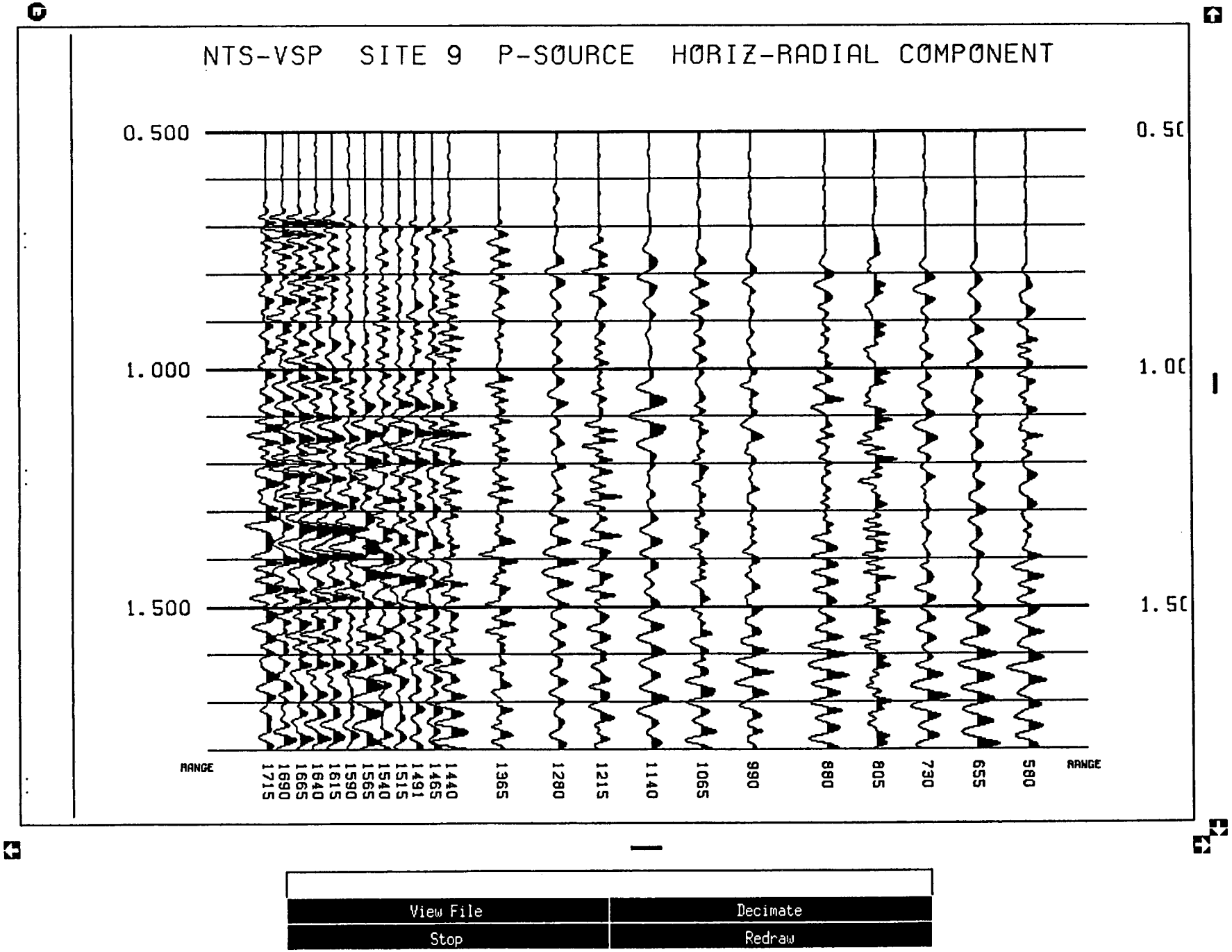
NTS-VSP SITE 9 P-SOURCE HORIZ-RADIAL COMPONENT
0.500
1.000
1.500
RANGE
1715
1690
1665
1640
1615
1590
1565
1540
1515
1491
1465
1440
1365
1280
1215
1140
1065
990
880
805
730
655
580
RANGE
View File
Decimate
Stop
Redraw

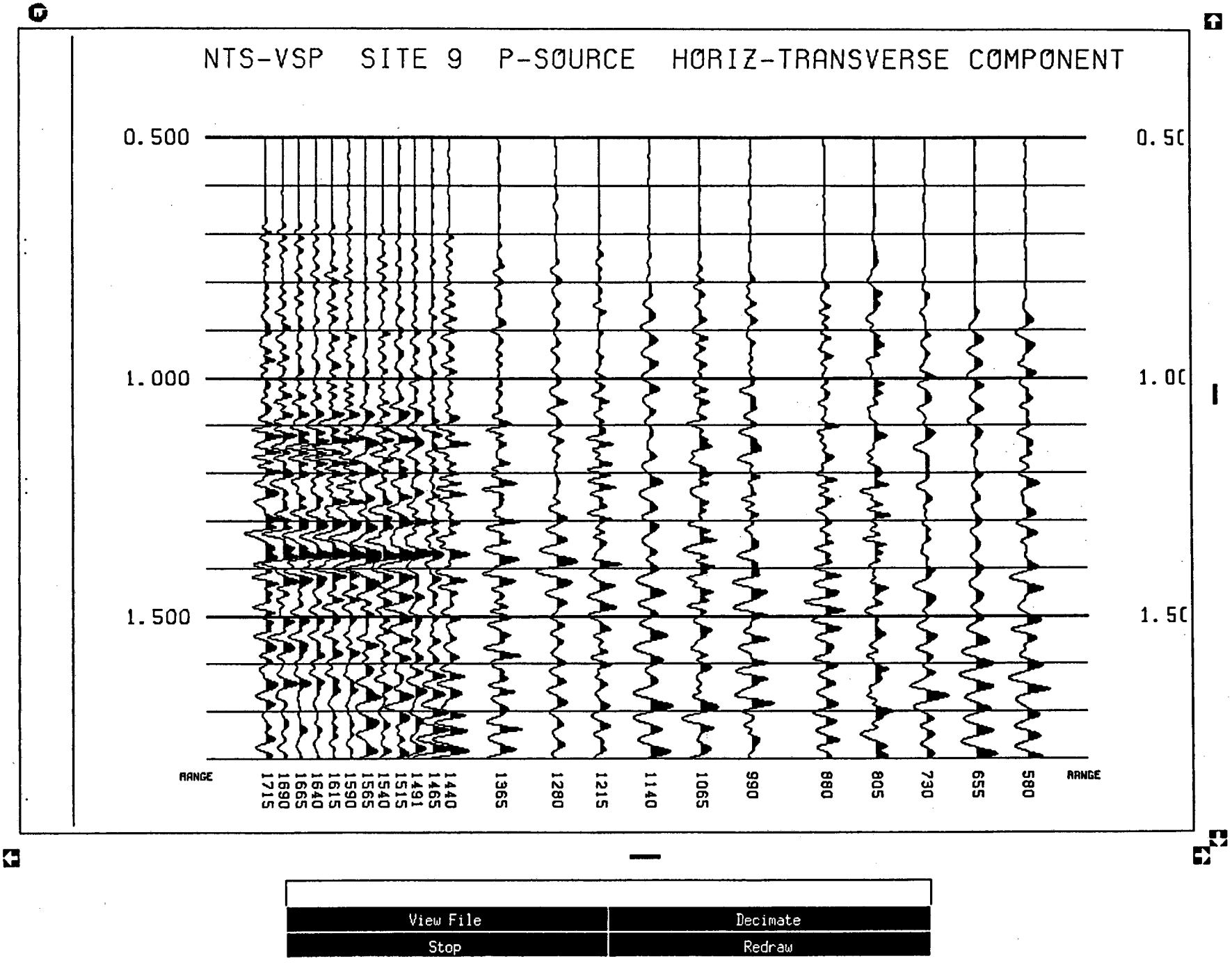
NTS-VSP SITE 9 P-SOURCE HORIZ-TRANSVERSE COMPONENT
0.500
1.000
1.500
0.50
1.00
1.50
RANGE
1715
1690
1665
1640
1615
1590
1565
1540
1515
1491
1465
1440
1365
1280
1215
1140
1065
990
880
805
730
655
580
RANGE
View File
Decimate
Stop
Redraw

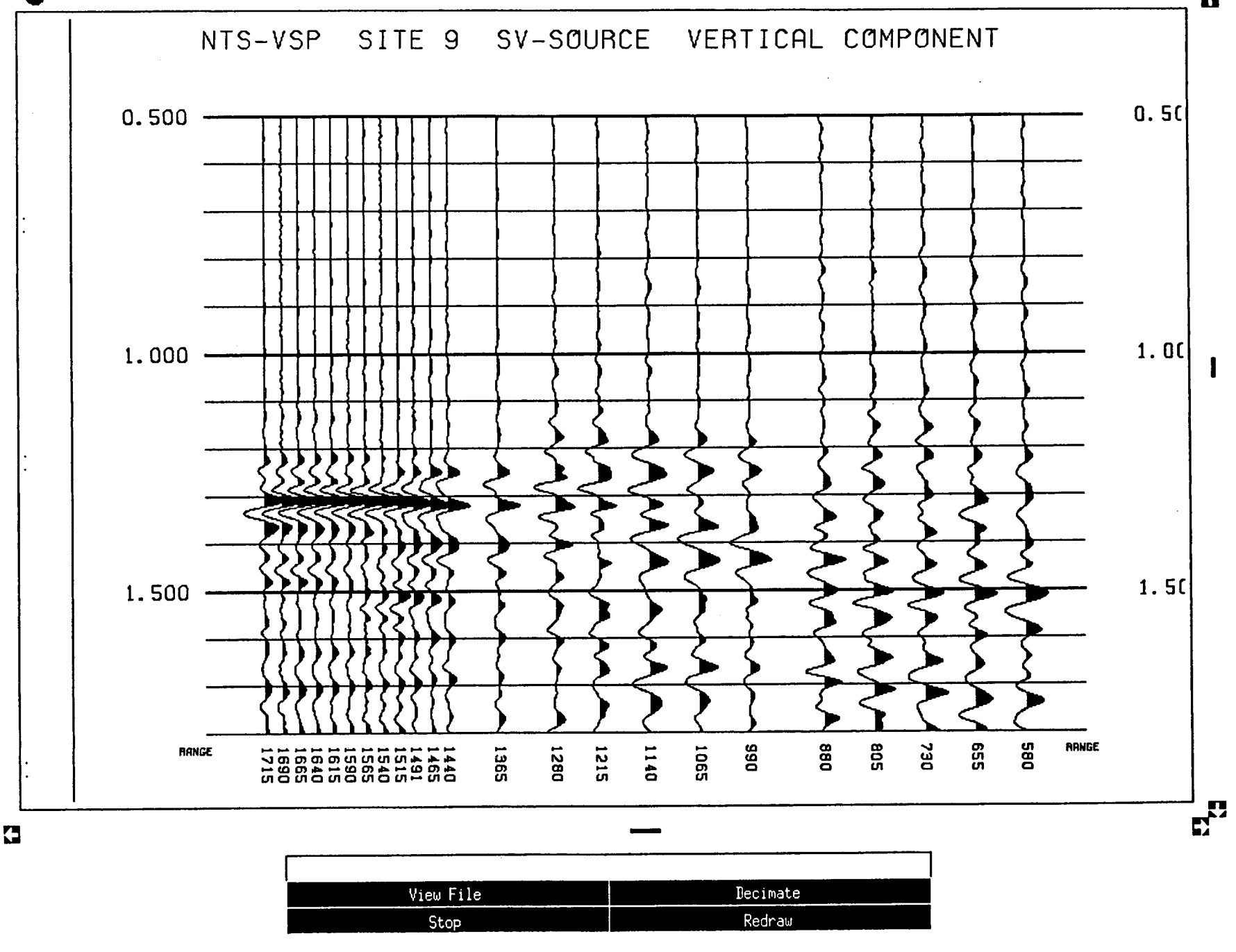
NTS-VSP SITE 9 SV-SOURCE VERTICAL COMPONENT
0.500
1.000
1.500
0.5C
1.0C
1.5C
RANGE
1715
1690
1665
1640
1615
1590
1565
1540
1515
1491
1465
1440
1365
1280
1215
1140
1065
990
880
805
730
655
580
RANGE
View File
Decimate
Stop
Redraw

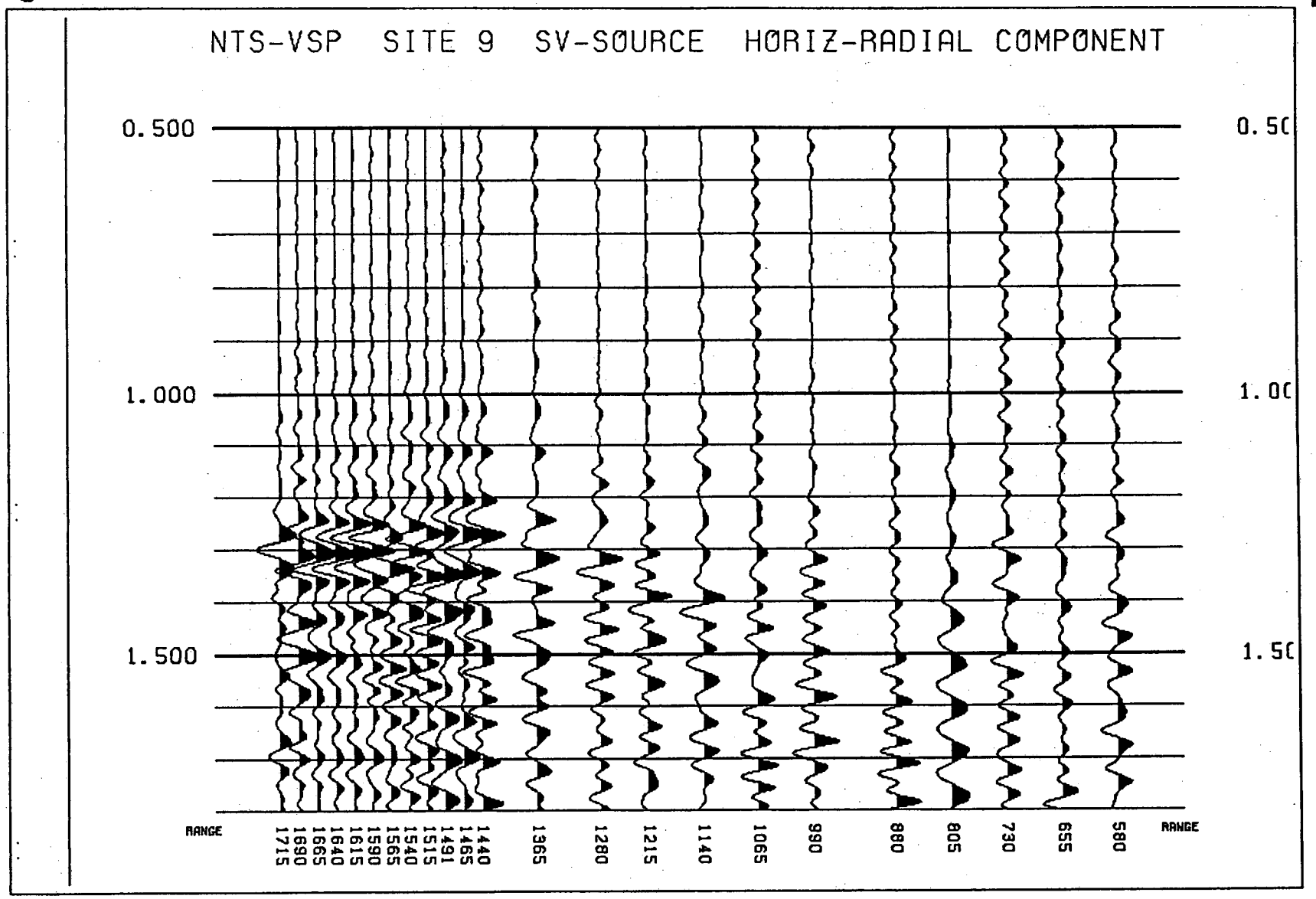

View File | Decimate

Stop | Redraw

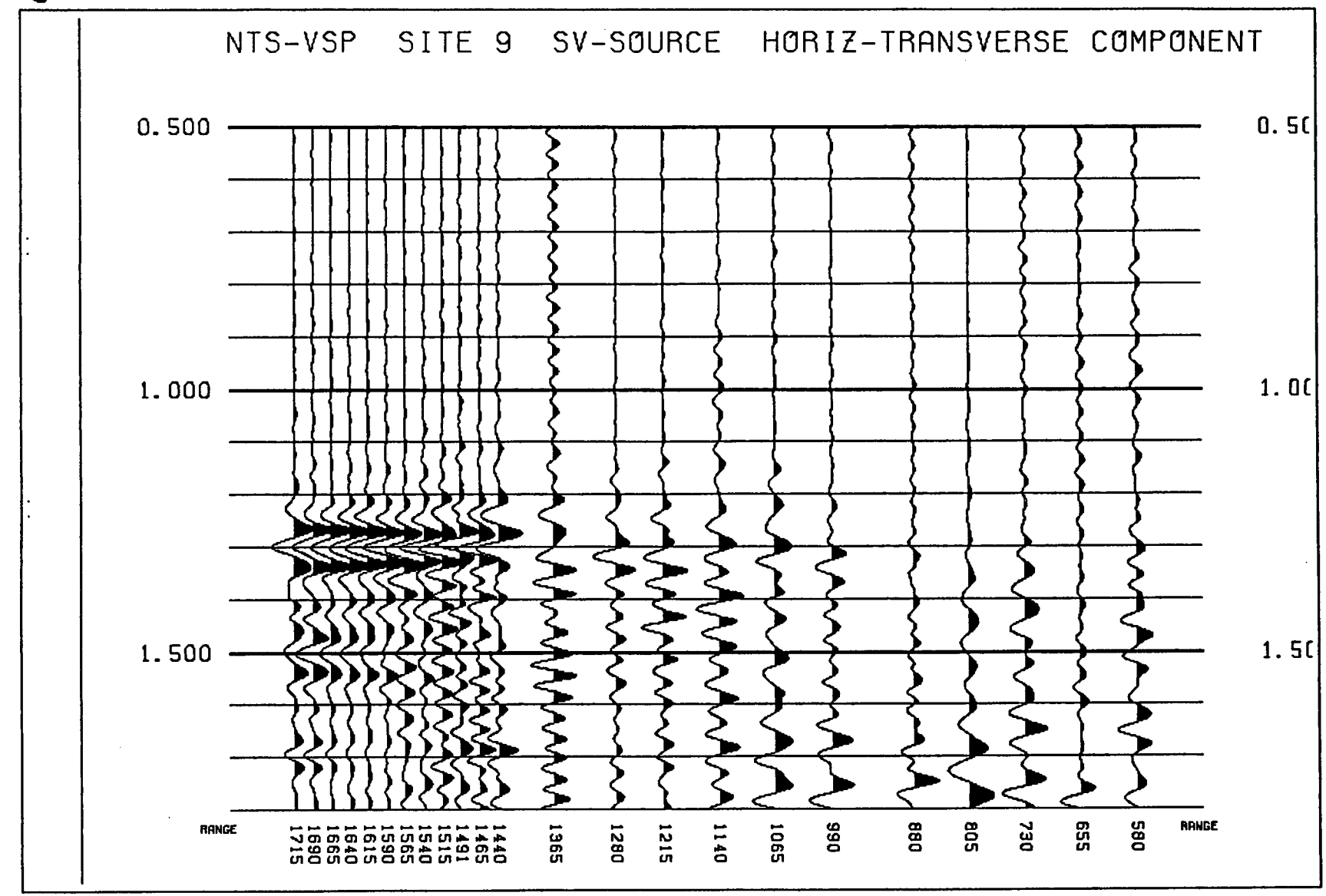

View File | Decimate
Stop | Redraw

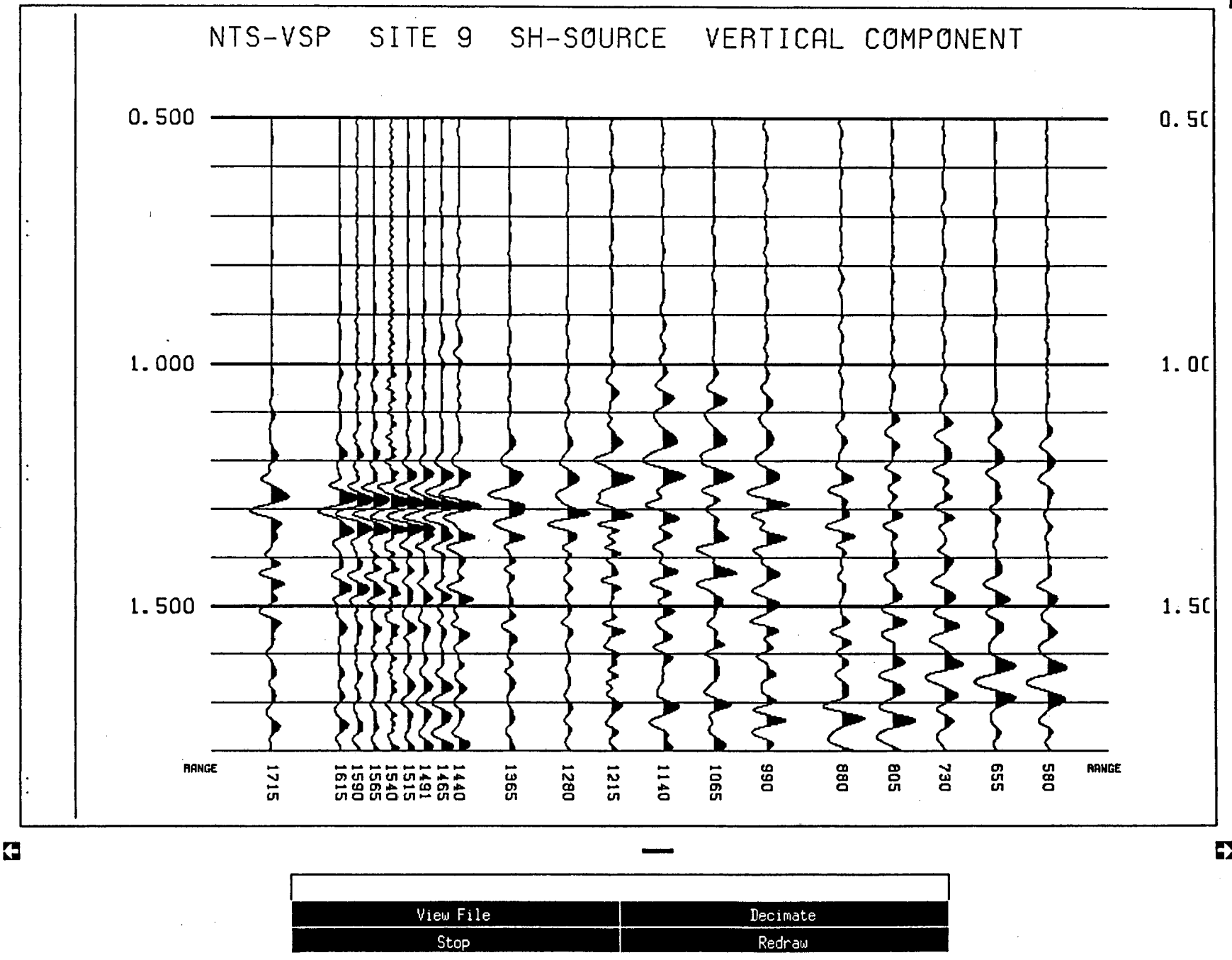
NTS-VSP SITE 9 SH-SOURCE VERTICAL COMPONENT
0.500
1.000
1.500
0.5C
1.0C
1.5C
RANGE
1715
1615
1590
1565
1540
1515
1491
1465
1440
1365
1280
1215
1140
1065
990
880
805
730
655
580
RANGE
View File
Decimate
Stop
Redraw

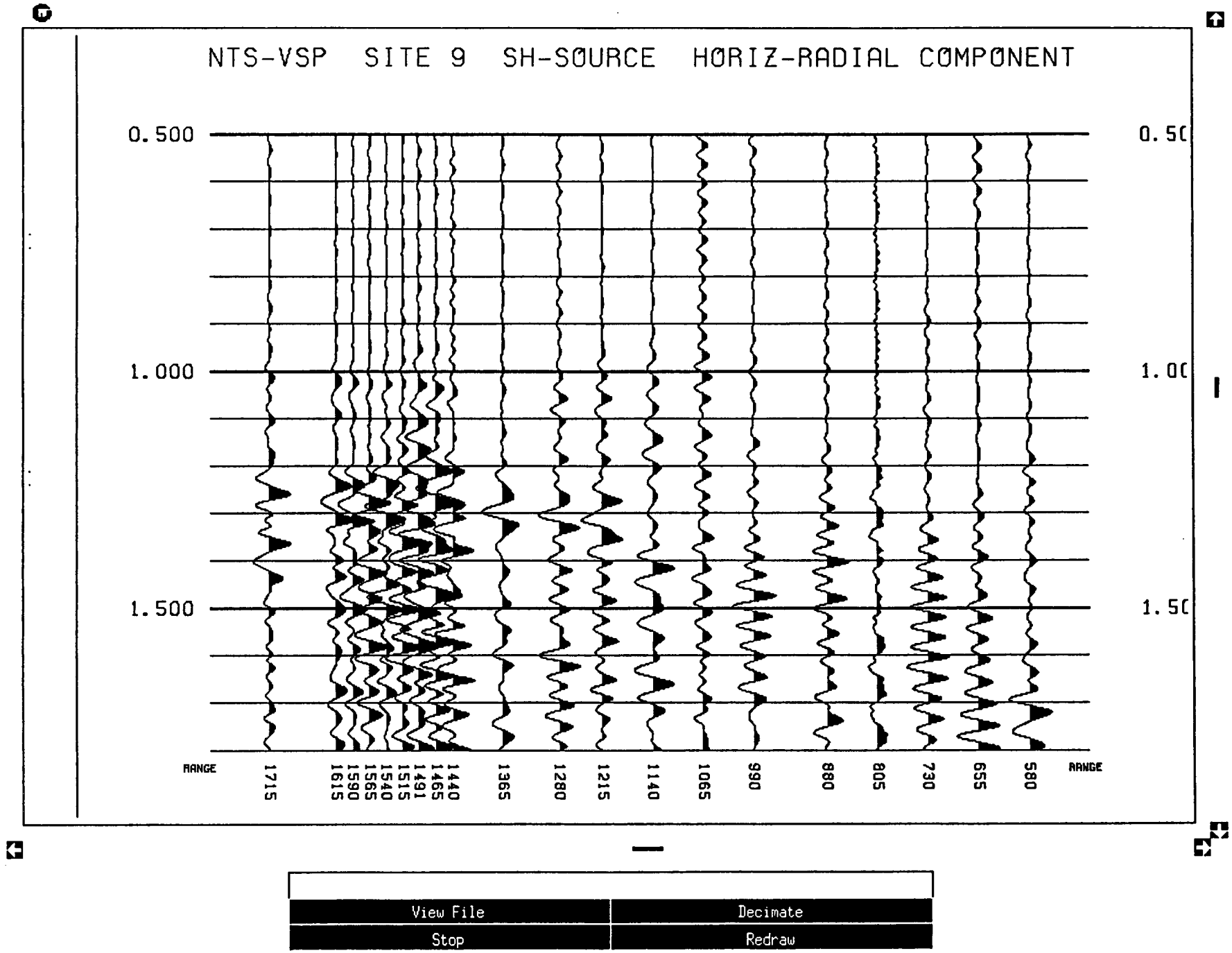
NTS-VSP SITE 9 SH-SOURCE HORIZ-RADIAL COMPONENT
0.500
1.000
1.500
0.5C
1.0C
1.5C
RANGE
1715
1615
1590
1565
1540
1515
1491
1465
1440
1365
1280
1215
1140
1065
990
880
805
730
655
580
RANGE
View File
Decimate
Stop
Redraw

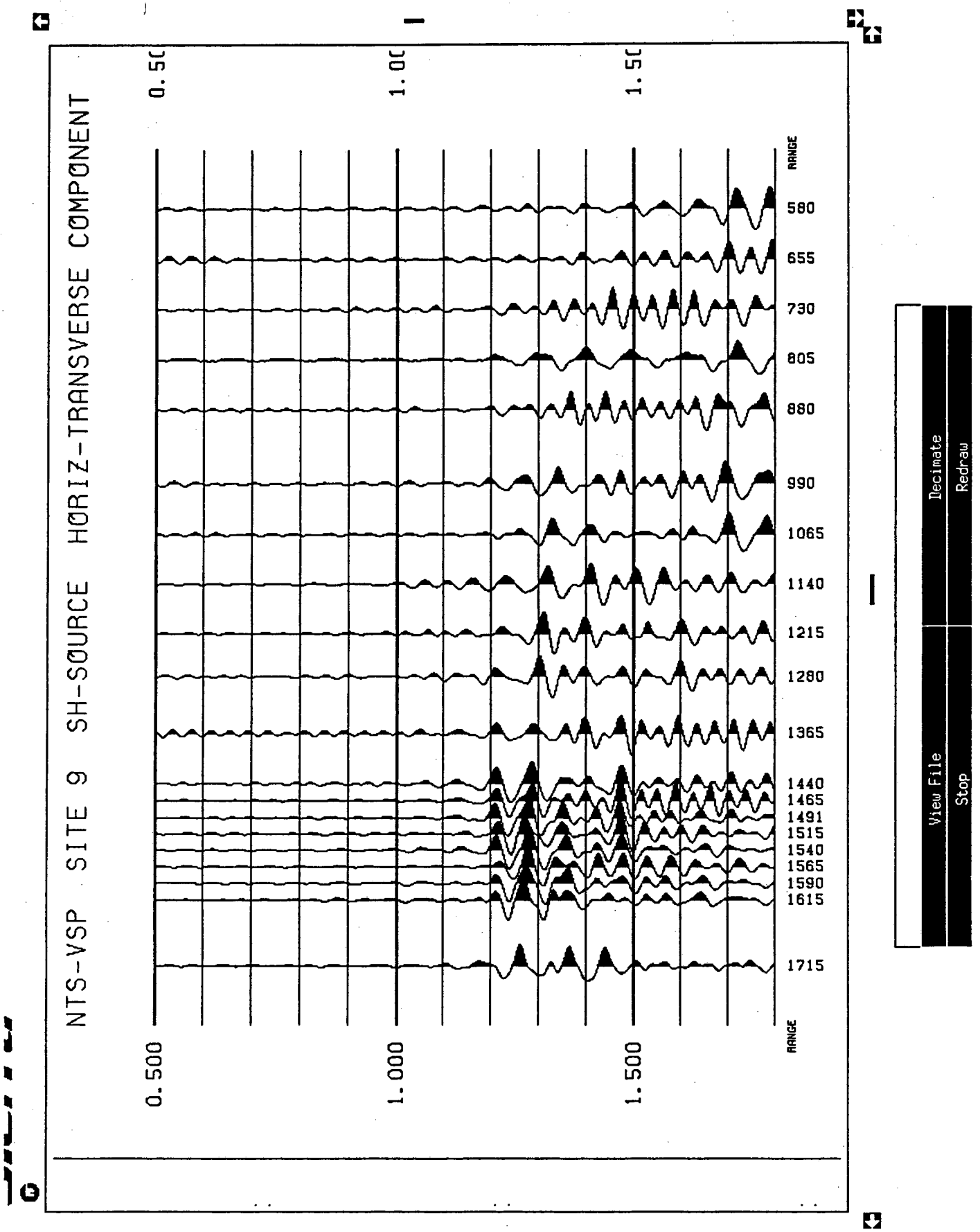
NTS-VSP SITE 9 SH-SOURCE HORIZ-TRANSVERSE COMPONENT
0.5
1.0
1.5
RANGE
580
655
730
805
880
990
1065
1140
1215
1280
1365
1440
1465
1491
1515
1540
1565
1590
1615
1715
RANGE
0.500
1.000
1.500
Decimate
Redraw
View File
Stop

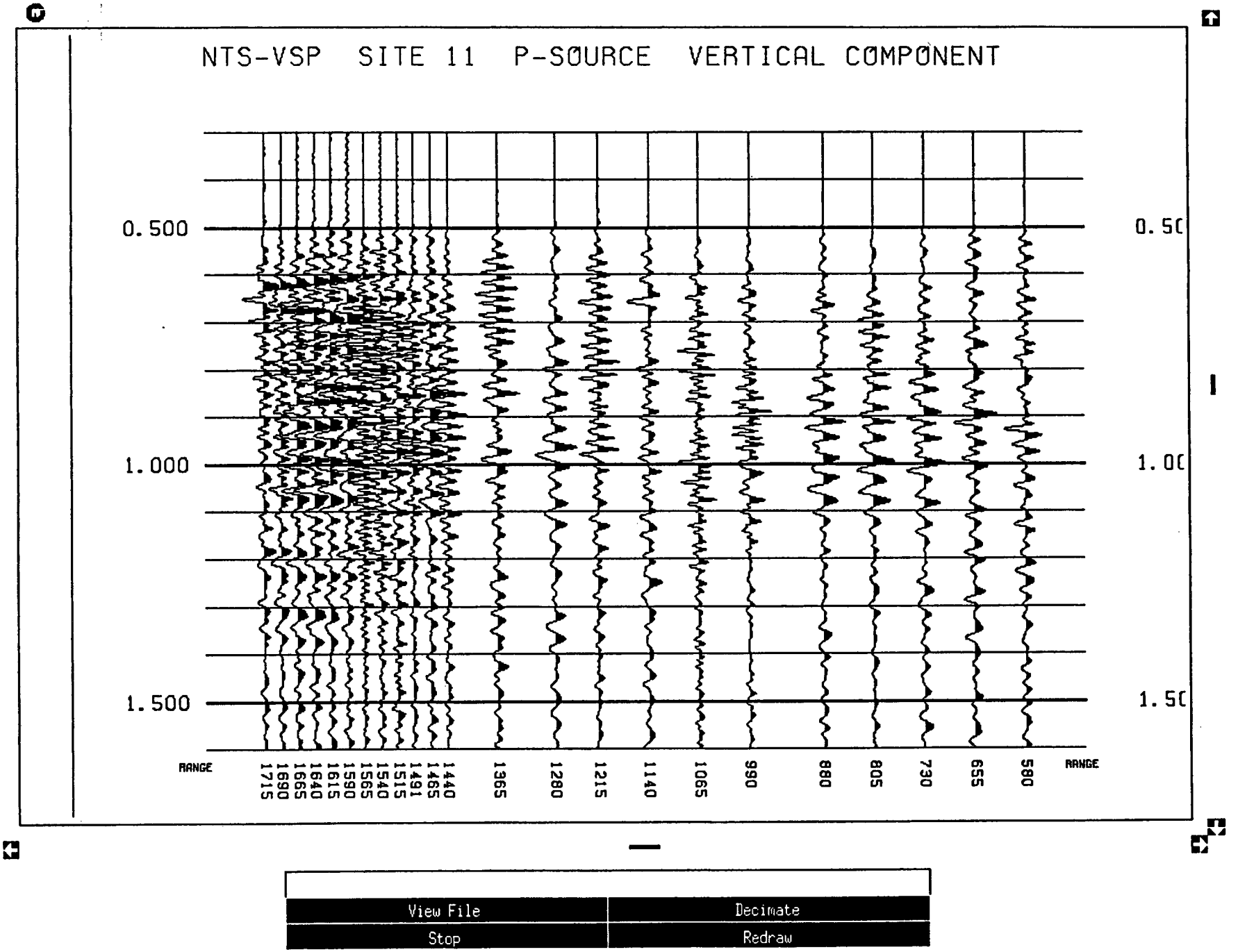
NTS-VSP SITE 11 P-SOURCE VERTICAL COMPONENT
0.500
1.000
1.500
RANGE
1715
1690
1665
1640
1615
1590
1565
1540
1515
1491
1465
1440
1365
1280
1215
1140
1065
990
880
805
730
655
580
RANGE
View File
Decimate
Stop
Redraw

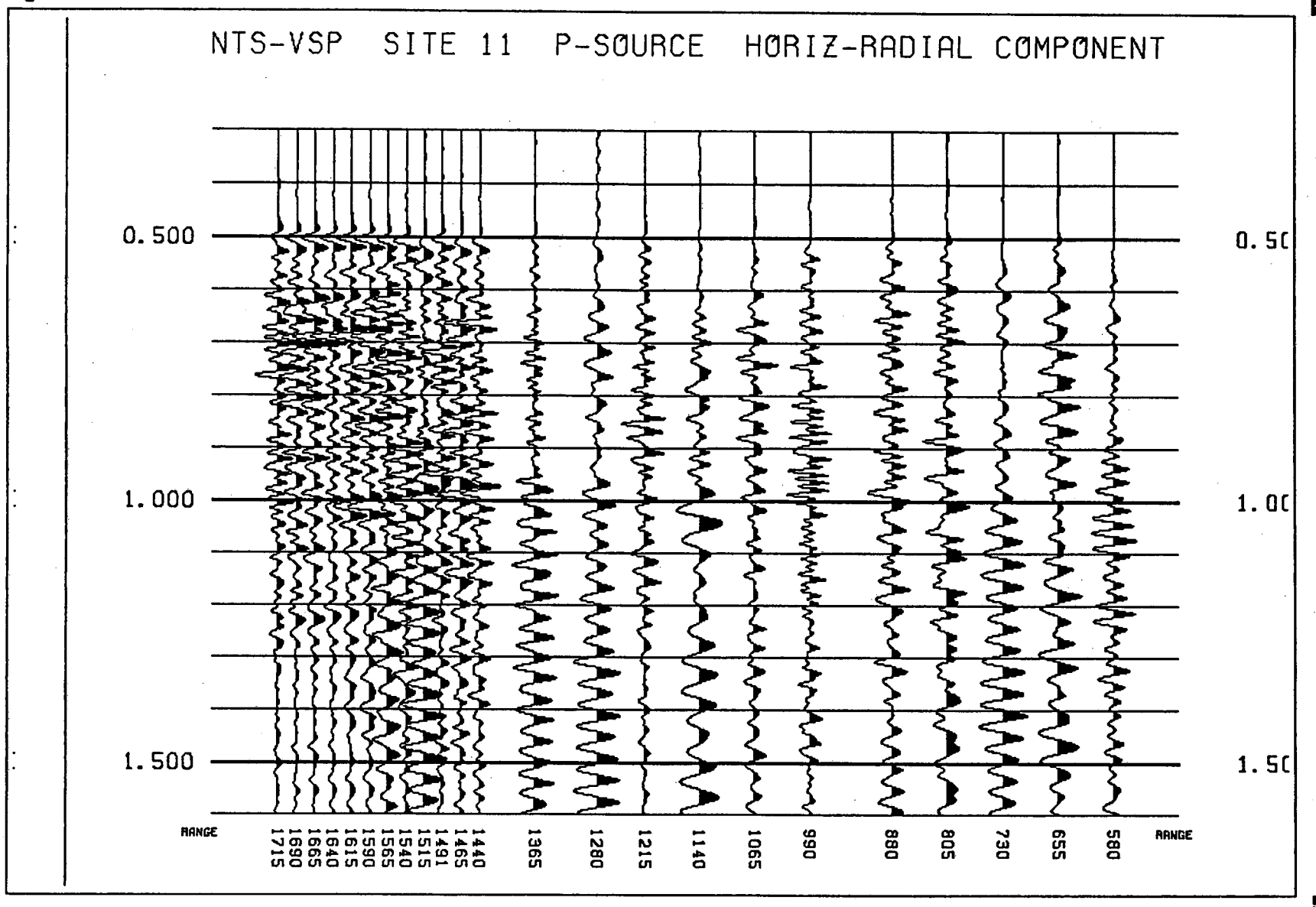
NTS-VSP SITE 11 P-SOURCE HORIZ-RADIAL COMPONENT
0.500
1.000
1.500
0.5C
1.0C
1.5C
RANGE
1715
1690
1665
1640
1615
1590
1565
1540
1515
1491
1465
1440
1365
1280
1215
1140
1065
990
880
805
730
655
580
RANGE
View File
Decimate
Stop
Redraw

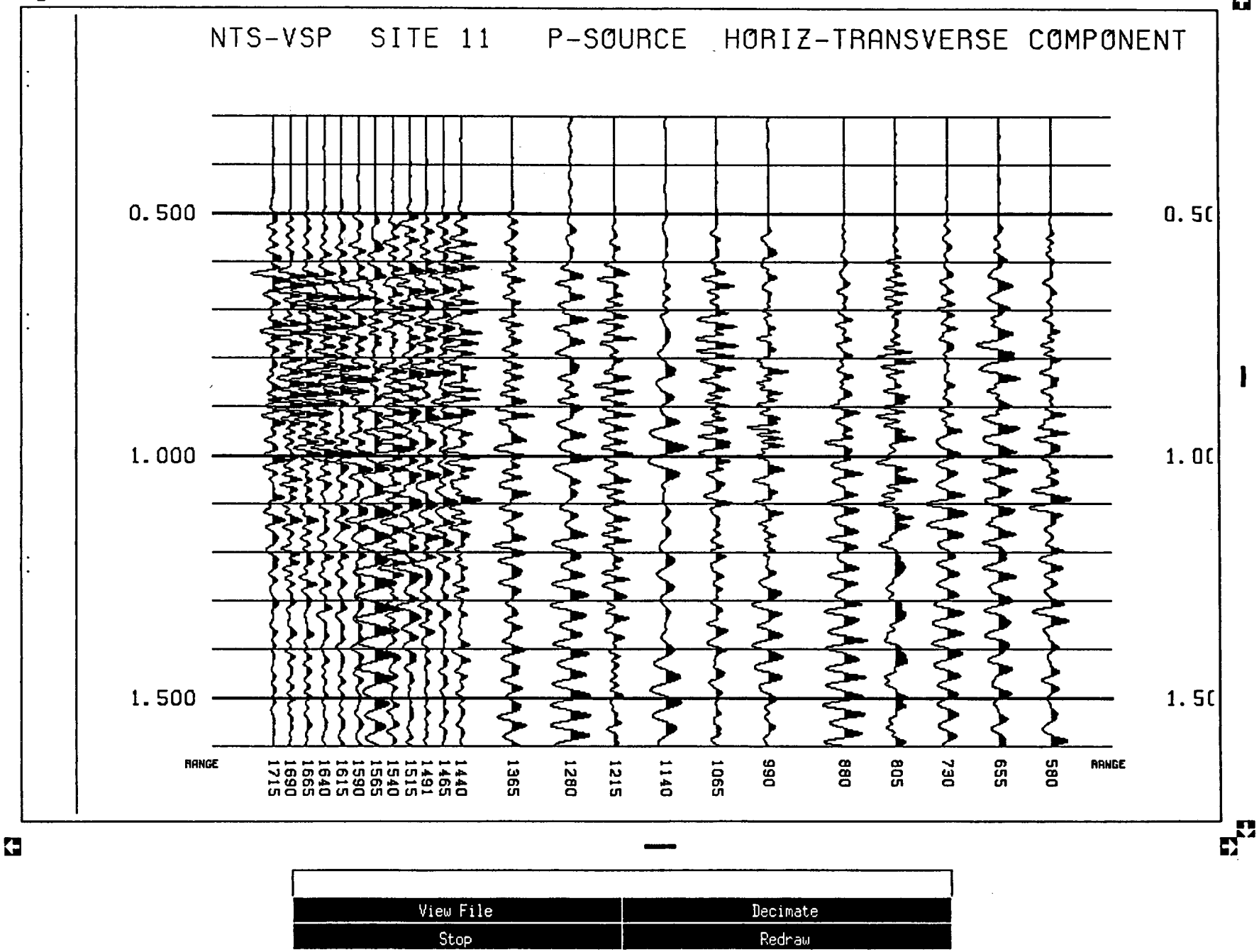
NTS-VSP SITE 11 P-SOURCE HORIZ-TRANSVERSE COMPONENT
0.500
1.000
1.500
0.5(
1.0(
1.5(
RANGE
1715
1690
1665
1640
1615
1590
1565
1540
1515
1491
1465
1440
1365
1280
1215
1140
1065
990
880
805
730
655
580
RANGE
View File
Decimate
Stop
Redraw

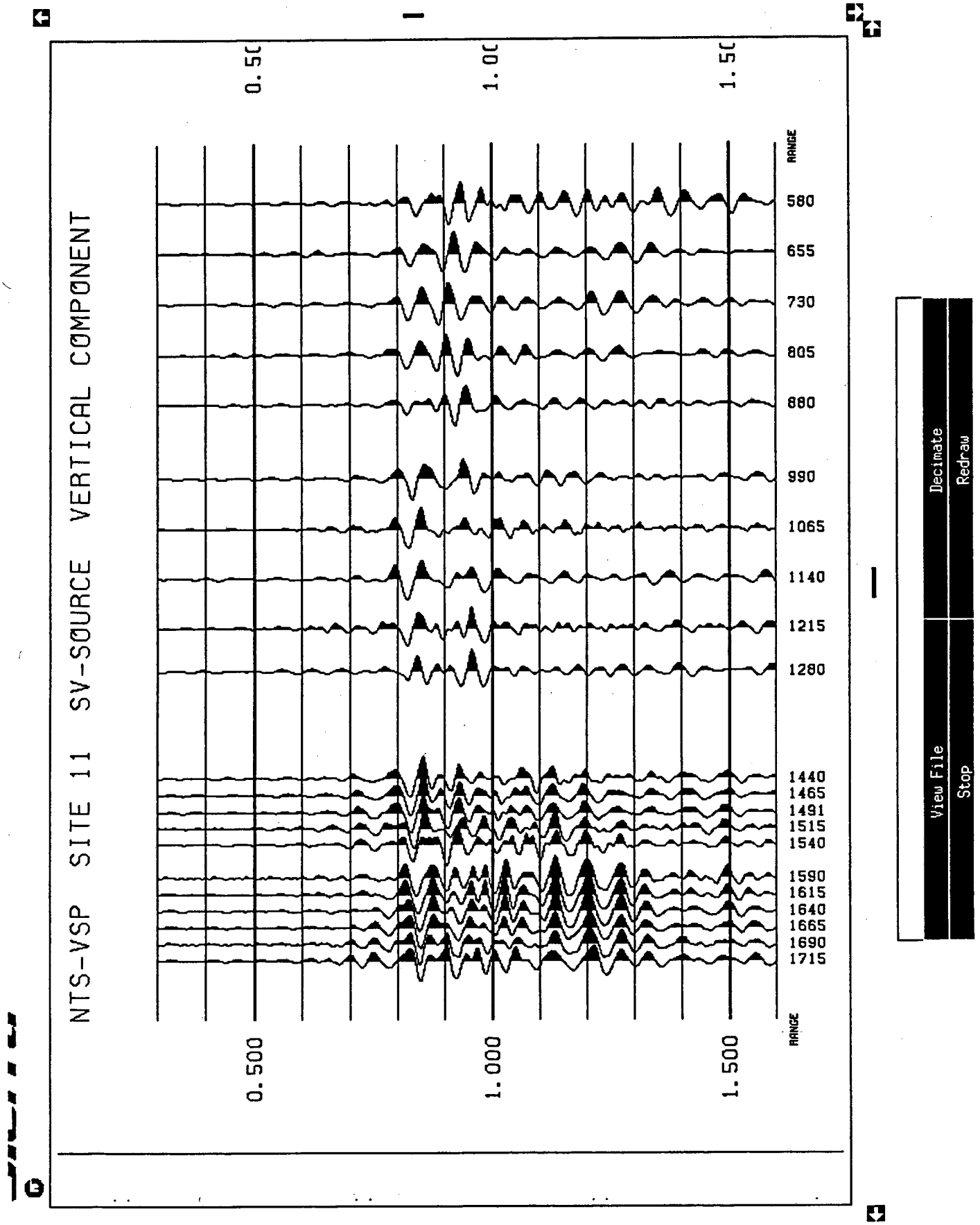
NTS-VSP SITE 11 SV-SOURCE VERTICAL COMPONENT
0.500
1.000
1.500
RANGE
580
655
730
805
880
990
1065
1140
1215
1280
1440
1465
1491
1515
1540
1590
1615
1640
1665
1690
1715
Decimate
Redraw
View File
Stop

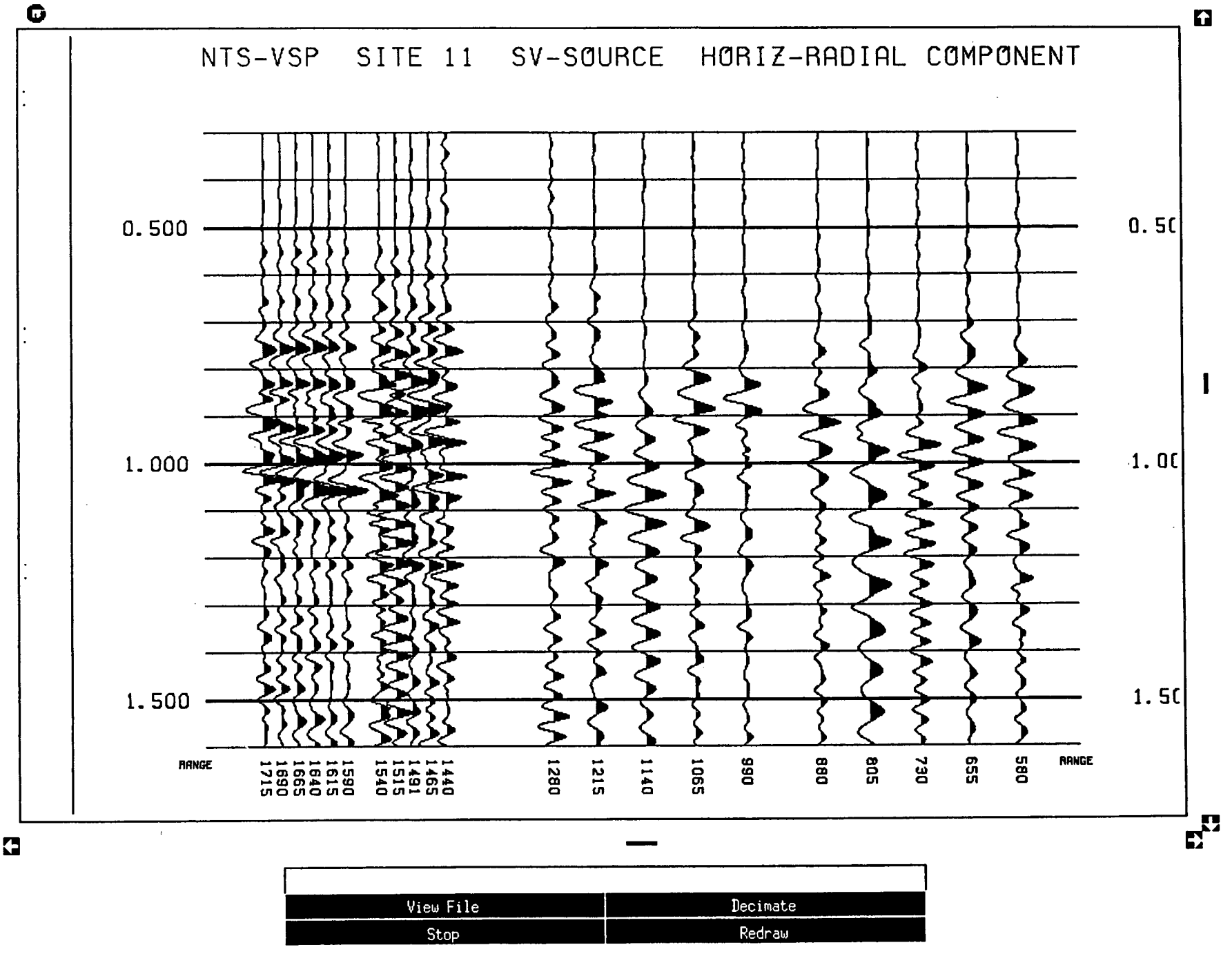
NTS-VSP SITE 11 SV-SOURCE HORIZ-RADIAL COMPONENT
0.500
1.000
1.500
RANGE
1715
1690
1665
1640
1615
1590
1540
1515
1491
1465
1440
1280
1215
1140
1065
990
880
805
730
655
580
RANGE
View File
Decimate
Stop
Redraw

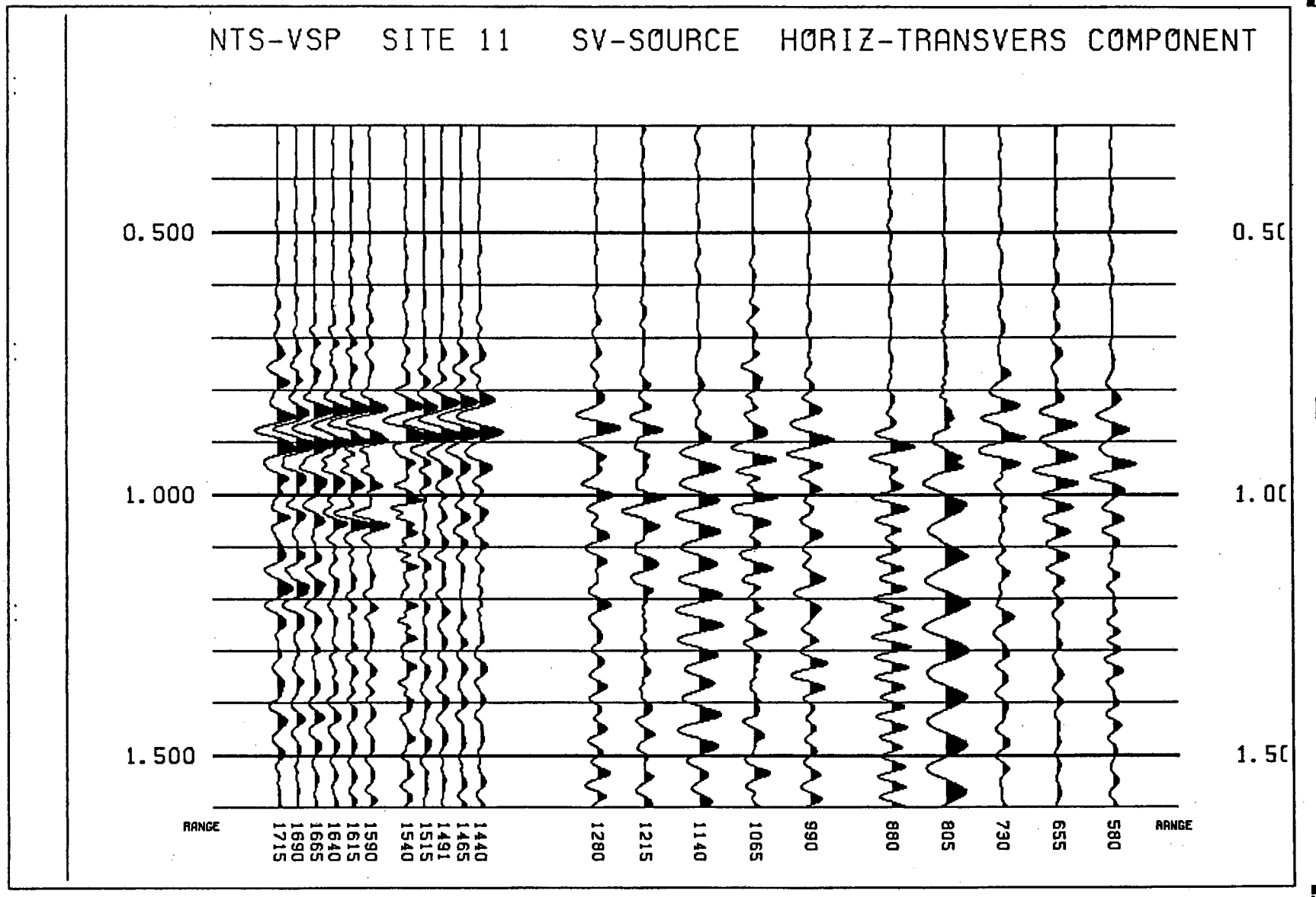
NTS-VSP SITE 11 SV-SOURCE HORIZ-TRANSVERS COMPONENT
0.500
1.000
1.500
0.50
1.00
1.50
RANGE
1715
1690
1665
1640
1615
1590
1540
1515
1491
1465
1440
1280
1215
1140
1065
990
880
805
730
655
580
RANGE
View File
Decimate
Stop
Redraw

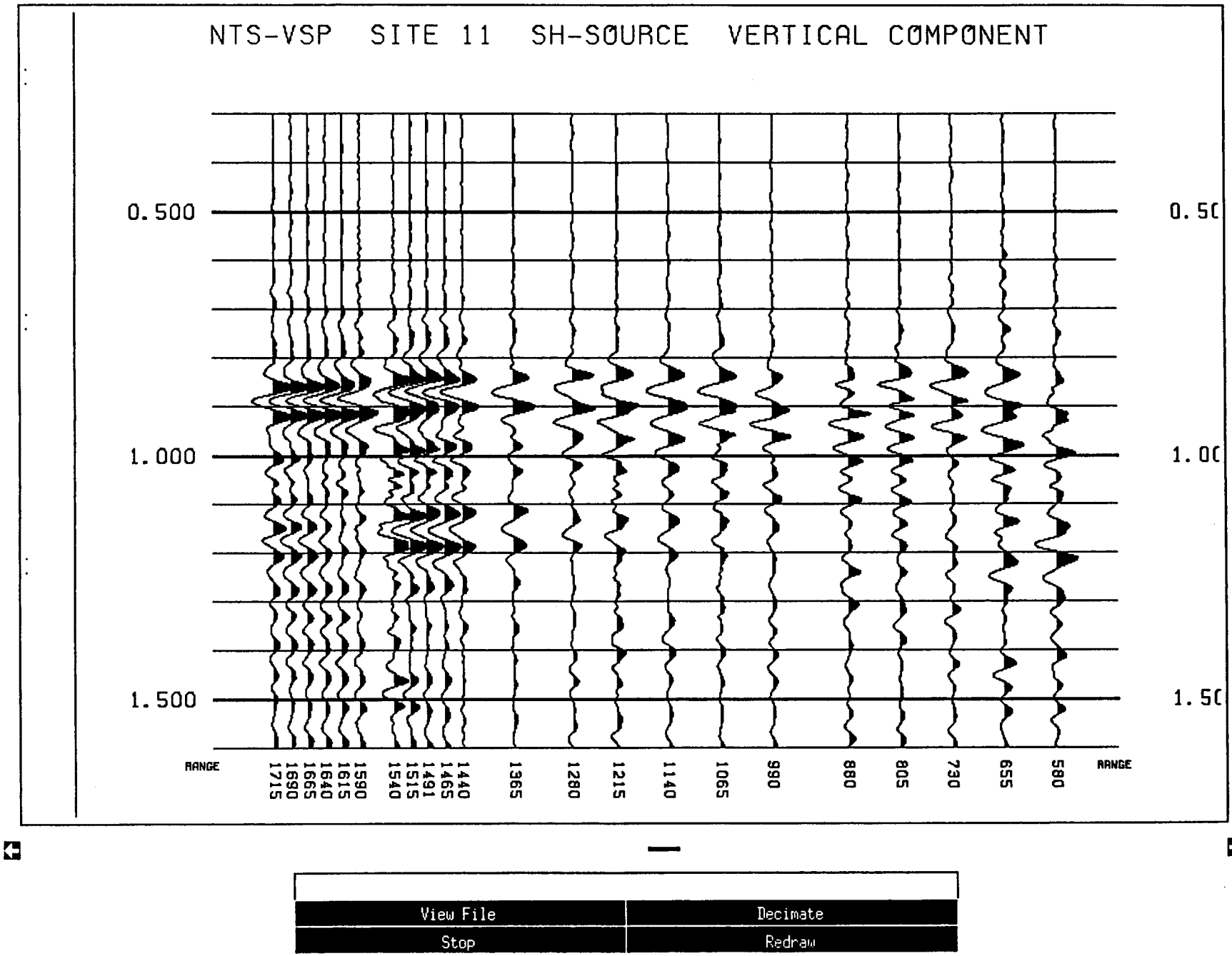
NTS-VSP SITE 11 SH-SOURCE VERTICAL COMPONENT
0.500
1.000
1.500
0.5C
1.0C
1.5C
RANGE
1715
1690
1665
1640
1615
1590
1540
1515
1491
1465
1440
1365
1280
1215
1140
1065
990
880
805
730
655
580
RANGE
View File
Decimate
Stop
Redraw

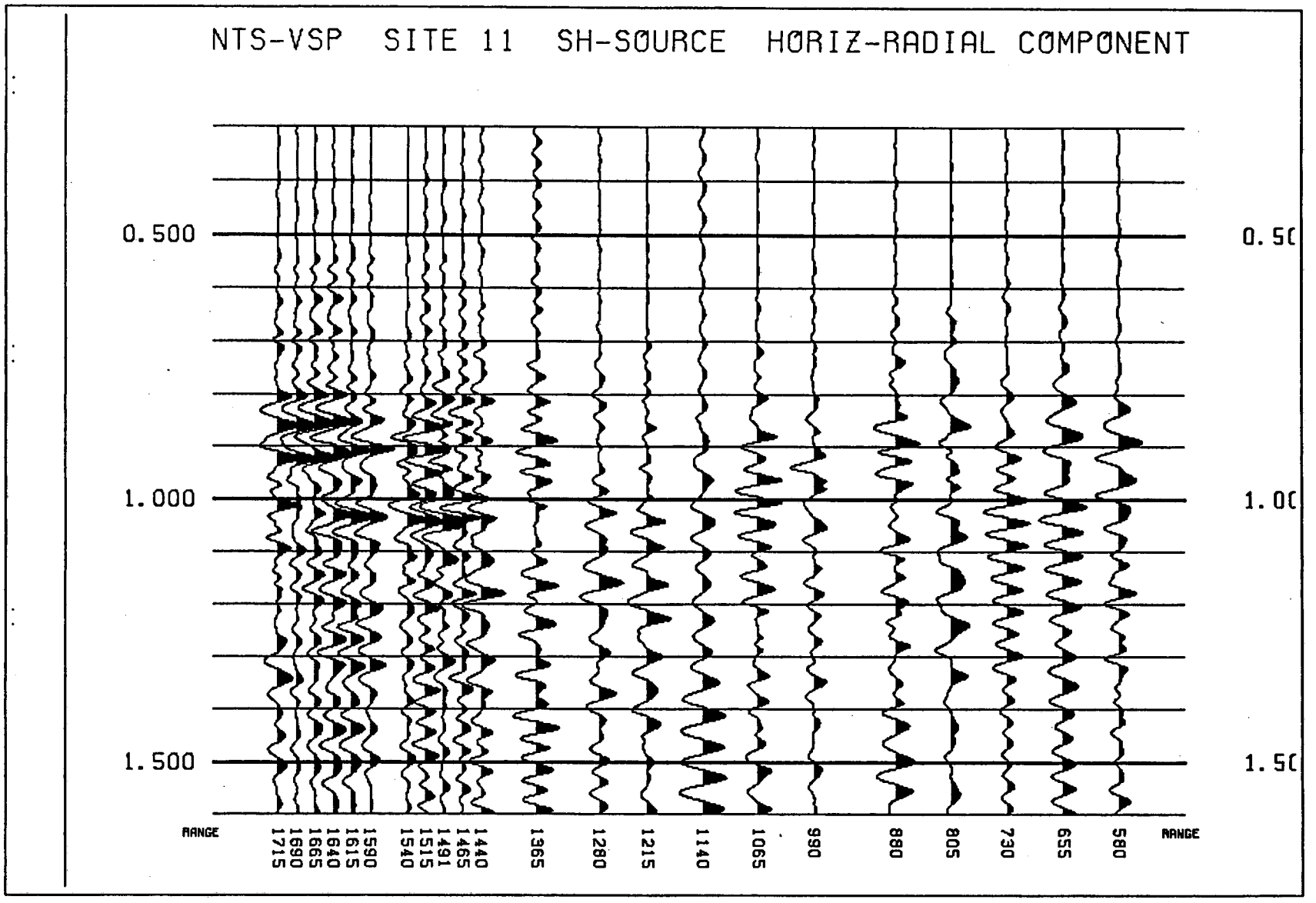

View File | Decimate

Stop | Redraw

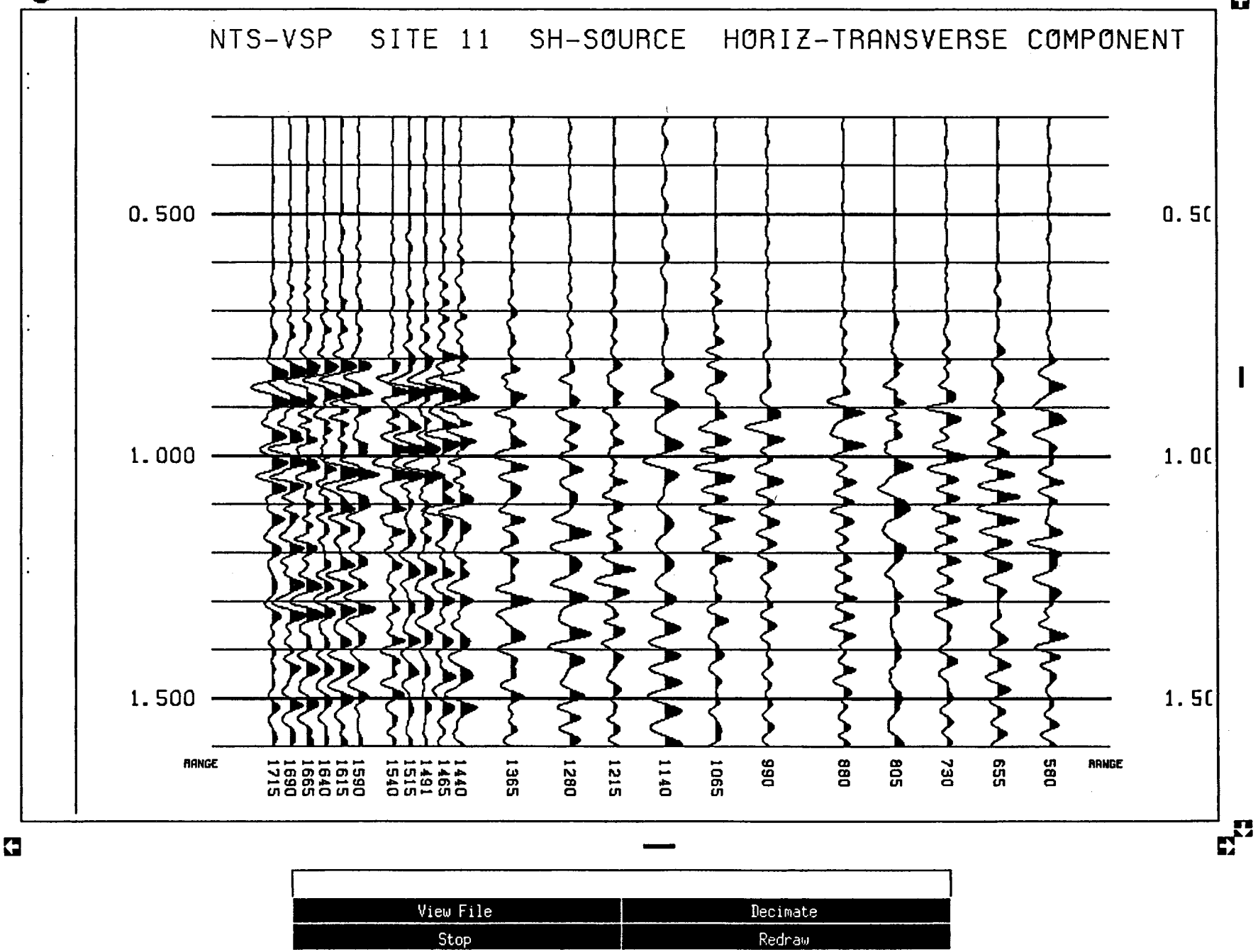
NTS-VSP SITE 11 SH-SOURCE HORIZ-TRANSVERSE COMPONENT
0.500
1.000
1.500
0.50
1.00
1.50
RANGE
1715
1690
1665
1640
1615
1590
1540
1515
1491
1465
1440
1365
1280
1215
1140
1065
990
880
805
730
655
580
RANGE
View File
Decimate
Stop
Redraw

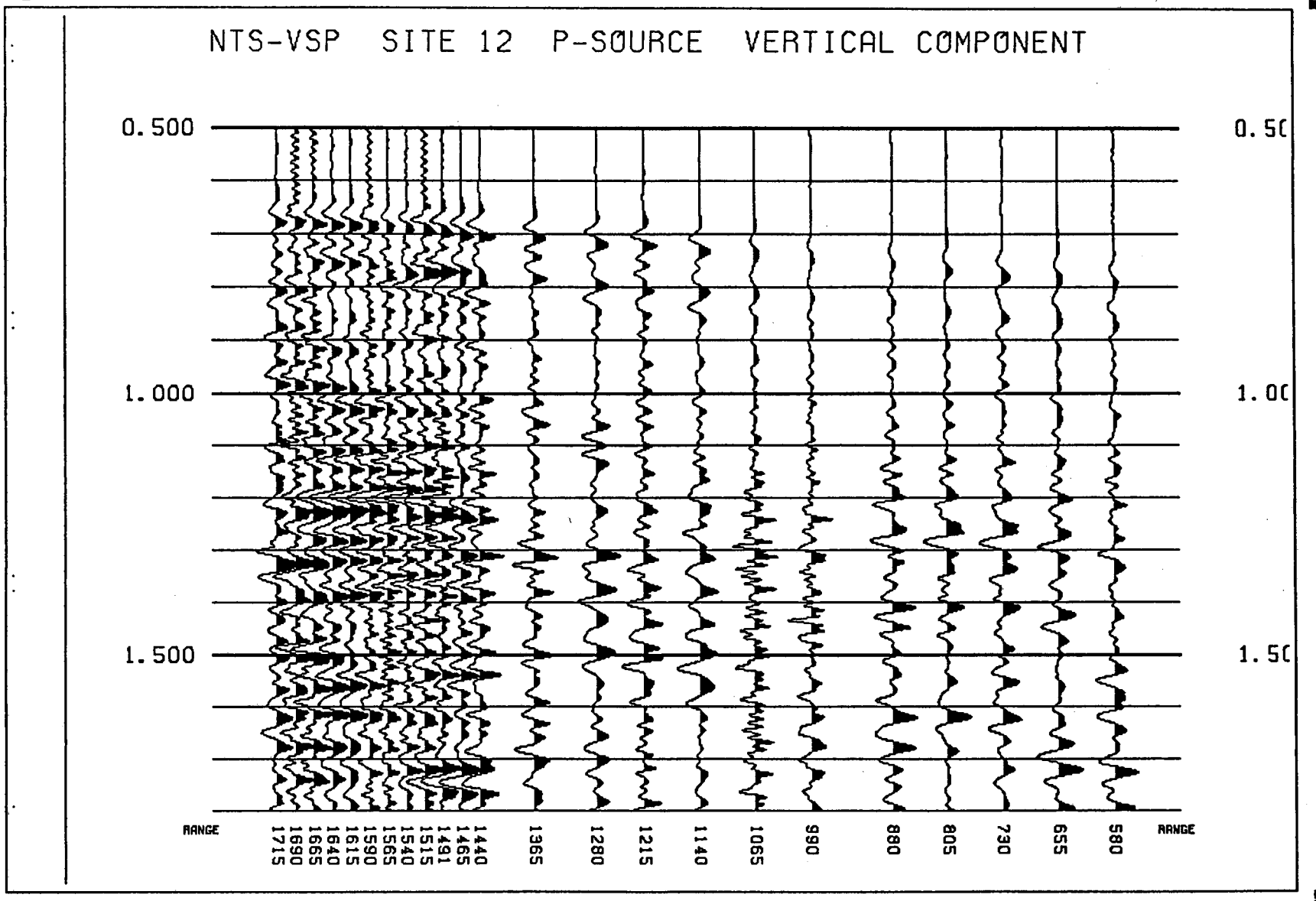
NTS-VSP SITE 12 P-SOURCE VERTICAL COMPONENT
0.500
1.000
1.500
0.5C
1.0C
1.5C
RANGE
1715
1690
1665
1640
1615
1590
1565
1540
1515
1491
1465
1440
1365
1280
1215
1140
1065
990
880
805
730
655
580
RANGE
View File
Decimate
Stop
Redraw

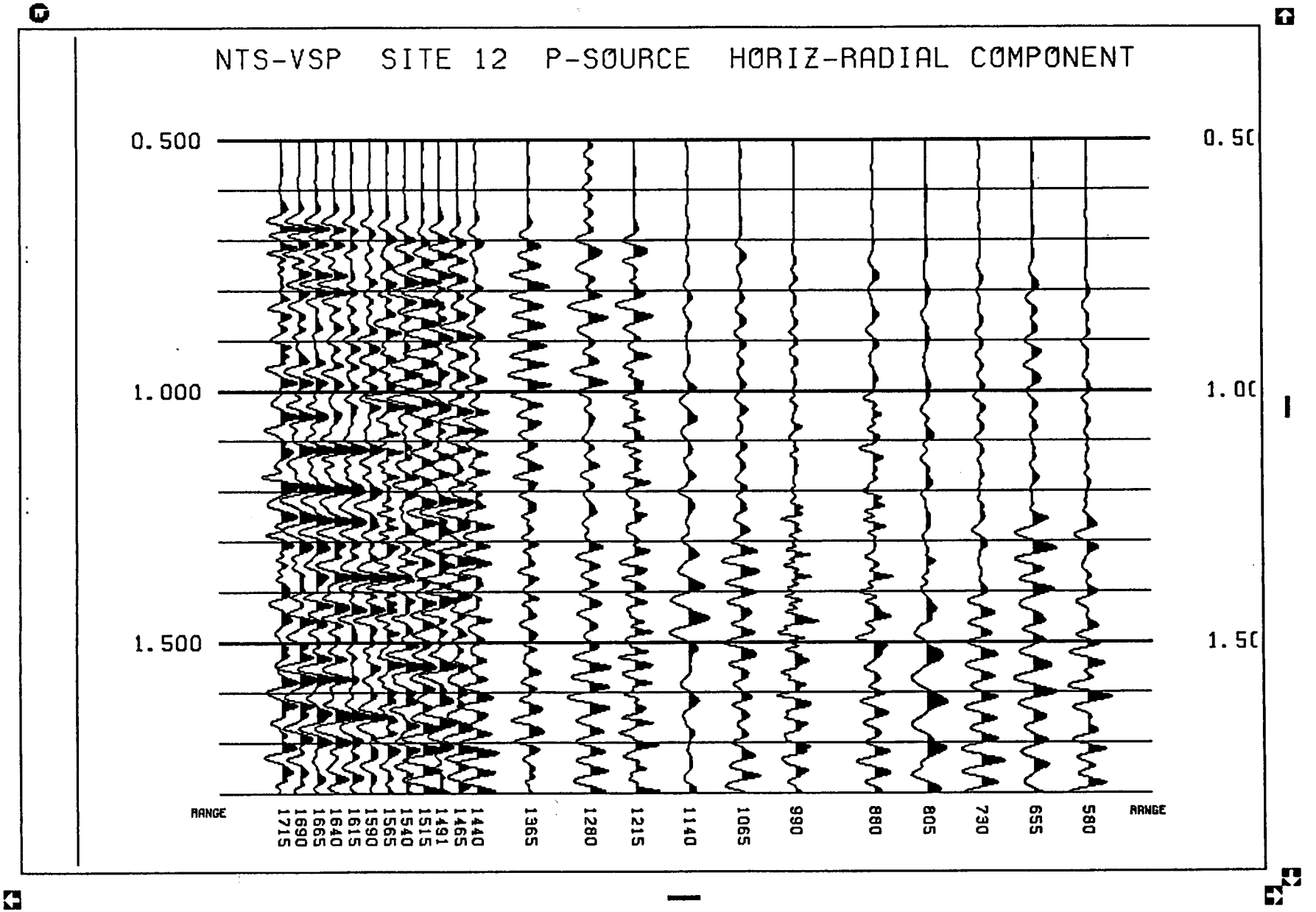
NTS-VSP SITE 12 P-SOURCE HORIZ-RADIAL COMPONENT
0.500
1.000
1.500
0.5C
1.0C
1.5C
RANGE
1715
1690
1665
1640
1615
1590
1565
1540
1515
1491
1465
1440
1365
1280
1215
1140
1065
990
880
805
730
655
580
RANGE
View File
Decimate
Stop
Redraw

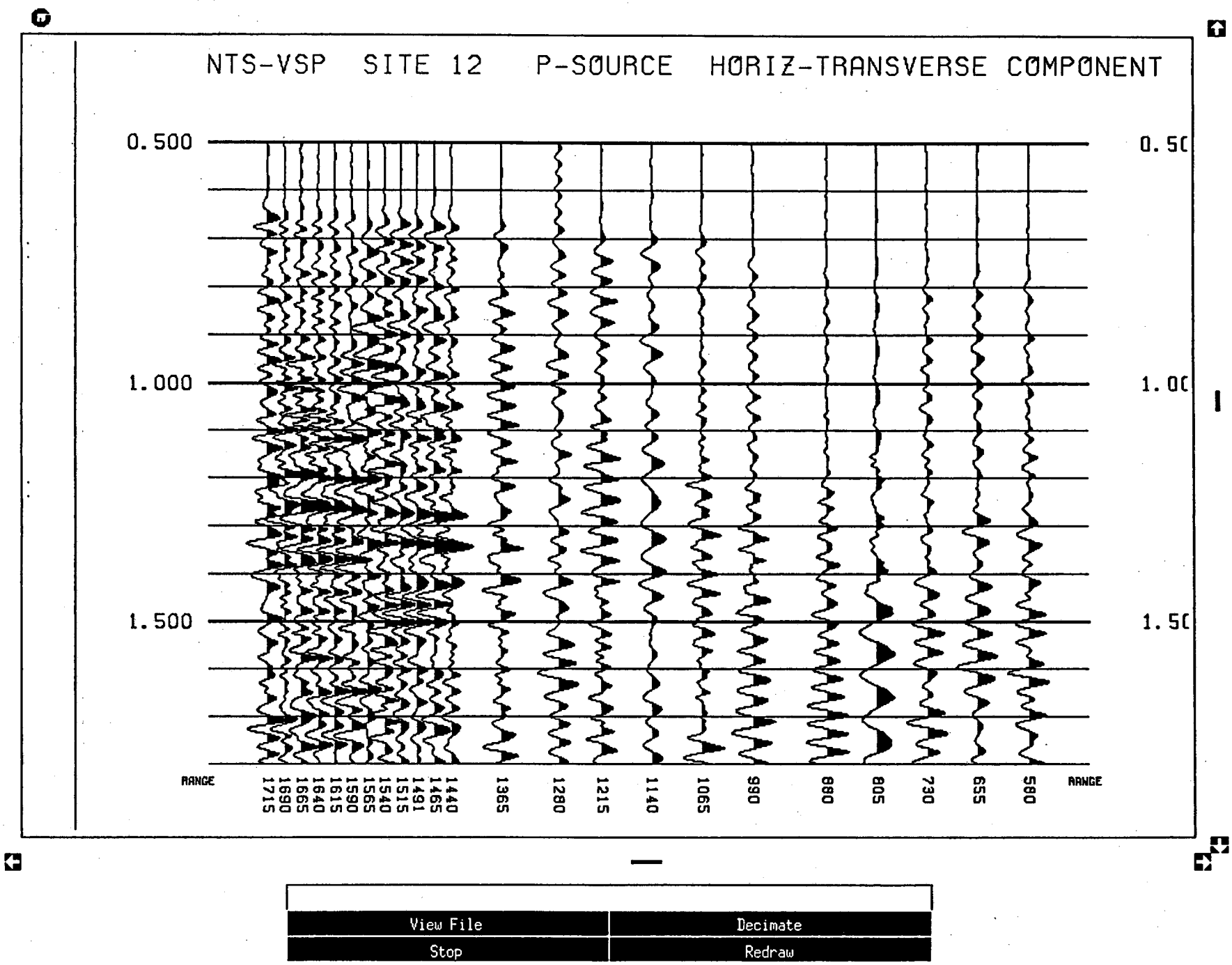
NTS-VSP SITE 12 P-SOURCE HORIZ-TRANSVERSE COMPONENT
0.500
1.000
1.500
0.5C
1.0C
1.5C
RANGE
1715
1690
1665
1640
1615
1590
1565
1540
1515
1491
1465
1440
1365
1280
1215
1140
1065
990
880
805
730
655
580
RANGE
View File
Decimate
Stop
Redraw

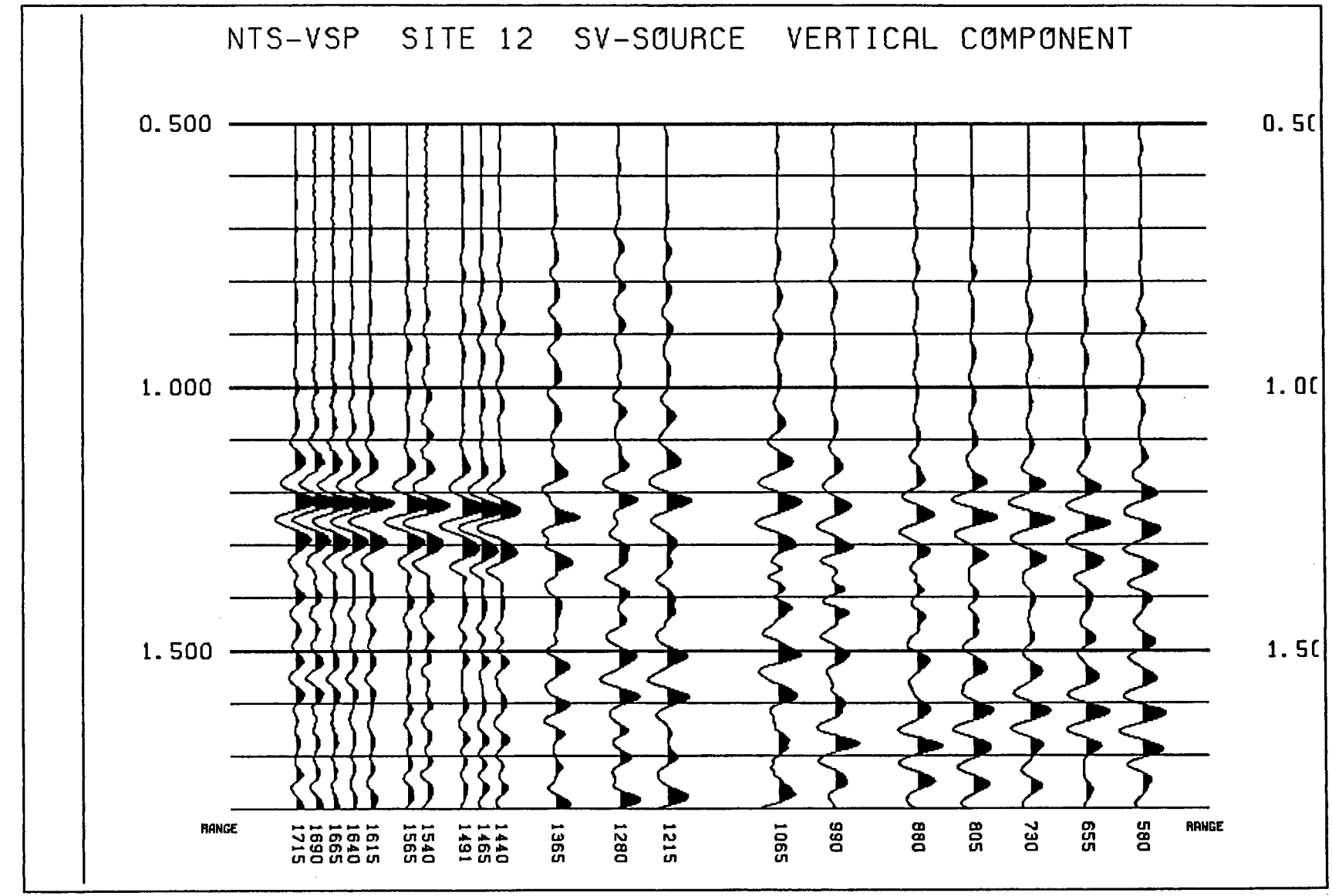
NTS-VSP SITE 12 SV-SOURCE VERTICAL COMPONENT
0.500
1.000
1.500
RANGE
1715
1690
1665
1640
1615
1565
1540
1491
1465
1440
1365
1280
1215
1065
990
880
805
730
655
580
RANGE
View File
Decimate
Stop
Redraw

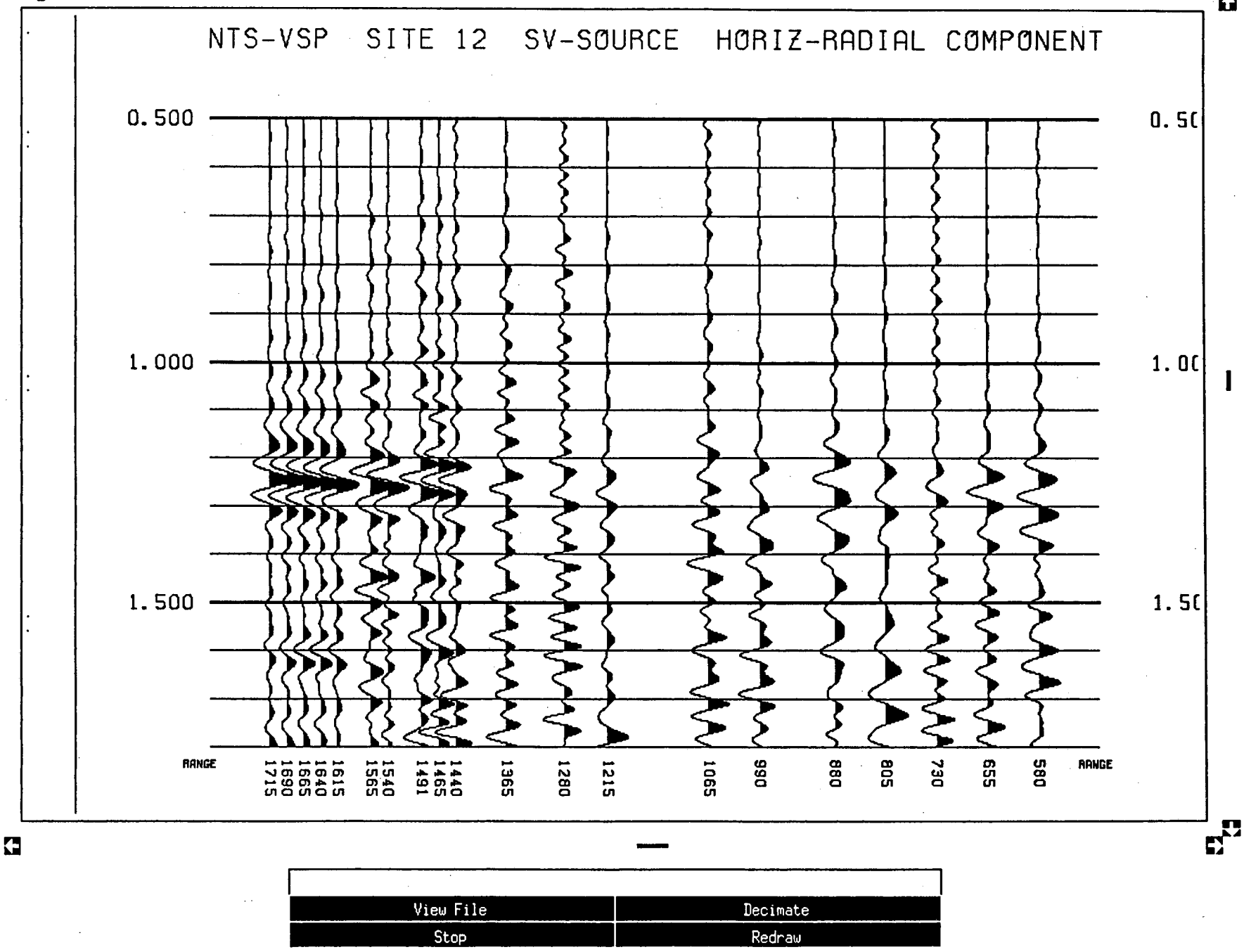
NTS-VSP SITE 12 SV-SOURCE HORIZ-RADIAL COMPONENT
0.500
1.000
1.500
RANGE
1715
1690
1665
1640
1615
1565
1540
1491
1465
1440
1365
1280
1215
1065
990
880
805
730
655
580
RANGE
View File
Decimate
Stop
Redraw

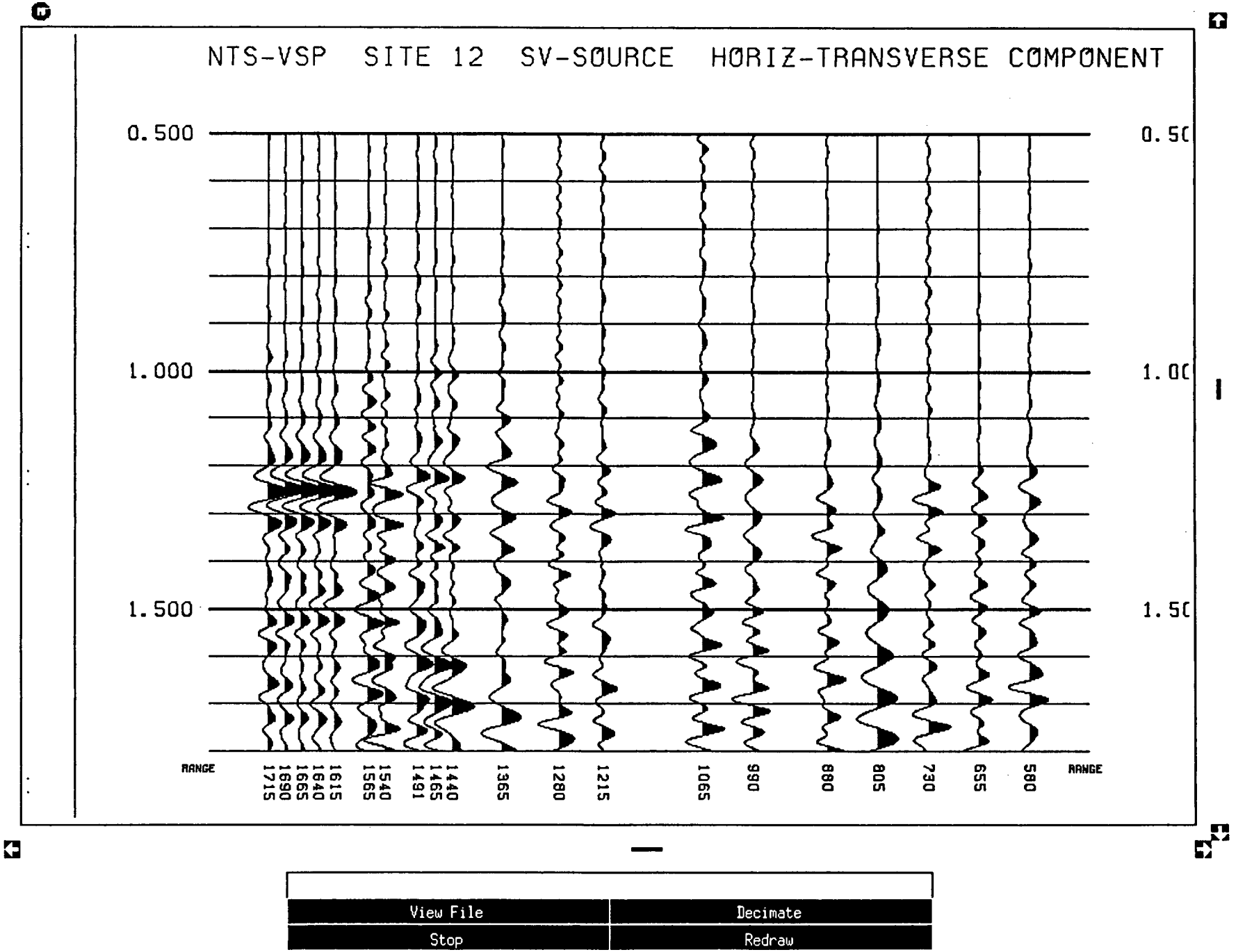
NTS-VSP SITE 12 SV-SOURCE HORIZ-TRANSVERSE COMPONENT
0.500
1.000
1.500
0.5(
1.0(
1.5(
RANGE
1715
1690
1665
1640
1615
1565
1540
1491
1465
1440
1365
1280
1215
1065
990
880
805
730
655
580
RANGE
View File
Decimate
Stop
Redraw

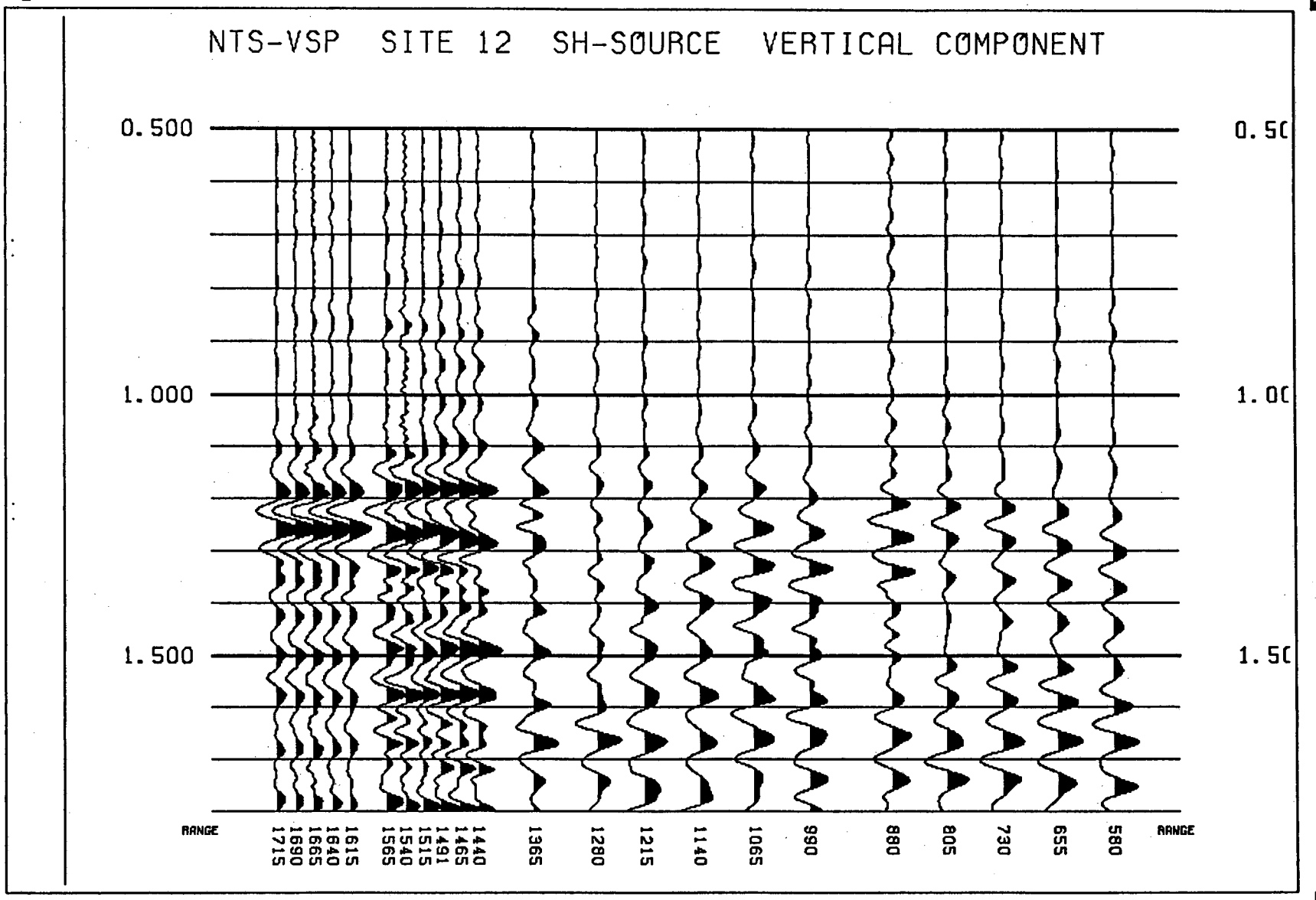
NTS-VSP SITE 12 SH-SOURCE VERTICAL COMPONENT
0.500
1.000
1.500
0.50
1.00
1.50
RANGE
1715
1690
1665
1640
1615
1565
1540
1515
1491
1465
1440
1365
1280
1215
1140
1065
990
880
805
730
655
580
RANGE
View File
Decimate
Stop
Redraw

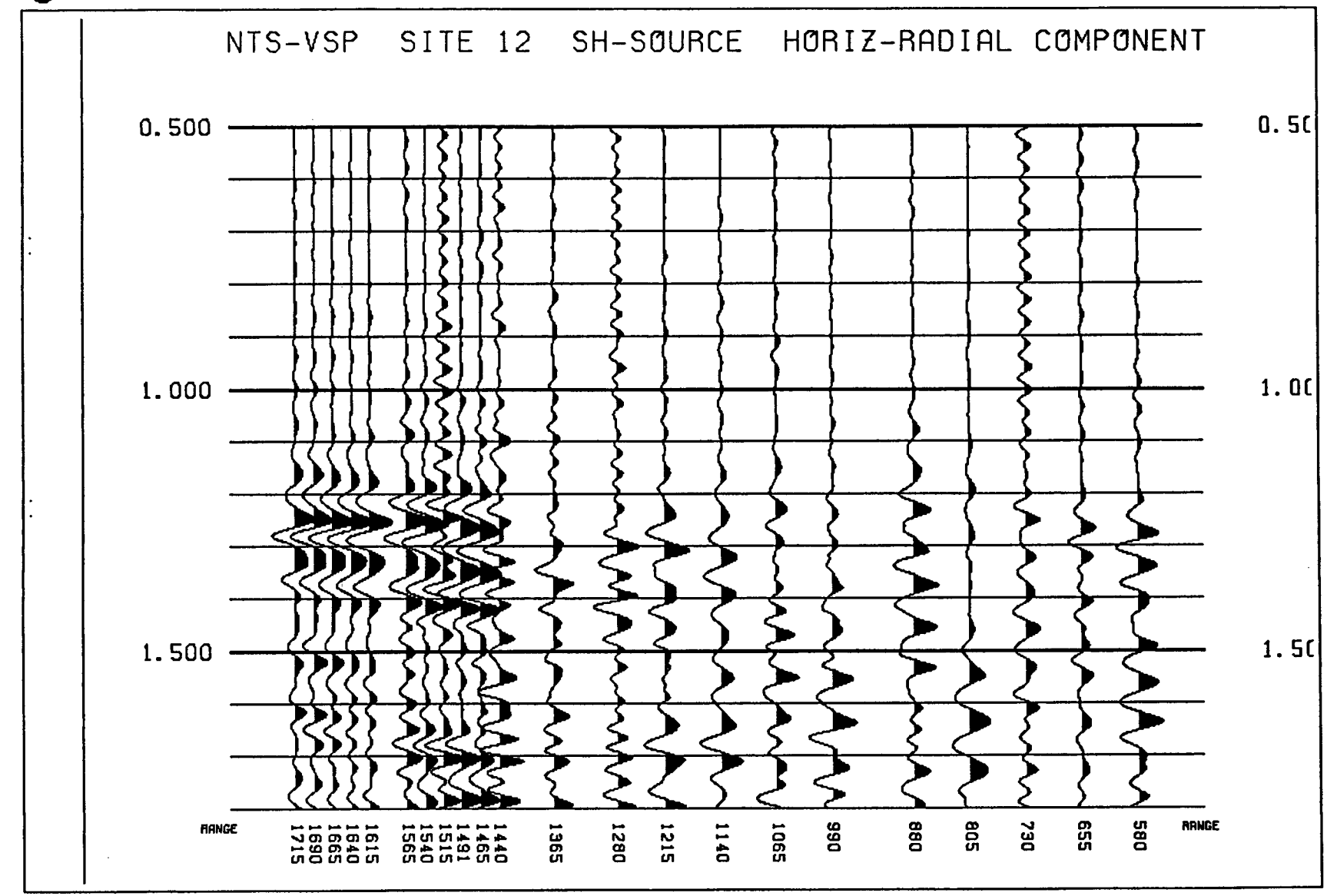
NTS-VSP SITE 12 SH-SOURCE HORIZ-RADIAL COMPONENT
0.500
1.000
1.500
0.50
1.00
1.50
RANGE
1715
1690
1665
1640
1615
1595
1540
1515
1491
1465
1440
1365
1280
1215
1140
1065
990
880
805
730
655
580
RANGE
View File
Decimate
Stop
Redraw

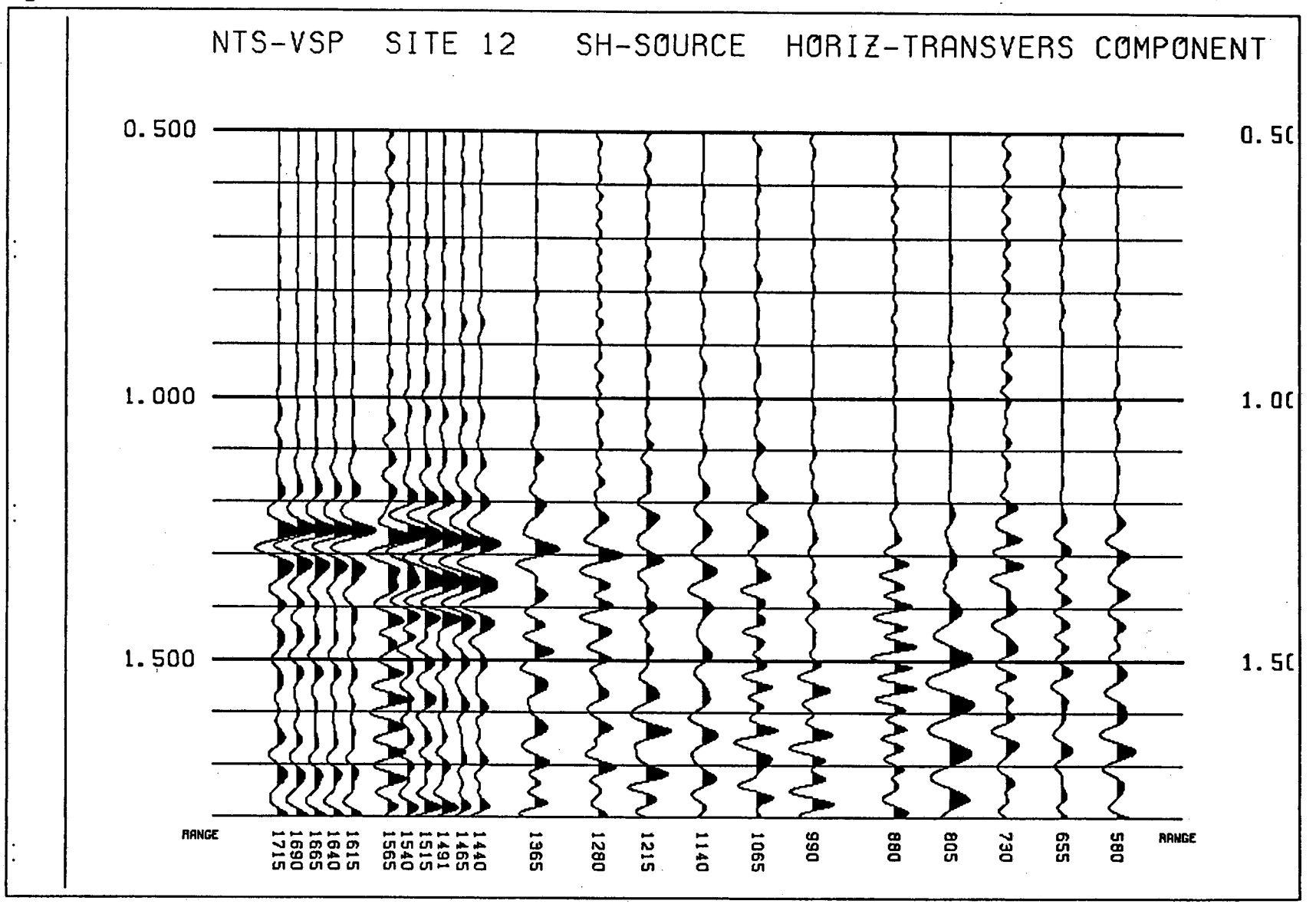
NTS-VSP SITE 12 SH-SOURCE HORIZ-TRANSVERS COMPONENT
0.500
1.000
1.500
0.50
1.00
1.50
RANGE
1715
1690
1665
1640
1615
1590
1565
1540
1515
1491
1465
1440
1365
1290
1215
1140
1065
990
880
805
730
655
580
RANGE
View File
Decimate
Stop
Redraw

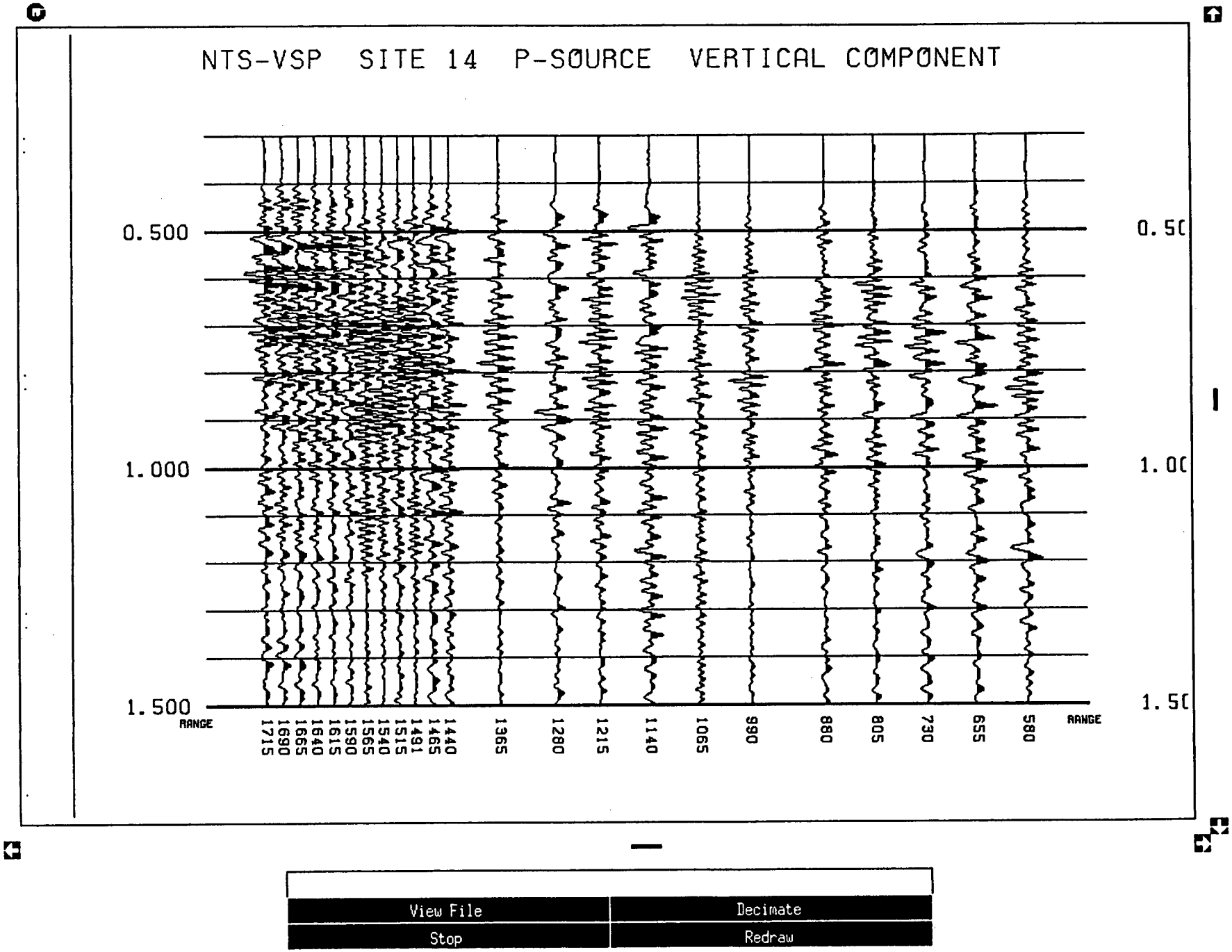
NTS-VSP SITE 14 P-SOURCE VERTICAL COMPONENT
0.500
1.000
1.500
RANGE
1715
1690
1665
1640
1615
1590
1565
1540
1515
1491
1465
1440
1365
1280
1215
1140
1065
990
880
805
730
655
580
RANGE
View File
Decimate
Stop
Redraw

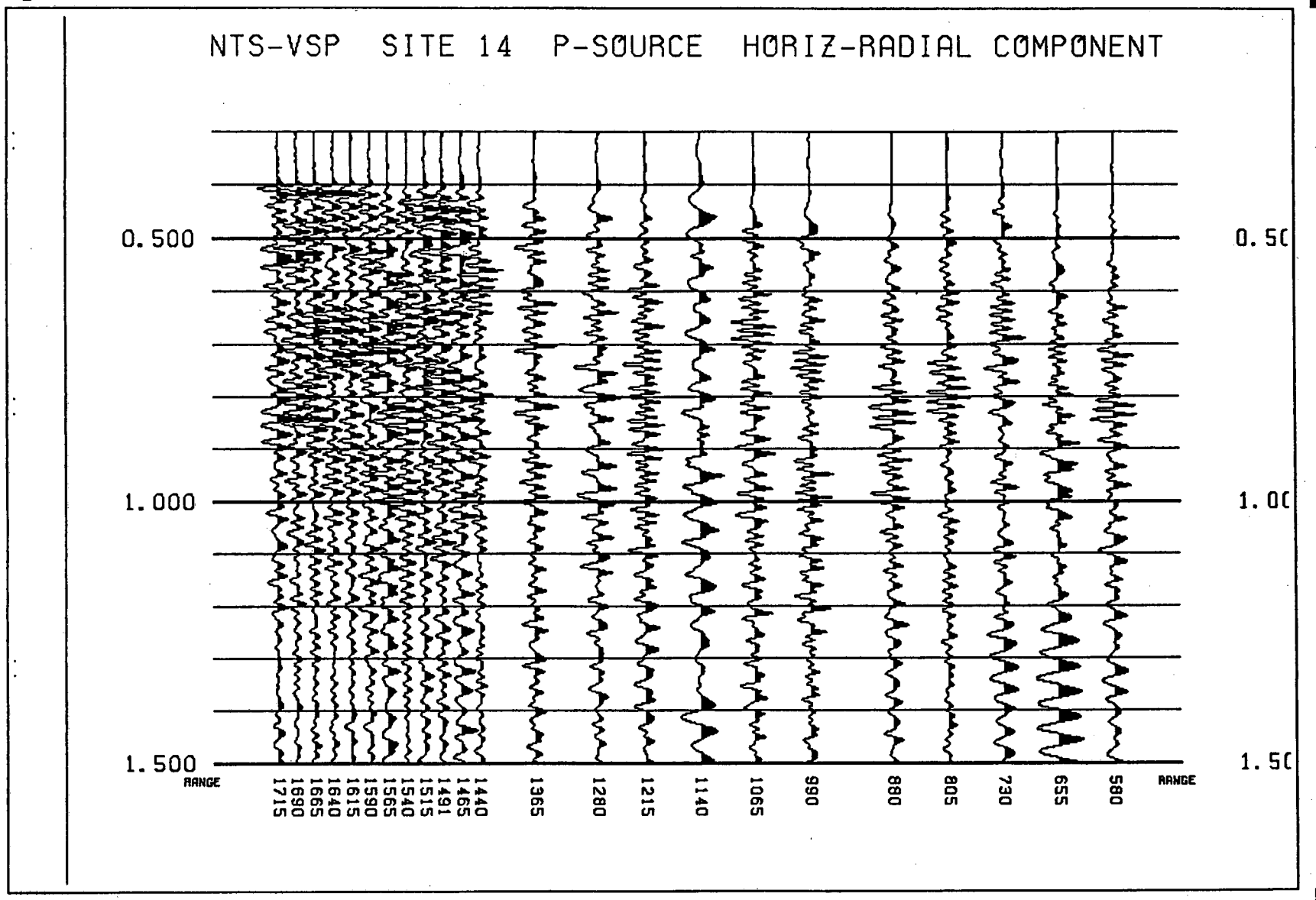
NTS-VSP SITE 14 P-SOURCE HORIZ-RADIAL COMPONENT
0.500
1.000
1.500
RANGE
1715
1690
1665
1640
1615
1590
1565
1540
1515
1491
1465
1440
1365
1290
1215
1140
1065
990
880
805
730
655
580
RANGE
View File
Decimate
Stop
Redraw

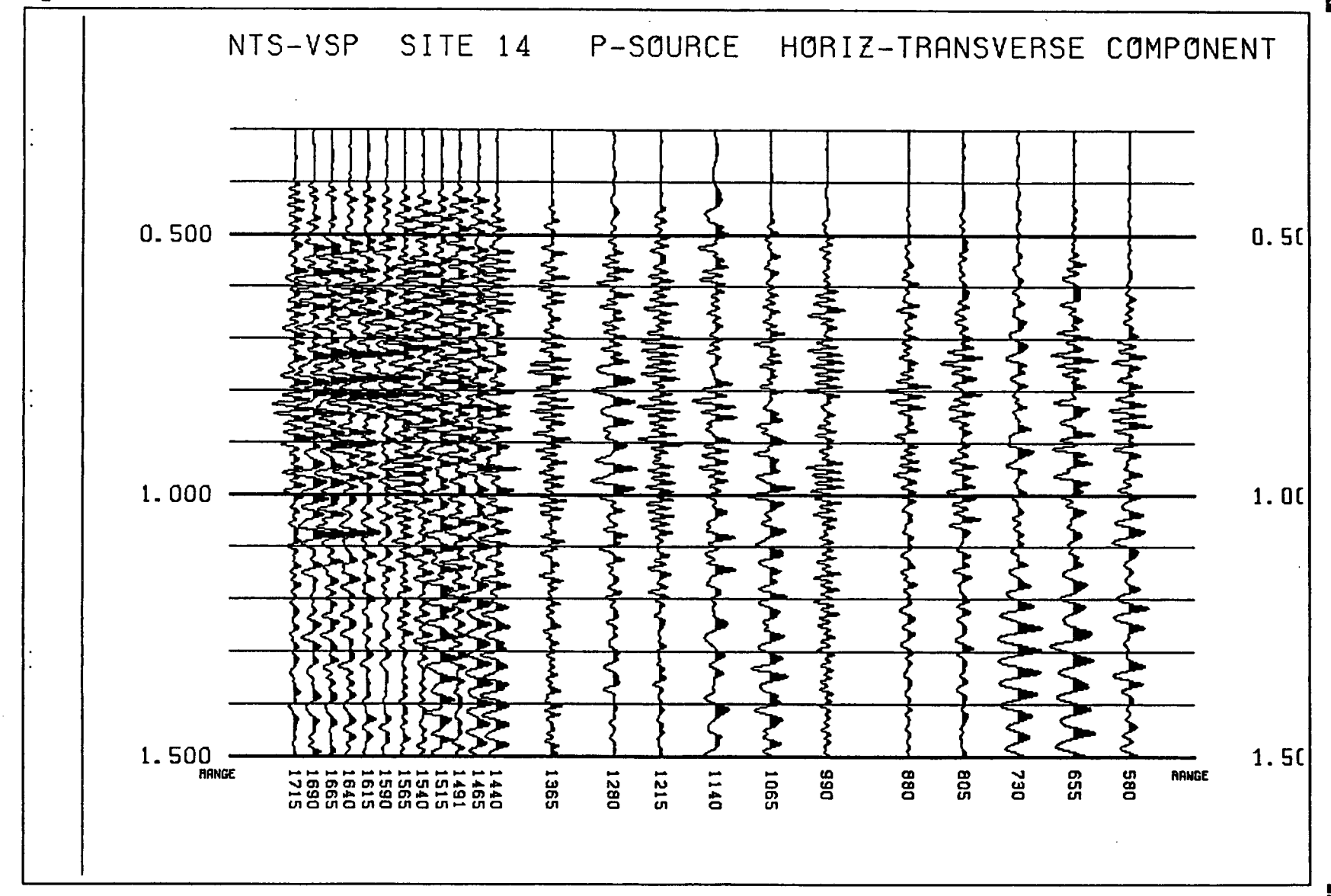
NTS-VSP SITE 14 P-SOURCE HORIZ-TRANSVERSE COMPONENT
0.500
1.000
1.500
0.50
1.00
1.50
RANGE
1715
1690
1665
1640
1615
1590
1565
1540
1515
1491
1465
1440
1365
1280
1215
1140
1065
990
880
805
730
655
580
RANGE
View File
Decimate
Stop
Redraw

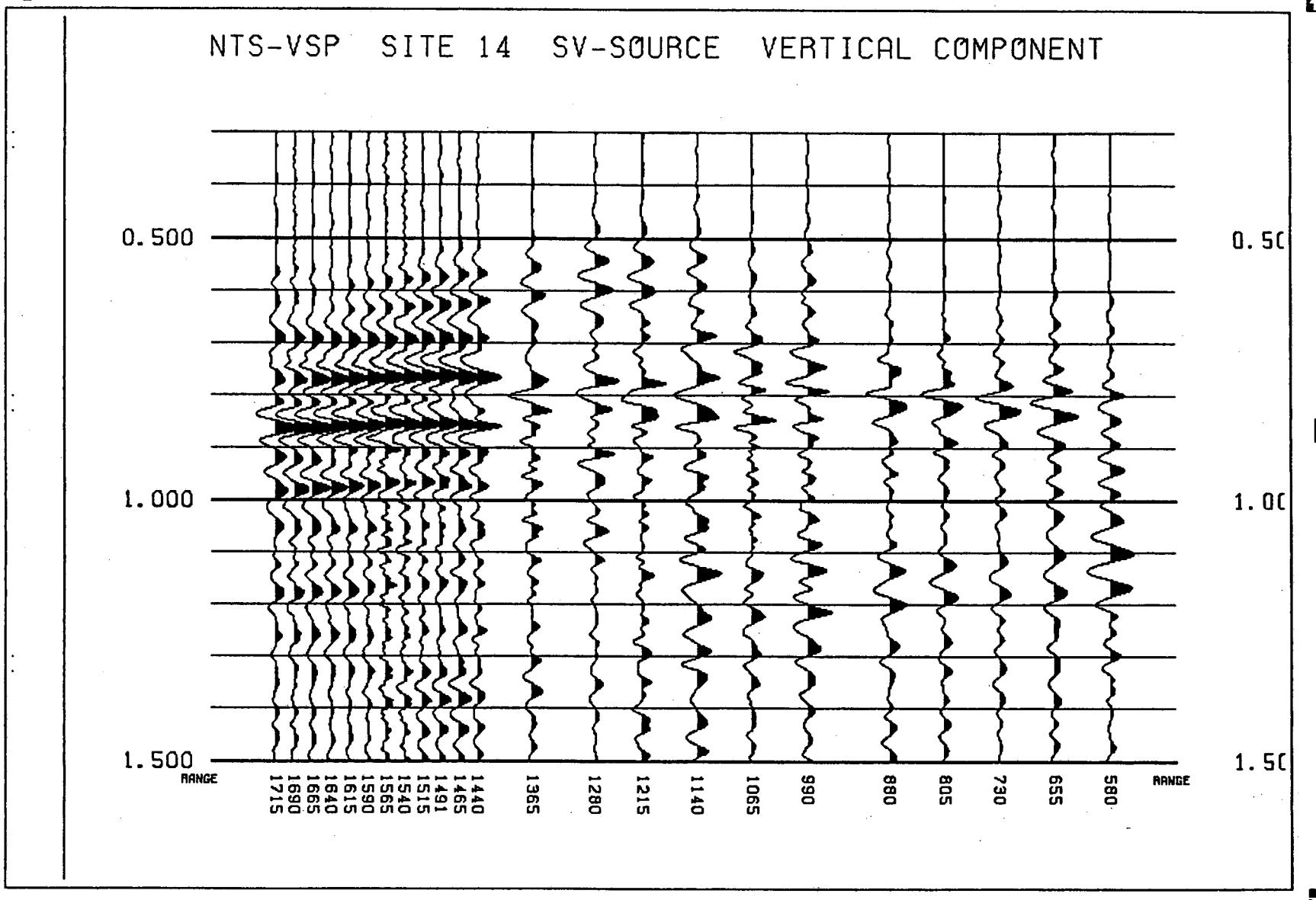

View File | Decimate

Stop | Redraw

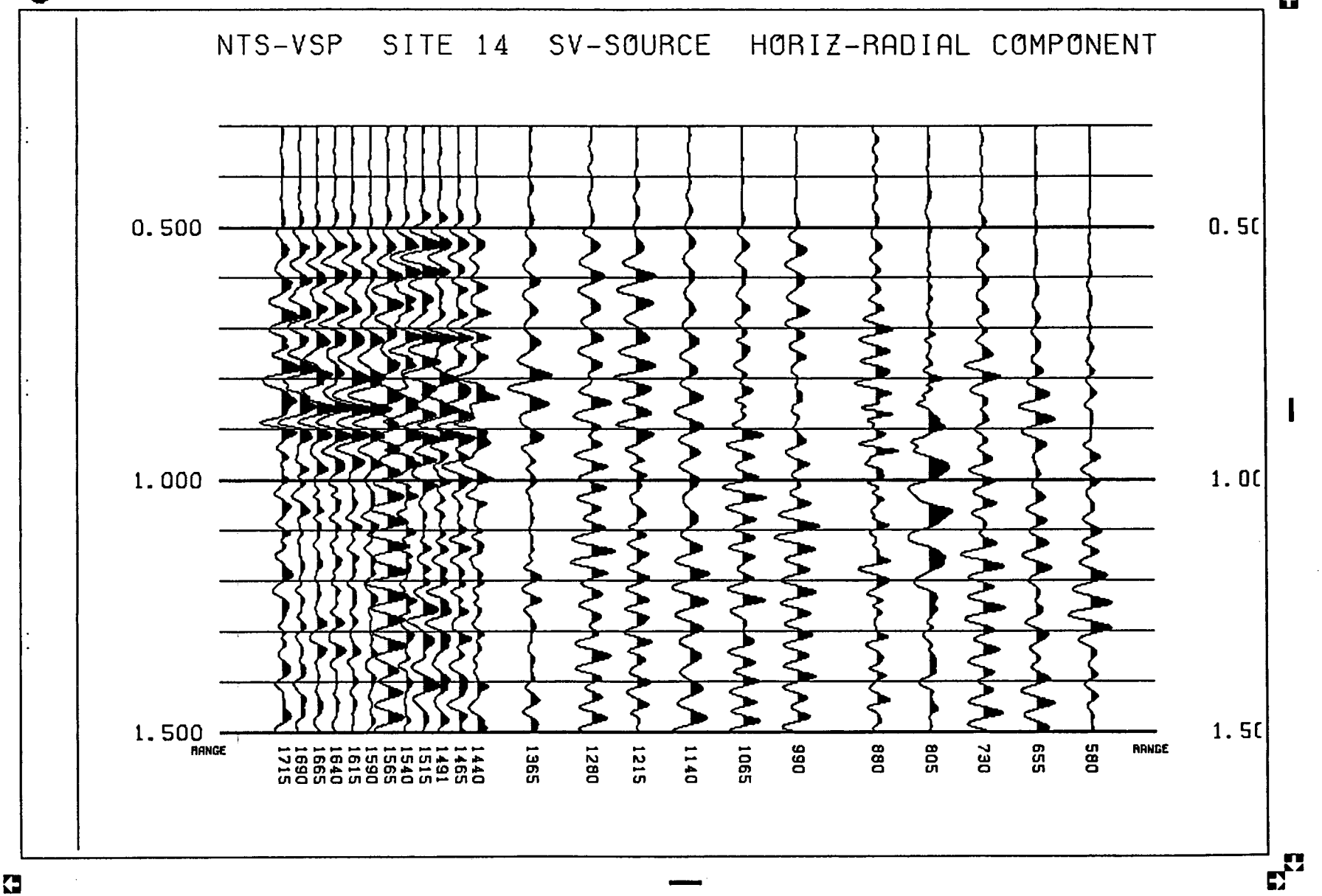
NTS-VSP SITE 14 SV-SOURCE HORIZ-RADIAL COMPONENT
0.500
1.000
1.500
0.5C
1.0C
1.5C
RANGE
1715
1690
1665
1640
1615
1590
1565
1540
1515
1491
1465
1440
1365
1280
1215
1140
1065
990
880
805
730
655
580
RANGE
View File
Decimate
Stop
Redraw

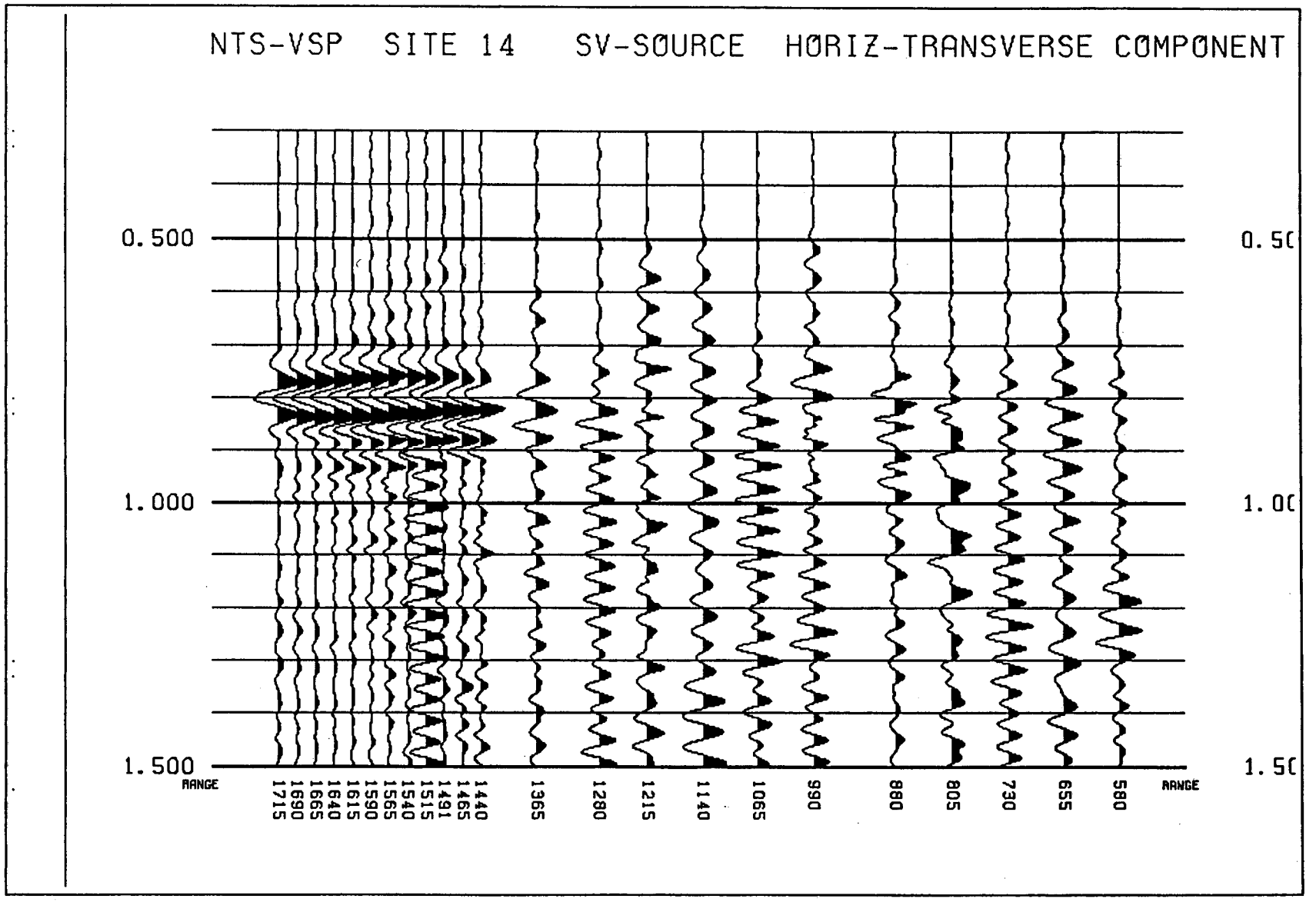
NTS-VSP SITE 14 SV-SOURCE HORIZ-TRANSVERSE COMPONENT
0.500
1.000
1.500
0.50
1.00
1.50
RANGE
1715
1690
1665
1640
1615
1590
1565
1540
1515
1491
1465
1440
1365
1280
1215
1140
1065
990
880
805
730
655
580
RANGE

View File
Decimate
Stop
Redraw

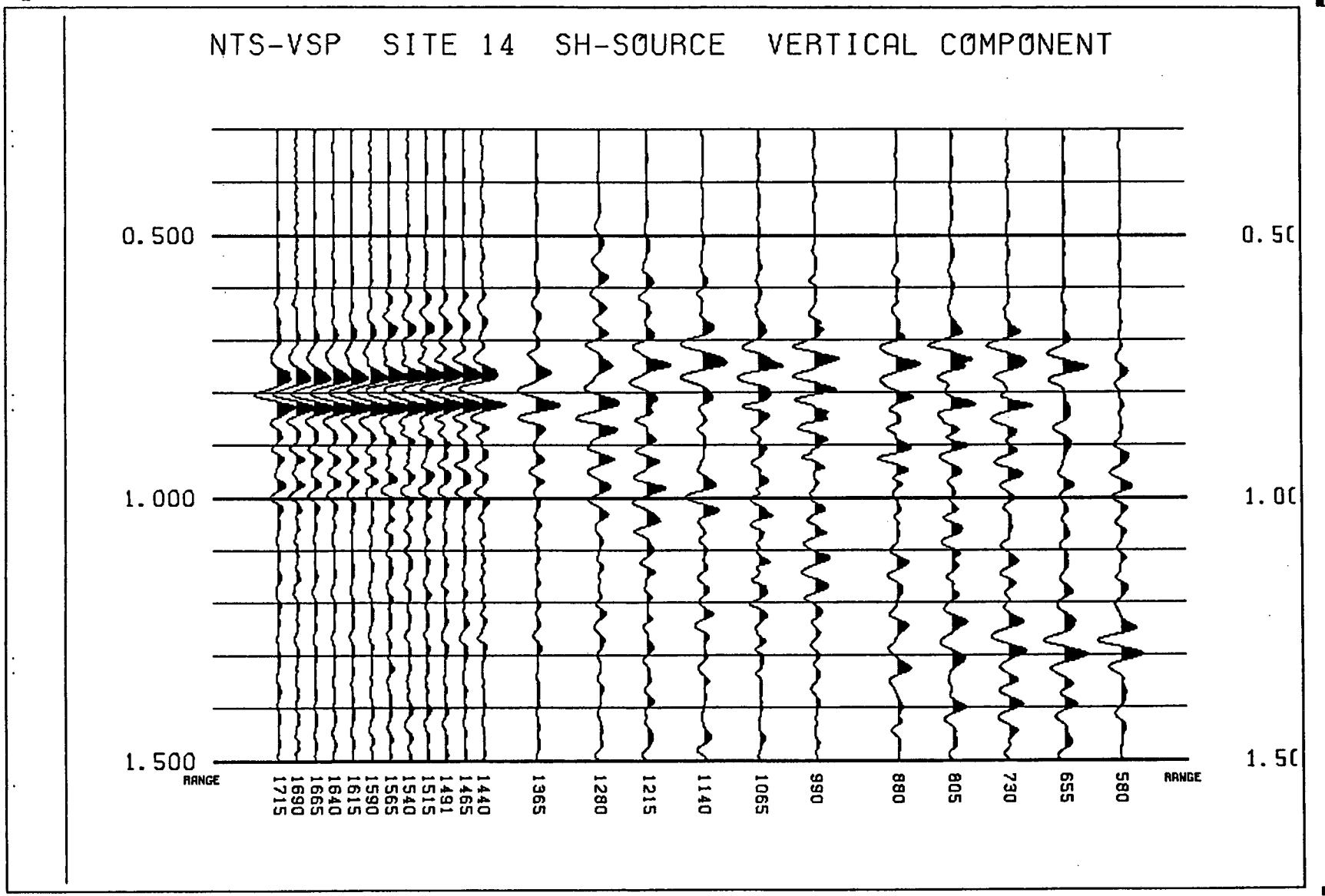

View File | Decimate

Stop | Redraw

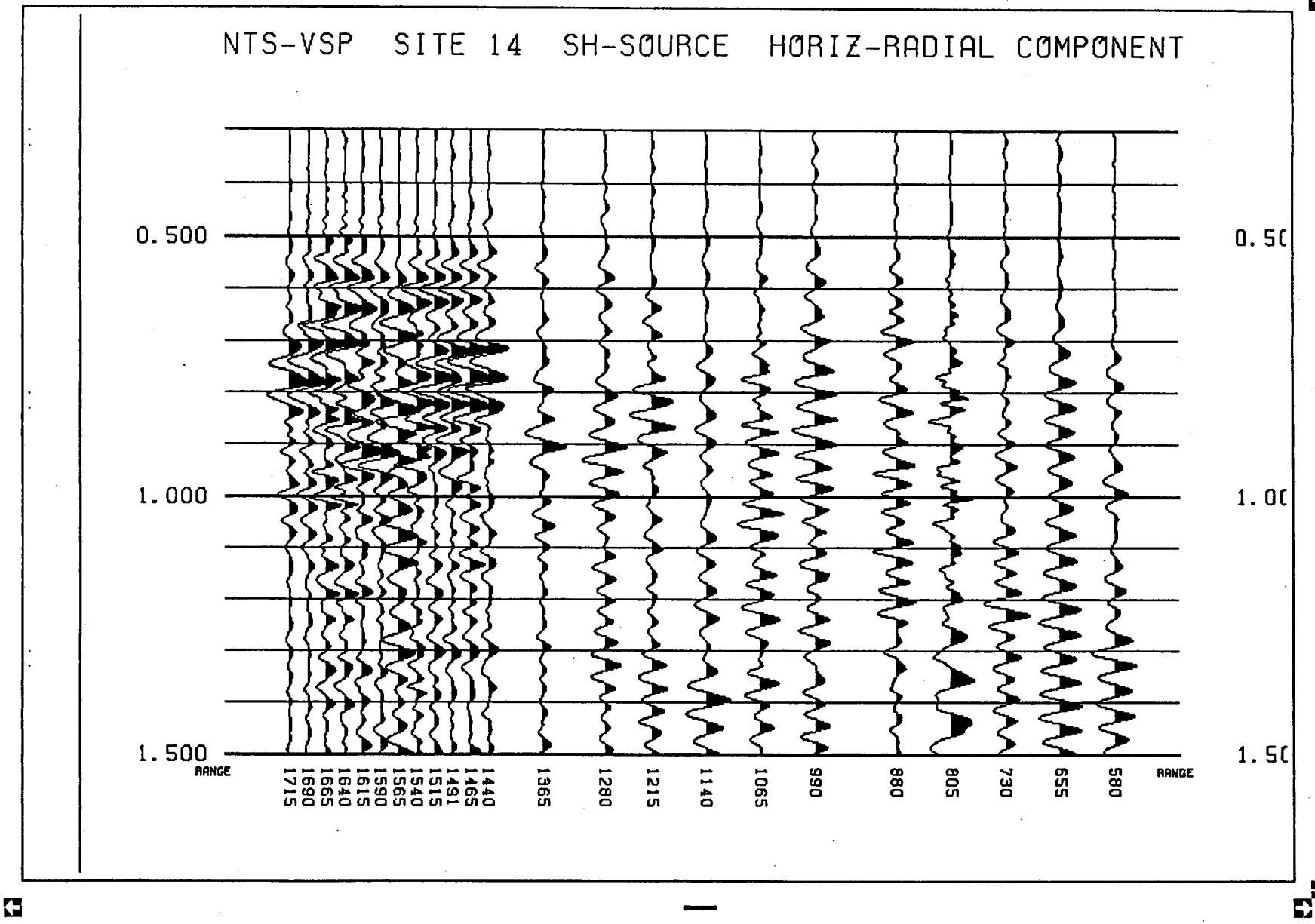
NTS-VSP SITE 14 SH-SOURCE HORIZ-RADIAL COMPONENT
0.500
1.000
1.500
RANGE
1715
1690
1665
1640
1615
1590
1565
1540
1515
1491
1465
1440
1365
1280
1215
1140
1065
990
880
805
730
655
580
RANGE
View File
Decimate
Stop
Redraw

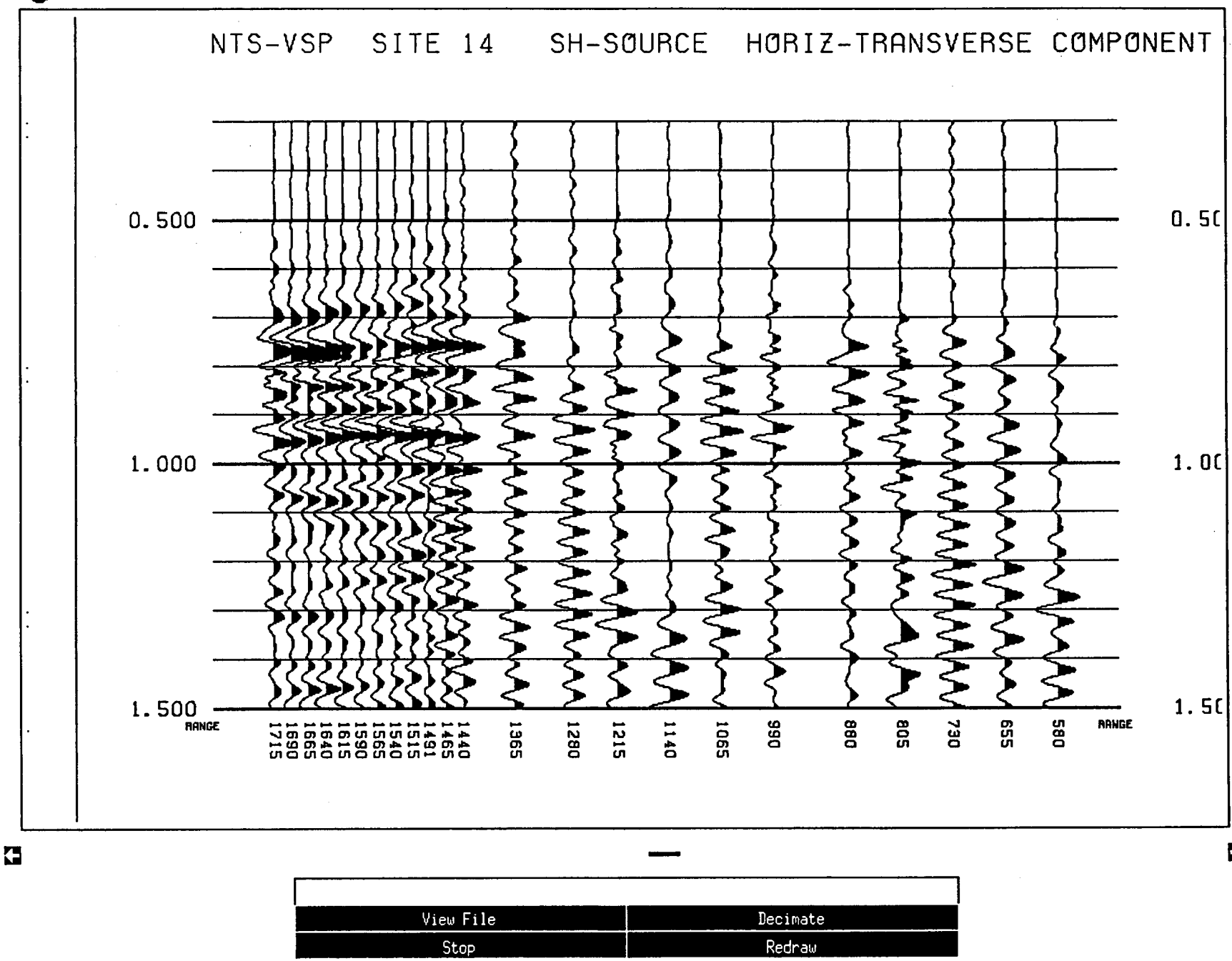
NTS-VSP SITE 14 SH-SOURCE HORIZ-TRANSVERSE COMPONENT
0.500
1.000
1.500
RANGE
1715
1690
1665
1640
1615
1590
1565
1540
1515
1491
1465
1440
1365
1280
1215
1140
1065
990
880
805
730
655
580
RANGE
View File
Decimate
Stop
Redraw

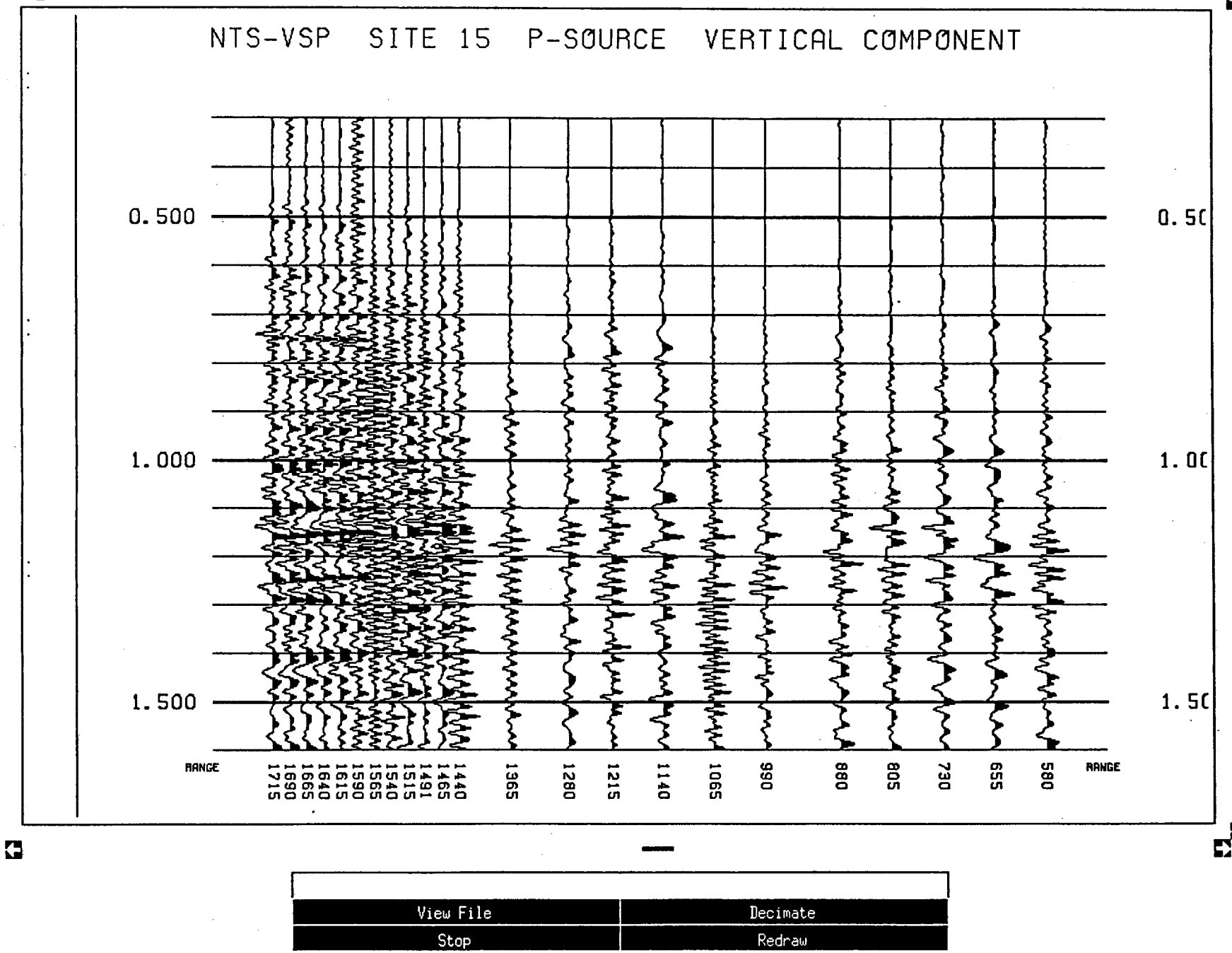
NTS-VSP SITE 15 P-SOURCE VERTICAL COMPONENT
0.500
1.000
1.500
RANGE
1715
1690
1665
1640
1615
1590
1565
1540
1515
1491
1465
1440
1365
1280
1215
1140
1065
990
880
805
730
655
580
RANGE
View File
Decimate
Stop
Redraw

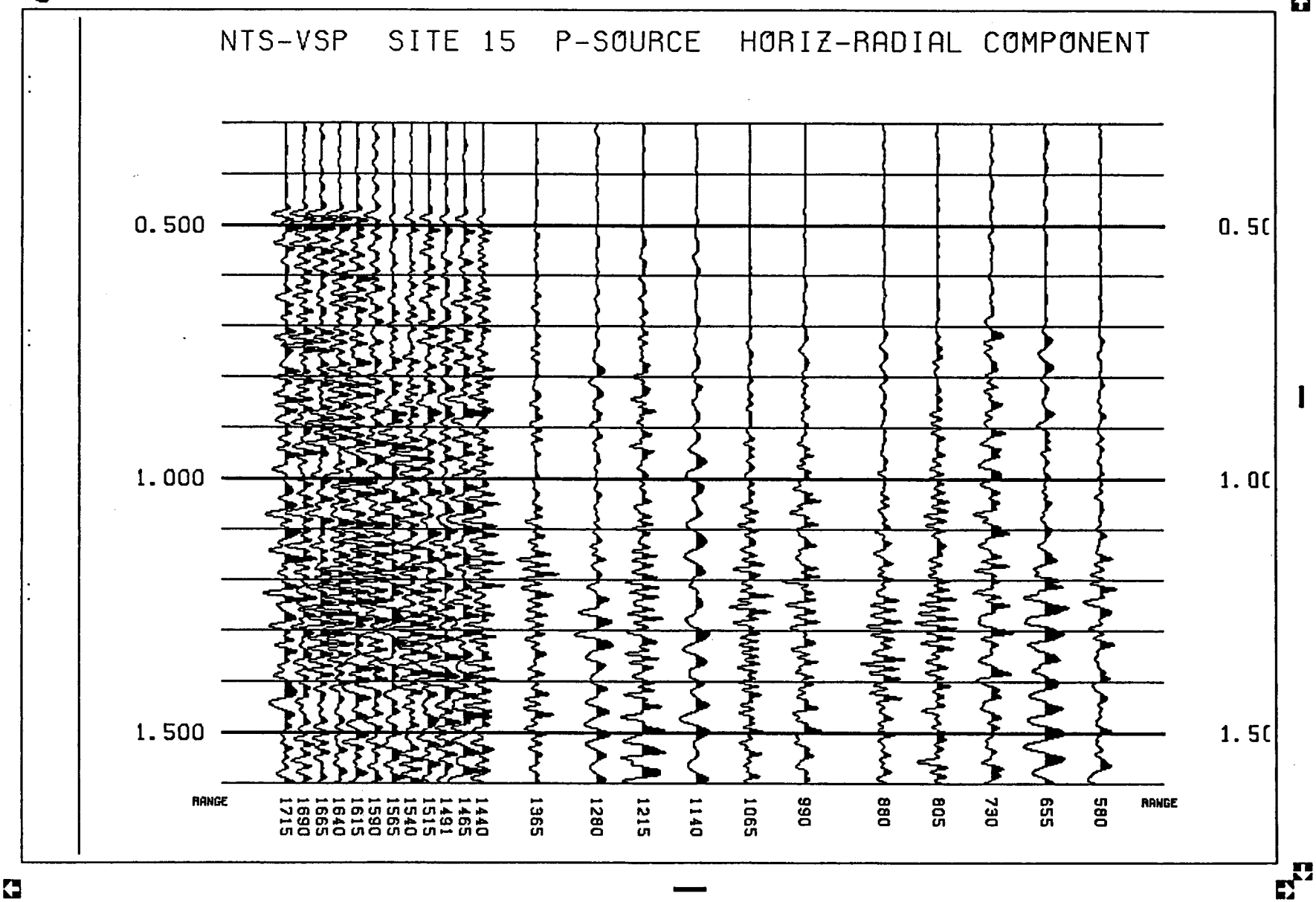
NTS-VSP SITE 15 P-SOURCE HORIZ-RADIAL COMPONENT
0.500
1.000
1.500
0.5C
1.0C
1.5C
RANGE
1715
1690
1665
1640
1615
1590
1565
1540
1515
1491
1465
1440
1365
1280
1215
1140
1065
990
880
805
730
655
580
RANGE
View File
Decimate
Stop
Redraw

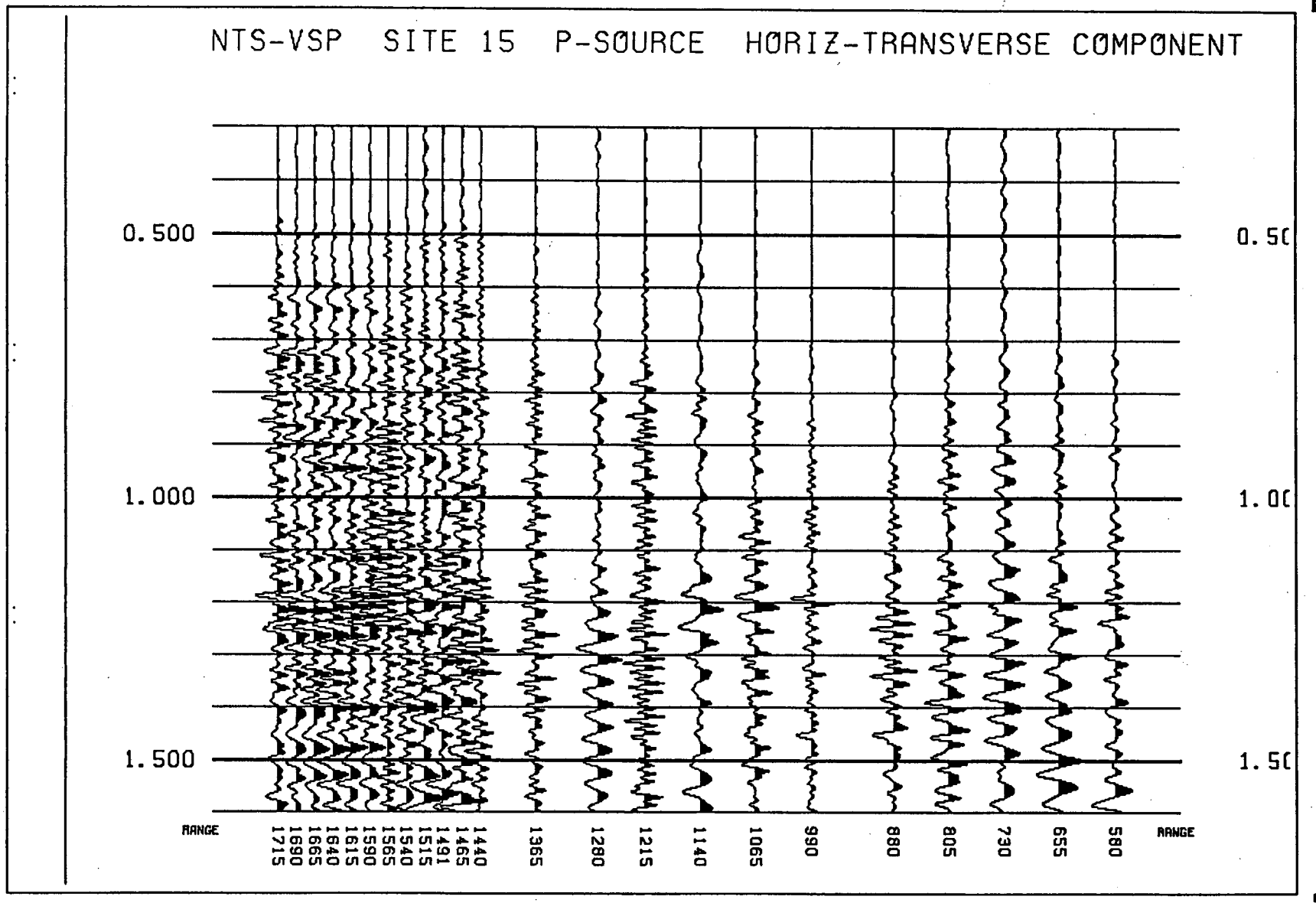

View File | Decimate

Stop | Redraw

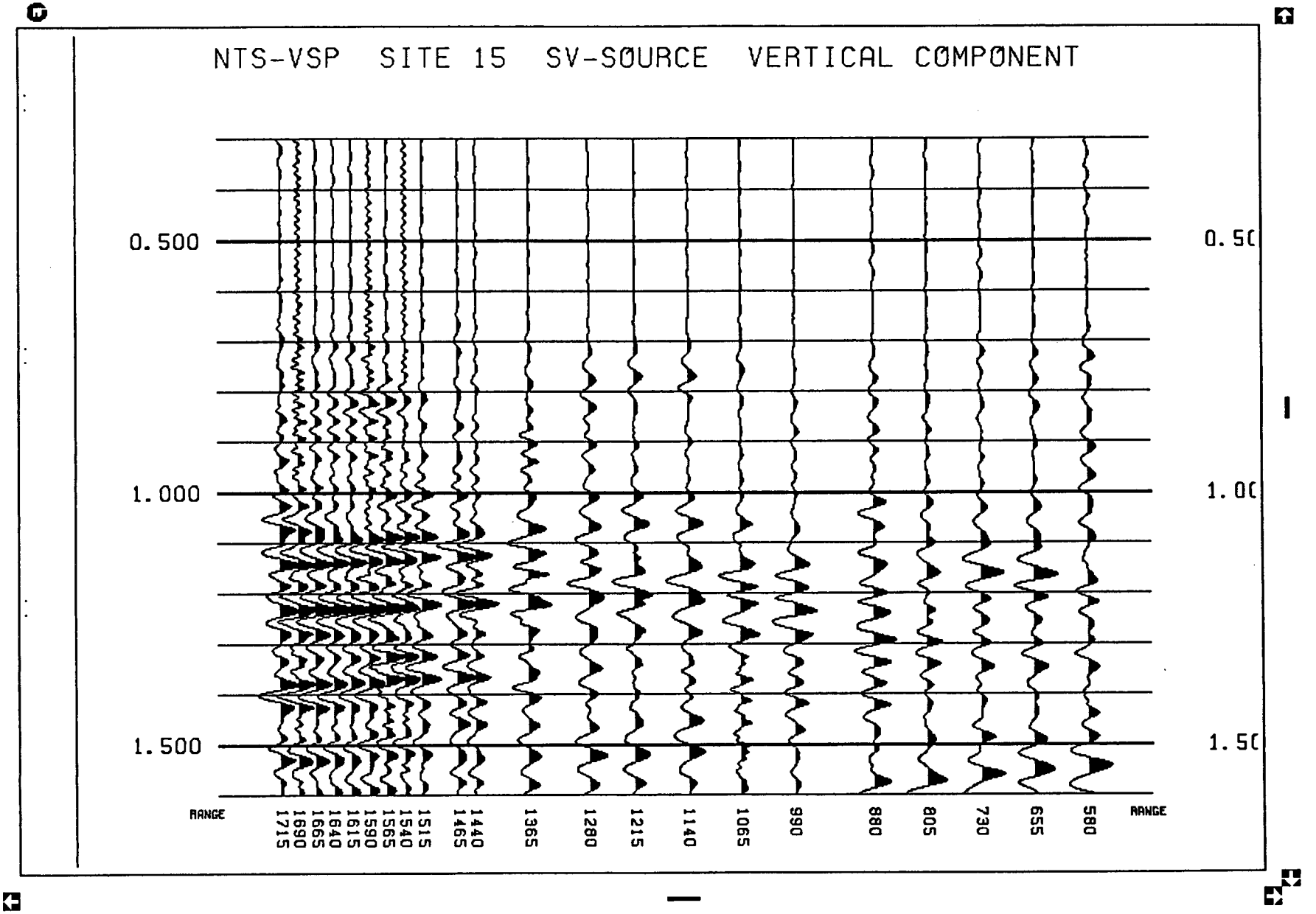
NTS-VSP SITE 15 SV-SOURCE VERTICAL COMPONENT
0.500
1.000
1.500
0.5C
1.0C
1.5C
RANGE
1715
1690
1665
1640
1615
1590
1565
1540
1515
1465
1440
1365
1280
1215
1140
1065
990
880
805
730
655
580
RANGE
View File
Decimate
Stop
Redraw

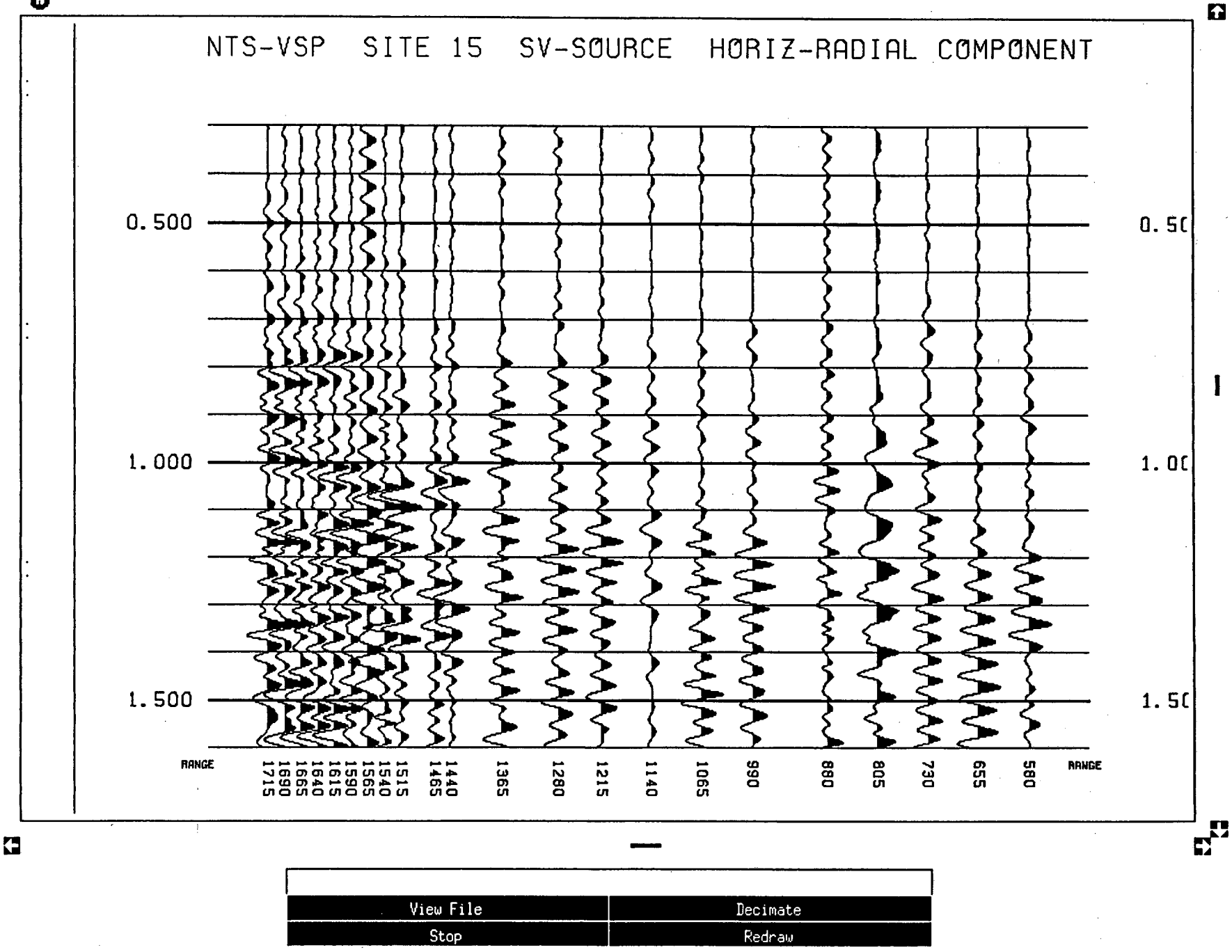
NTS-VSP SITE 15 SV-SOURCE HORIZ-RADIAL COMPONENT
0.500
1.000
1.500
0.5(
1.0(
1.5(
RANGE
1715
1690
1665
1640
1615
1590
1565
1540
1515
1465
1440
1365
1280
1215
1140
1065
990
880
805
730
655
580
RANGE
View File
Decimate
Stop
Redraw

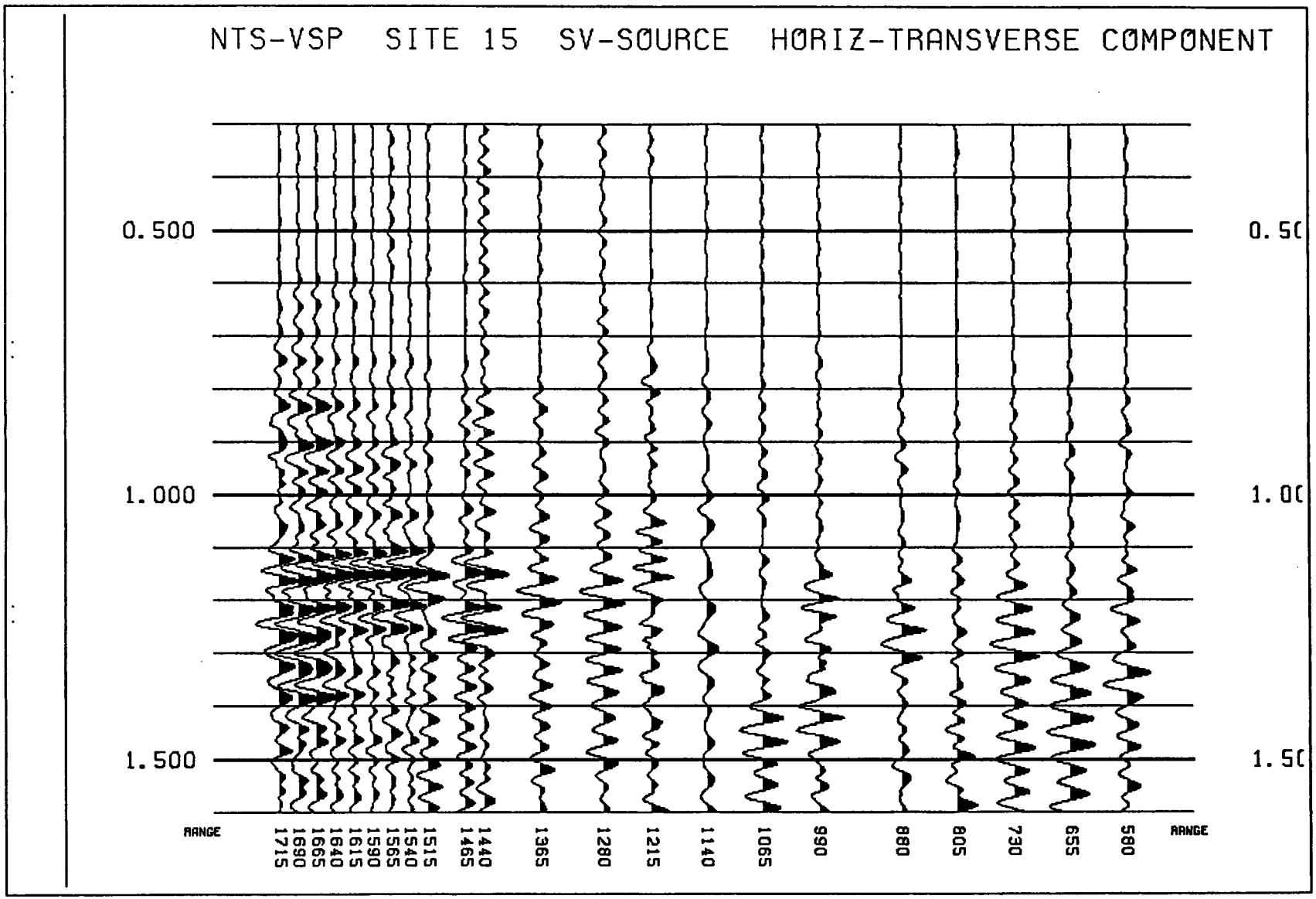

View File	Decimate
Stop	Redraw

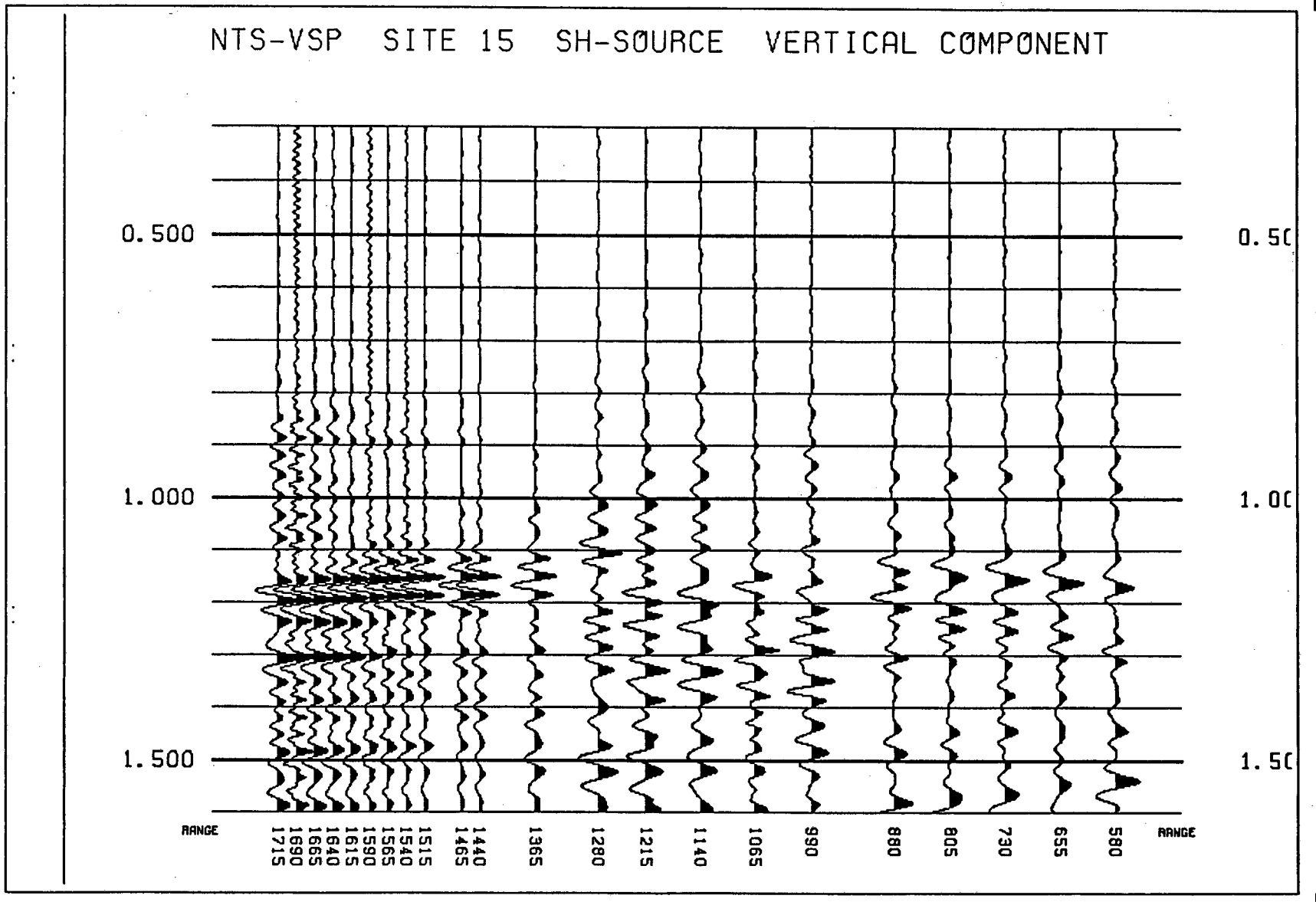

View File | Decimate
Stop | Redraw

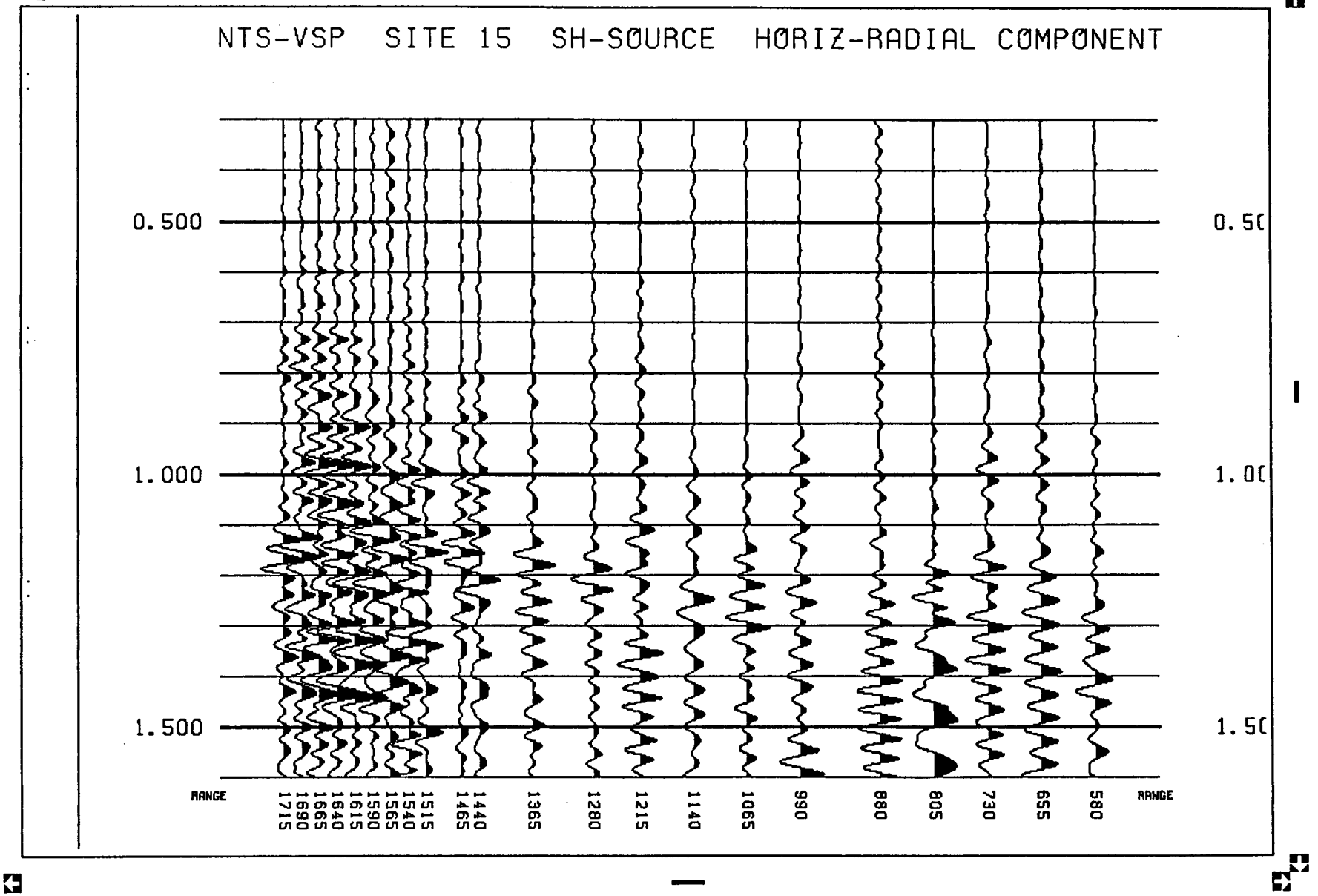
NTS-VSP SITE 15 SH-SOURCE HORIZ-RADIAL COMPONENT
0.500
1.000
1.500
0.5C
1.0C
1.5C
RANGE
1715
1690
1665
1640
1615
1590
1565
1540
1515
1465
1440
1365
1280
1215
1140
1065
990
880
805
730
655
580
RANGE
View File
Decimate
Stop
Redraw

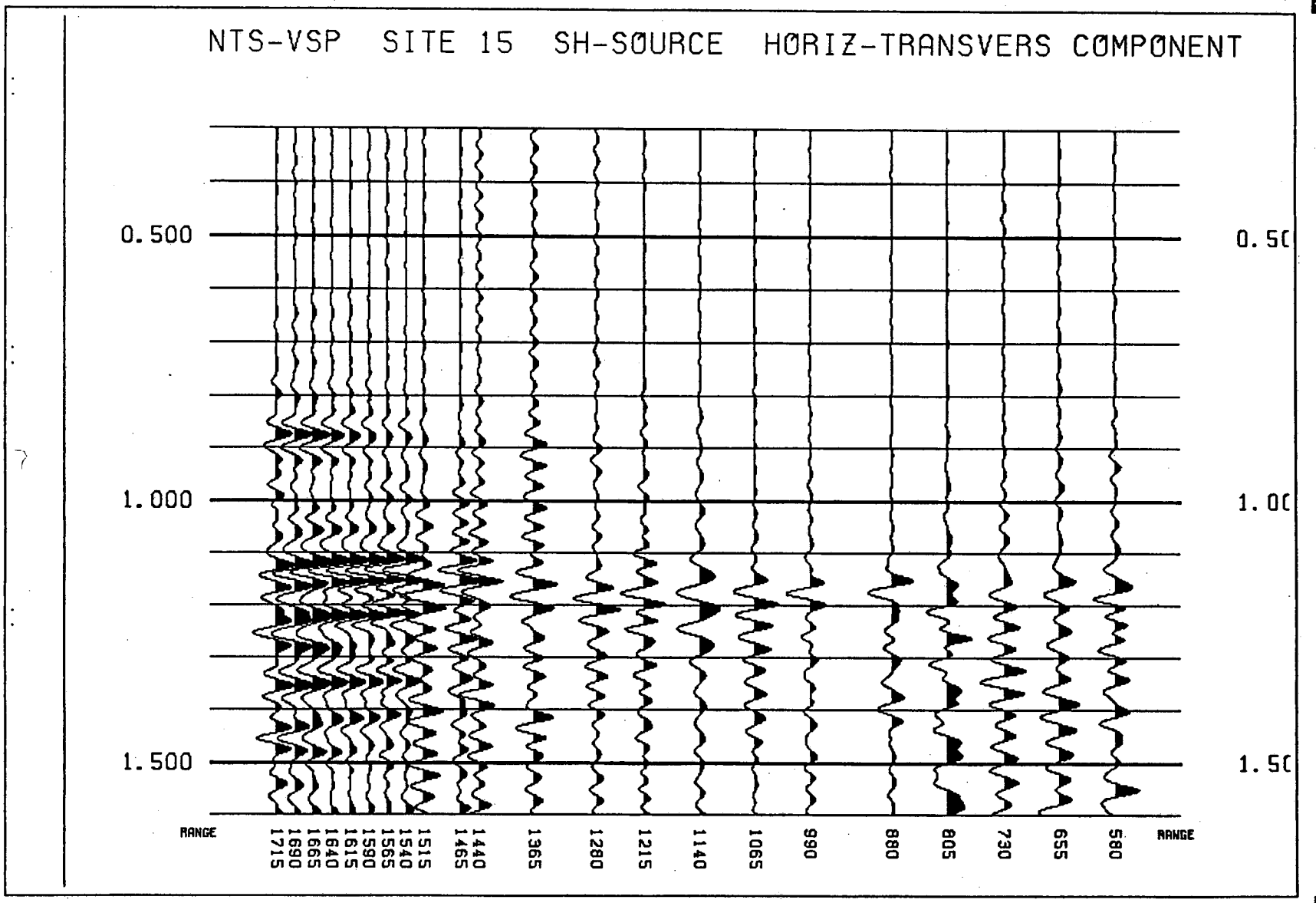
NTS-VSP SITE 15 SH-SOURCE HORIZ-TRANSVERS COMPONENT
0.500
1.000
1.500
0.5(
1.0(
1.5(
RANGE
1715
1690
1665
1640
1615
1590
1565
1540
1515
1465
1440
1365
1280
1215
1140
1065
990
880
805
730
655
580
RANGE
View File
Decimate
Stop
Redraw

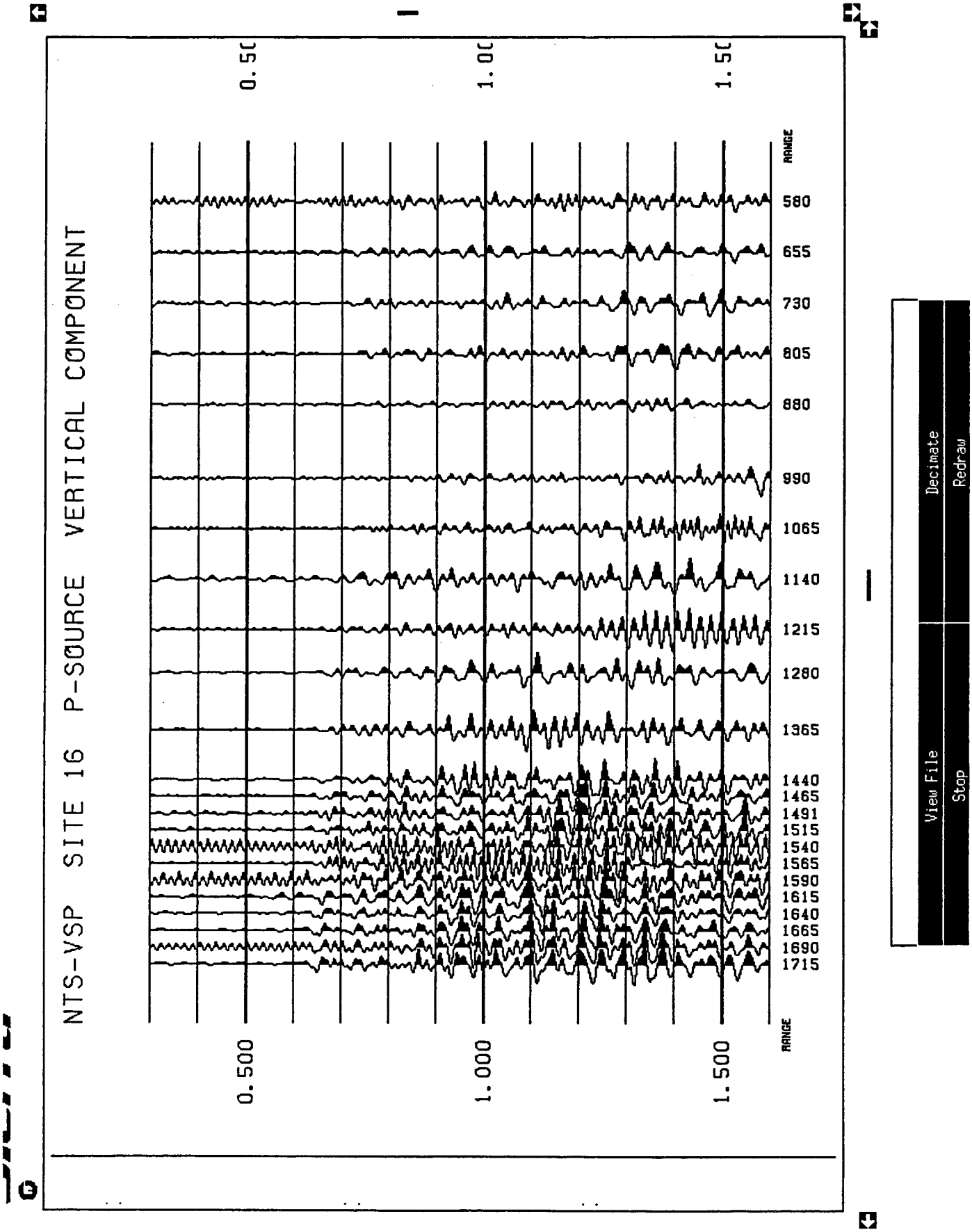
NTS-VSP SITE 16 P-SOURCE VERTICAL COMPONENT
0.5
1.0
1.5
RANGE
580
655
730
805
880
990
1065
1140
1215
1280
1365
1440
1465
1491
1515
1540
1565
1590
1615
1640
1665
1690
1715
0.500
1.000
1.500
Decimate
Redraw
View File
Stop

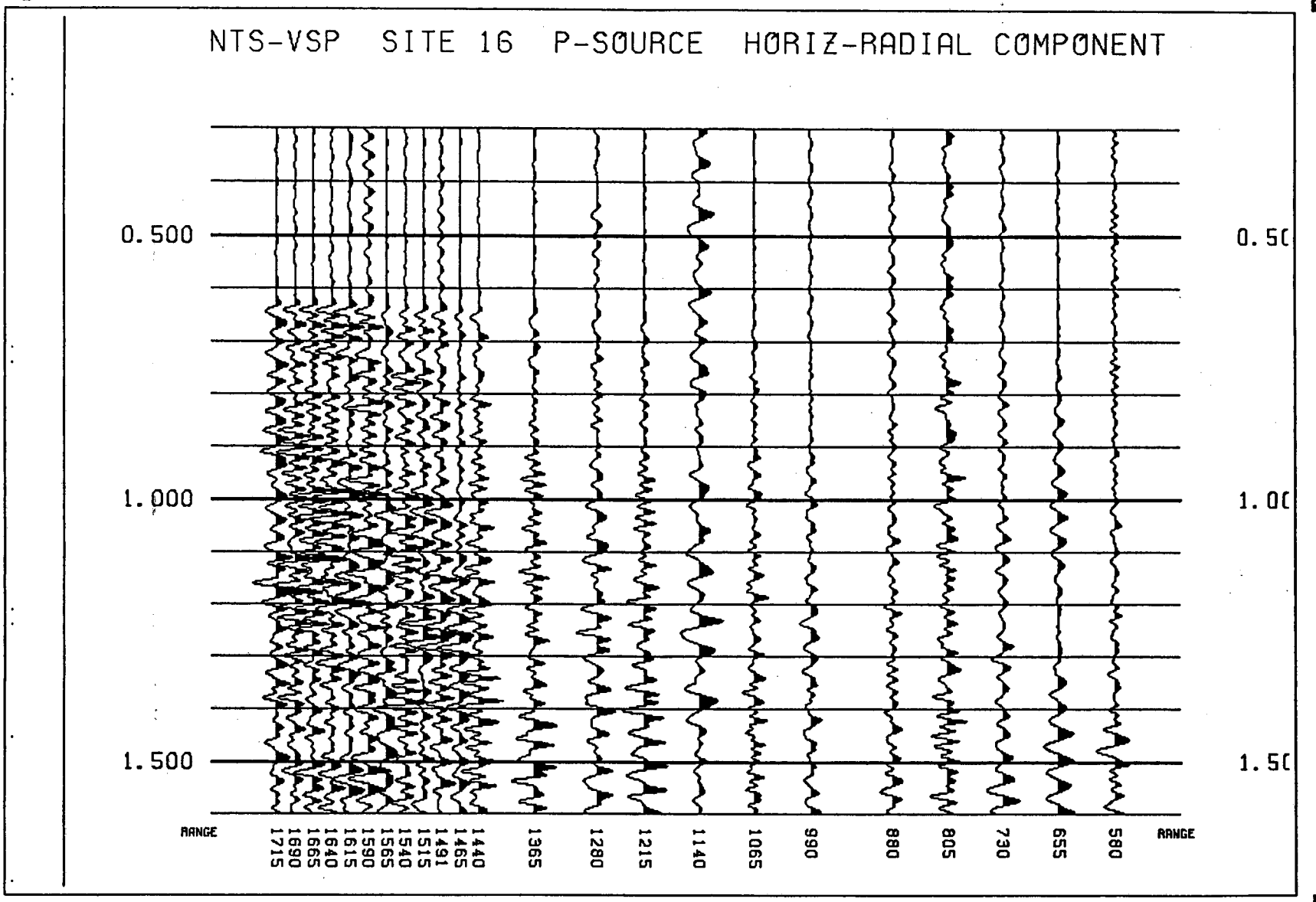
NTS-VSP SITE 16 P-SOURCE HORIZ-RADIAL COMPONENT
0.500
1.000
1.500
0.50
1.00
1.50
RANGE
1715
1690
1665
1640
1615
1590
1565
1540
1515
1491
1465
1440
1365
1280
1215
1140
1065
990
880
805
730
655
580
RANGE
View File
Decimate
Stop
Redraw

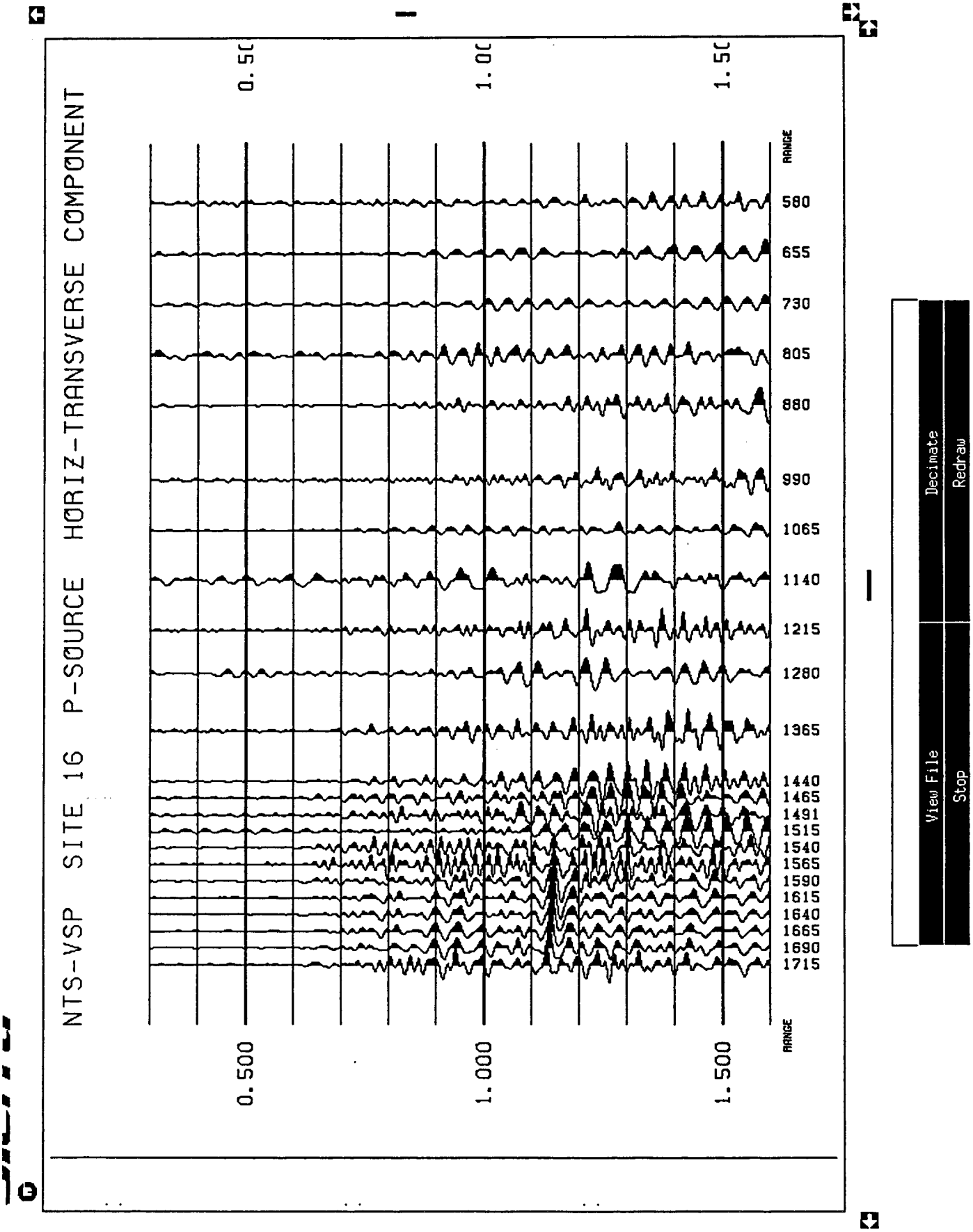
NTS-VSP SITE 16 P-SOURCE HORIZ-TRANSVERSE COMPONENT
0.5
1.0
1.5
RANGE
580
655
730
805
880
990
1065
1140
1215
1280
1365
1440
1465
1491
1515
1540
1565
1590
1615
1640
1665
1690
1715
RANGE
0.500
1.000
1.500
Decimate
Redraw
View File
Stop

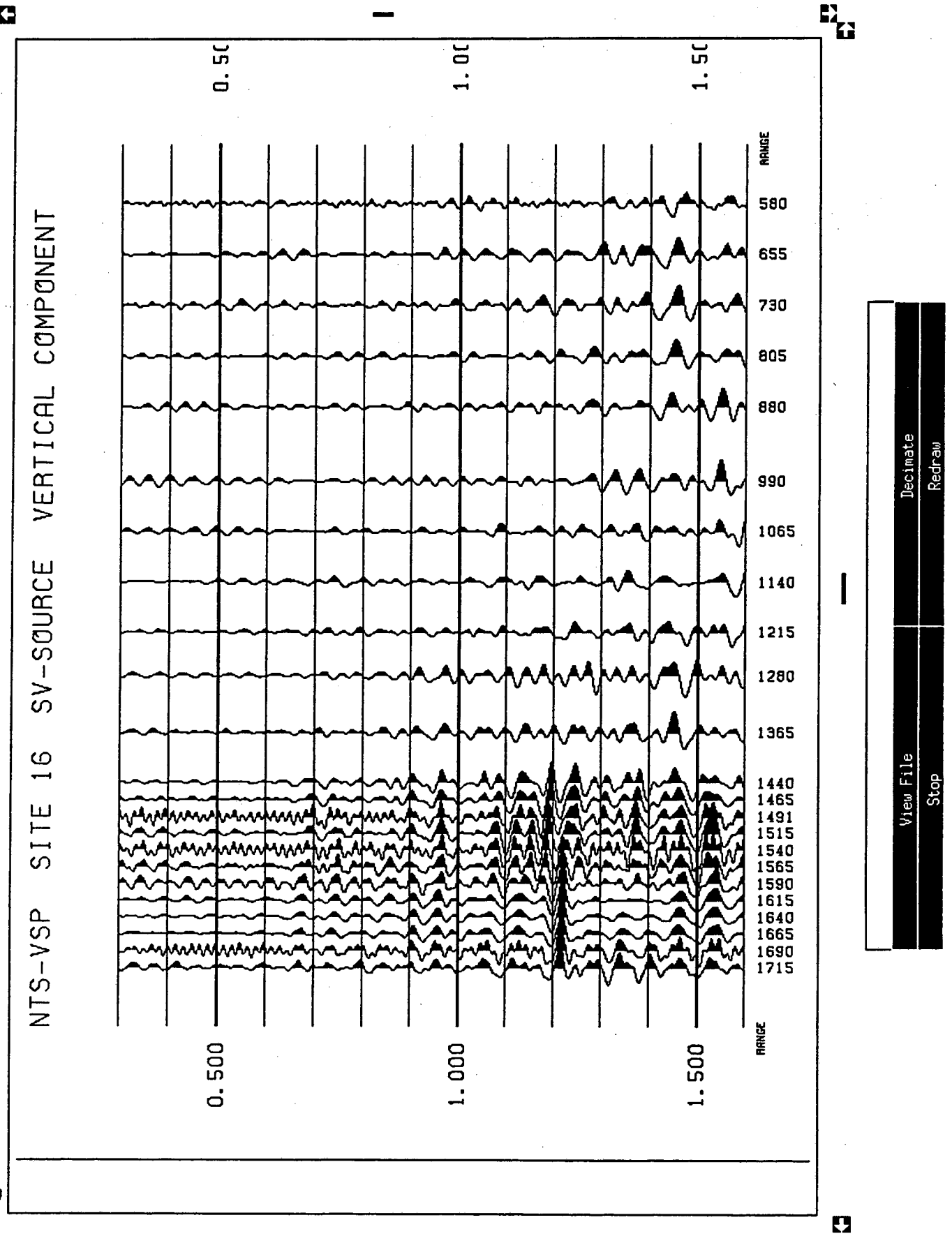
NTS-VSP SITE 16 SV-SOURCE VERTICAL COMPONENT
0.5
1.0
1.5
RANGE
580
655
730
805
880
990
1065
1140
1215
1280
1365
1440
1465
1491
1515
1540
1565
1590
1615
1640
1665
1690
1715
0.500
1.000
1.500
Decimate
Redraw
View File
Stop

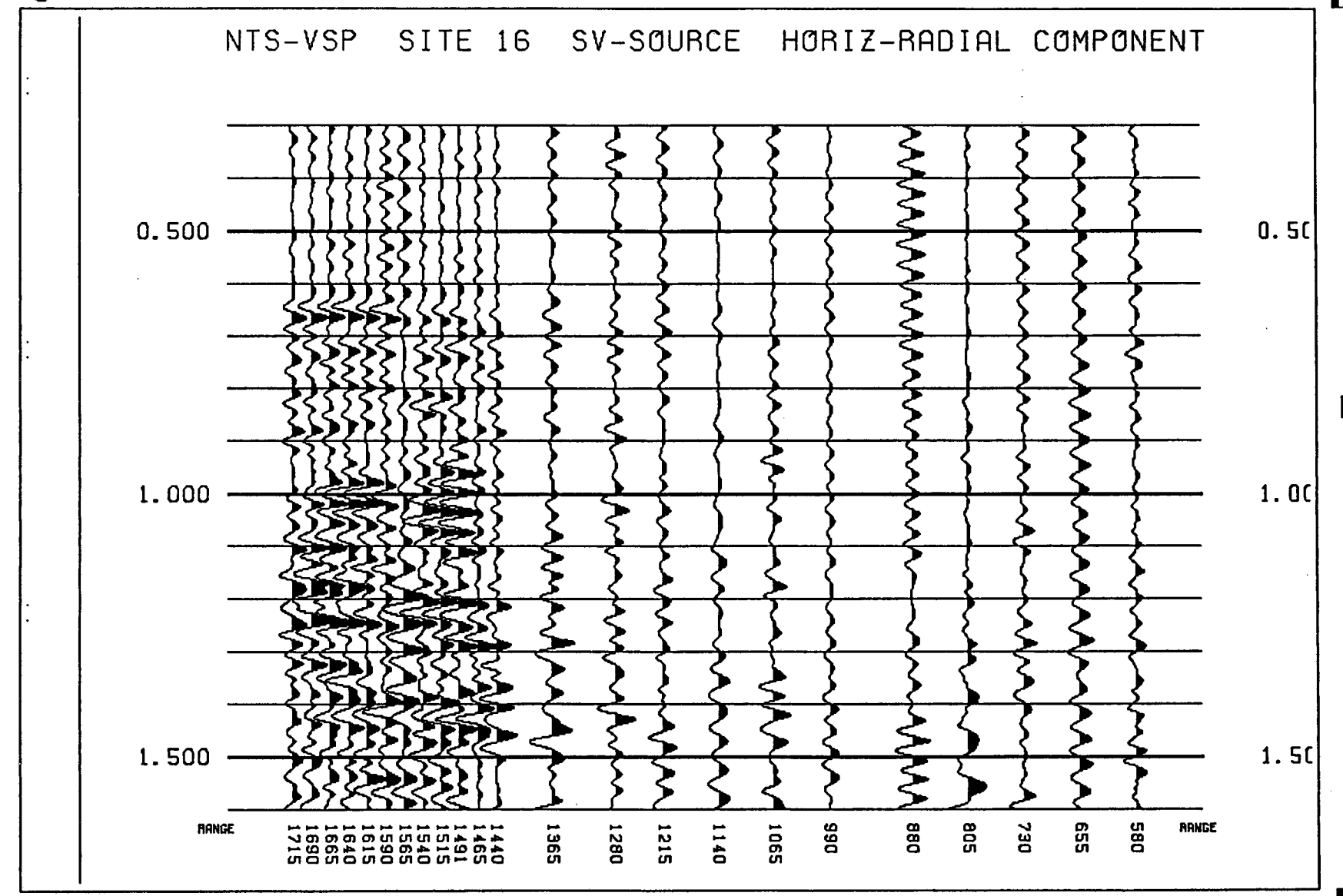
NTS-VSP SITE 16 SV-SOURCE HORIZ-RADIAL COMPONENT
0.500
1.000
1.500
RANGE
1715
1690
1665
1640
1615
1590
1565
1540
1515
1491
1465
1440
1365
1280
1215
1140
1065
990
880
805
730
655
580
RANGE
View File
Decimate
Stop
Redraw

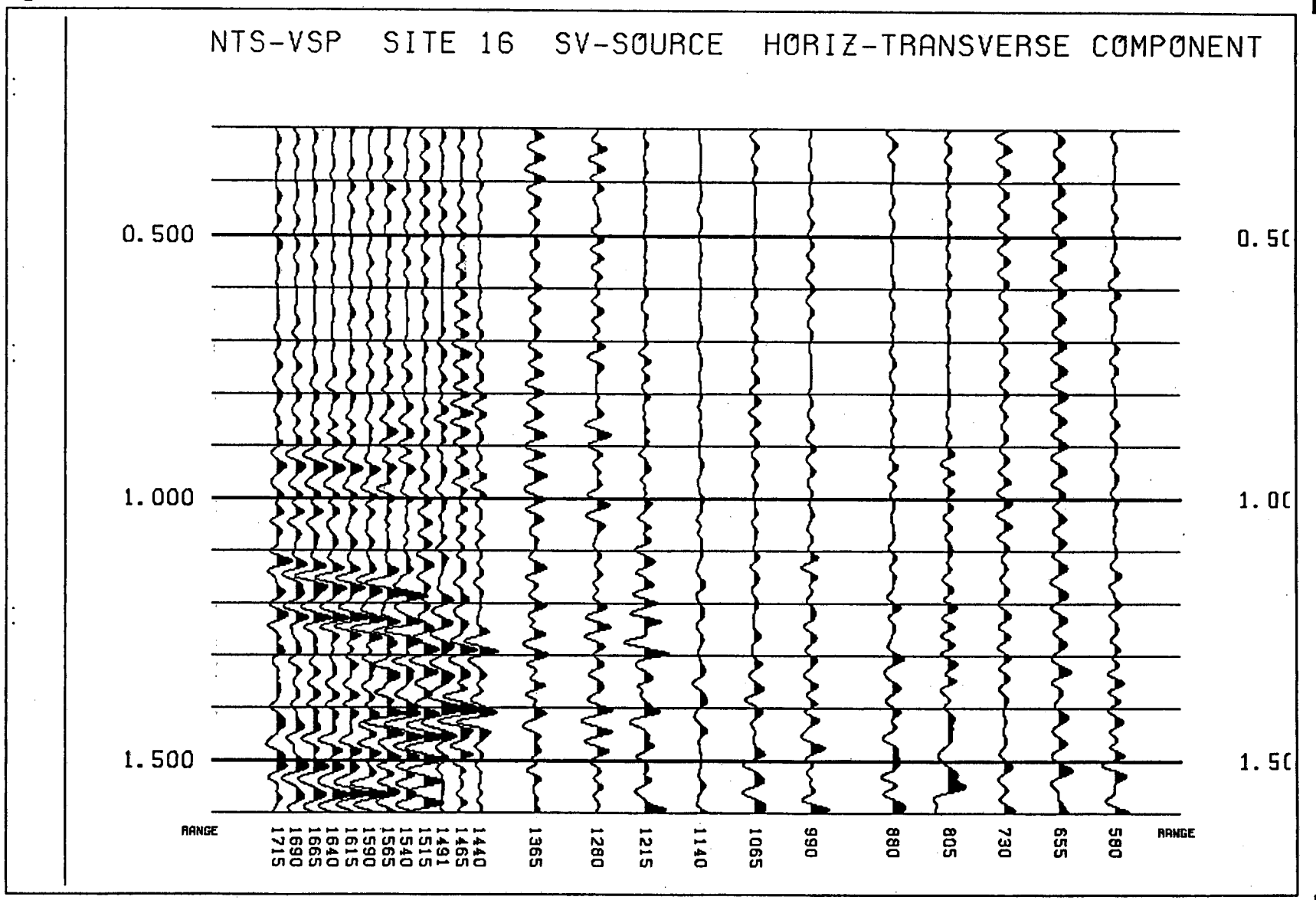
NTS-VSP SITE 16 SV-SOURCE HORIZ-TRANSVERSE COMPONENT
0.500
1.000
1.500
0.5(
1.0(
1.5(
RANGE
1715
1690
1665
1640
1615
1590
1565
1540
1515
1491
1465
1440
1365
1280
1215
1140
1065
990
880
805
730
655
580
RANGE
View File
Decimate
Stop
Redraw

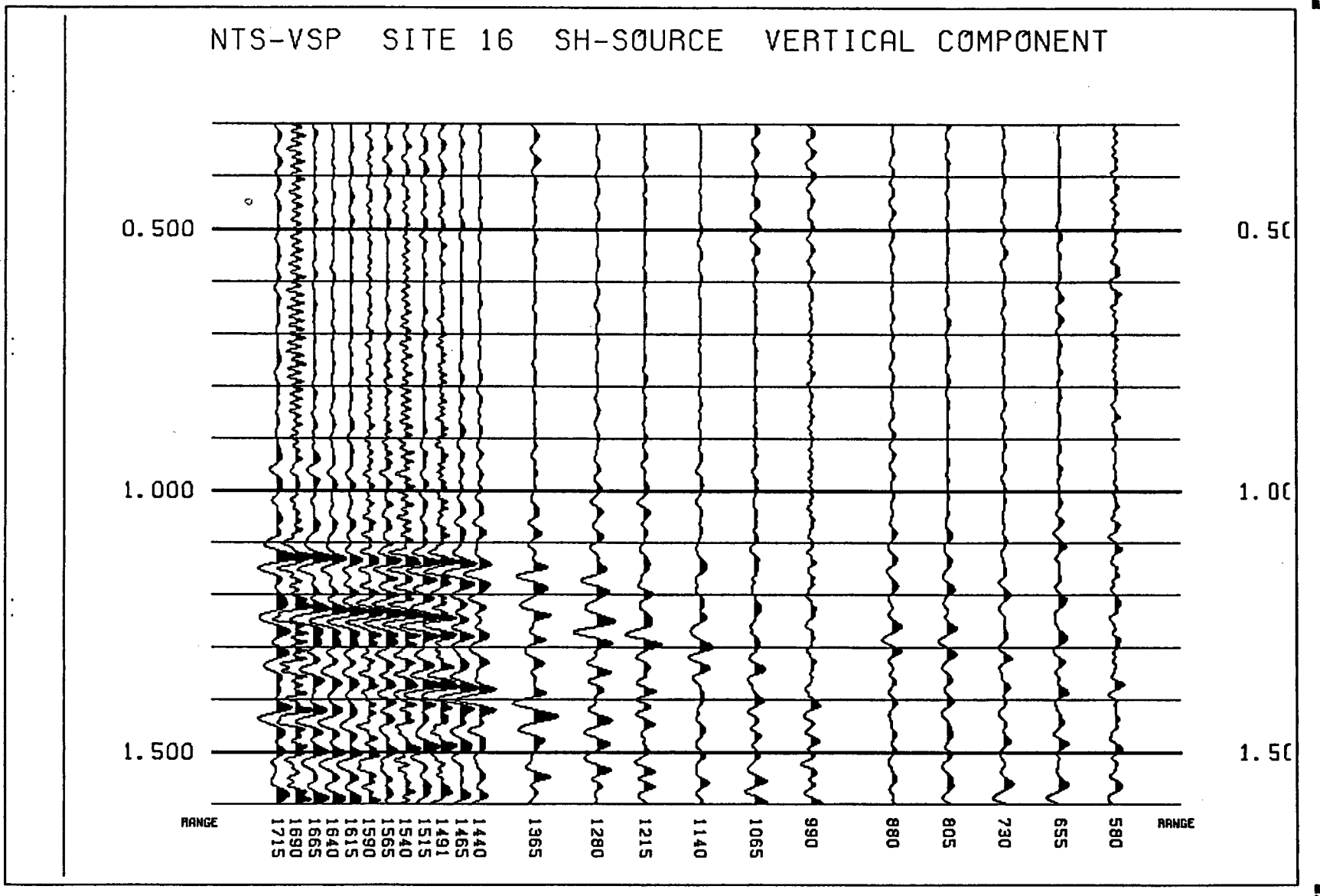

View File | Decimate
Stop | Redraw

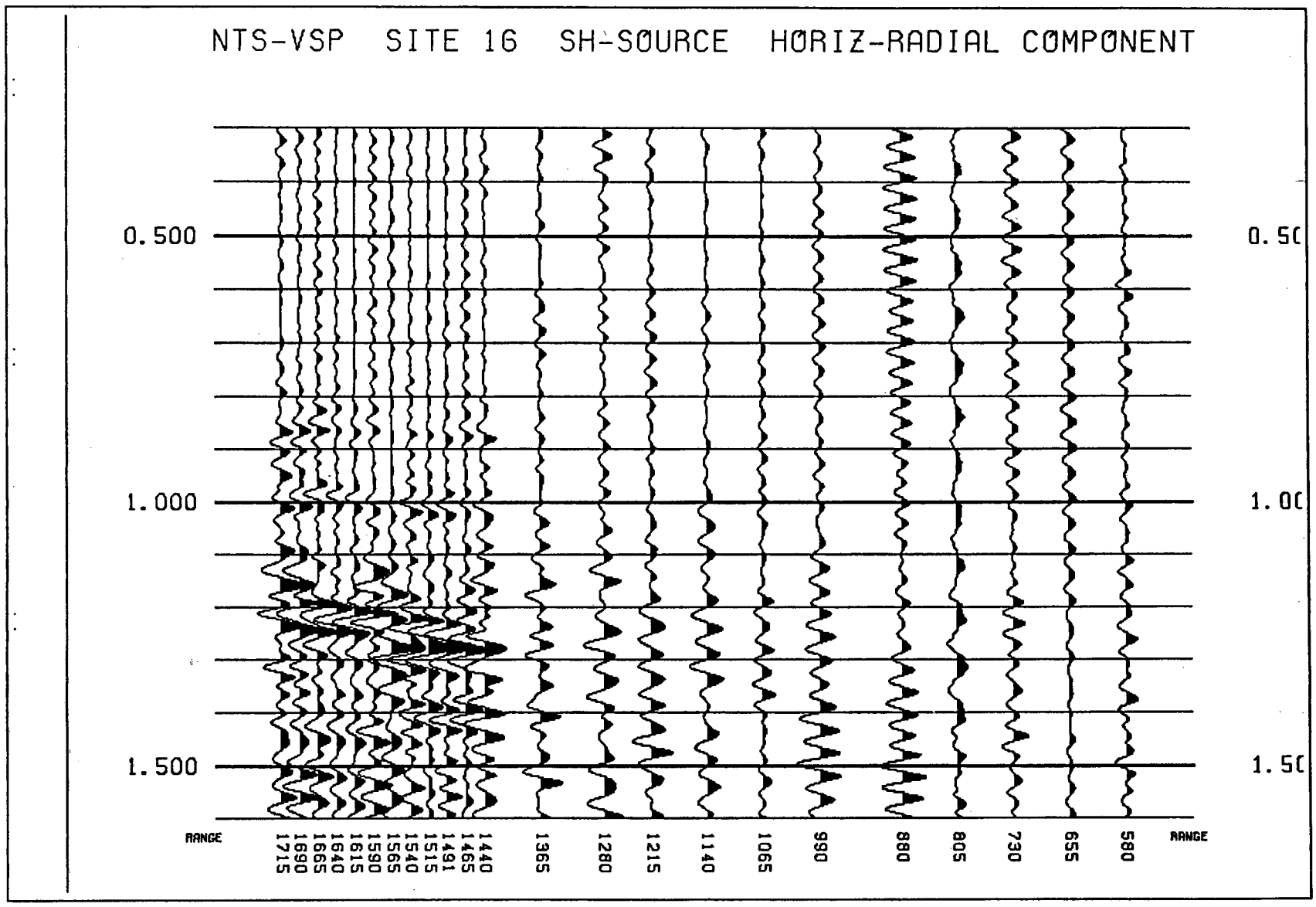
NTS-VSP SITE 16 SH-SOURCE HORIZ-RADIAL COMPONENT
0.500
1.000
1.500
0.5C
1.0C
1.5C
RANGE
1715
1690
1665
1640
1615
1590
1565
1540
1515
1491
1465
1440
1365
1280
1215
1140
1065
990
880
805
730
655
580
RANGE
View File
Decimate
Stop
Redraw

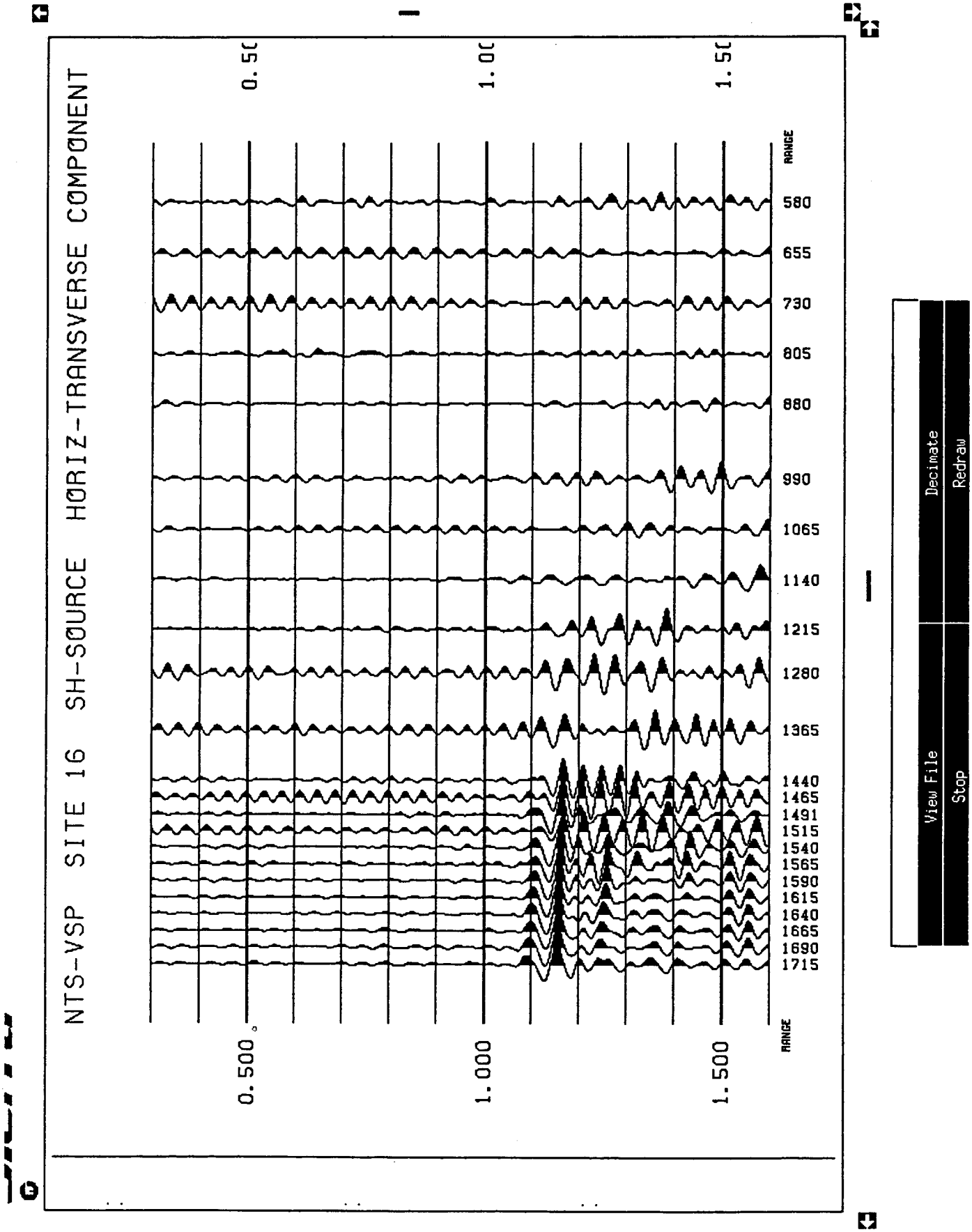
NTS-VSP SITE 16 SH-SOURCE HORIZ-TRANSVERSE COMPONENT
0.5
1.0
1.5
RANGE
580
655
730
805
880
990
1065
1140
1215
1280
1365
1440
1465
1491
1515
1540
1565
1590
1615
1640
1665
1690
1715
0.500
1.000
1.500
RANGE
Decimate
Redraw
View File
Stop

LAWRENCE BERKELEY LABORATORY
UNIVERSITY OF CALIFORNIA
INFORMATION RESOURCES DEPARTMENT
BERKELEY, CALIFORNIA 94720